Fluidized Bed Torrefaction of Agro-industrial Residues: the Case Study of Residues from Campania Region, Italy

Paola Brachi

Department of Industrial Engineering

Ph.D. Course in Chemical Engineering
(XIV Cycle-New Series)

Fluidized Bed Torrefaction of Agro-Industrial Residues: the Case Study of Residues from Campania Region, Italy

Supervisor   **Ph.D. student**
Prof. Michele Miccio   *Paola Brachi*

Scientific Referees
Ing. Giovanna Ruoppolo (IRC-CNR)
Dott.ssa. Letizia Magaldi (Magaldi Industrie S.r.l.)

Ph.D. Course Coordinator
Prof. Paolo Ciambelli

To my beloved "Mamma"

List of publications

This thesis includes the work contained in the following papers:

Paola Brachi*, Francesco Miccio, Michele Miccio, Giovanna Ruoppolo, On the torrefaction of tomato peel residues in fluidized bed of inert particles, Energy & Fuels, SUBMITTED.

Paola Brachi*, Francesco Miccio, Michele Miccio, Giovanna Ruoppolo, Non-isothermal decomposition kinetics of tomato peels based on isoconversional method and deconvolution procedure, Fuel Processing Technology, SUBMITTED.

Paola Brachi*, Francesco Miccio, Michele Miccio, Giovanna Ruoppolo, Isoconversional kinetic analysis of olive pomace decomposition under torrefaction operating conditions. Fuel Processing Technology 130 (**2015**). ISSN: 0378-3820 - DOI: 10.1016/j.fuproc.2014.09.04.

Conference contributions included in the thesis:

Paola Brachi*, Francesco Miccio, Michele Miccio, Giovanna Ruoppolo, Fluidized bed torrefaction of industrial tomato peels: set-up of a new batch lab-scale test rig and preliminary experimental results. Proceedings of the 22nd International Conference On Fluidized Bed Conversion previously "International Conference on Fluidized Bed Combustion" - Turku, Finland, June 14-17, 2015. ISBN: 978-952-12-3222-0.

Publications not included in the thesis:

Giovanna Ruoppolo, Francesco Miccio, Paola Brachi, Antonio Picarelli*, Riccardo Chirone. In Situ Carbon Dioxide Capture during Biomass Fluidized Bed Gasification. Chemical Engineering Transactions 43 (**2015**). ISBN 978-88-95608-34-1; ISSN 2283-9216.

Paola Brachi*, Francesco Miccio, Michele Miccio, Antonio Picarelli, Giovanna Ruoppolo. Fluidized bed co-gasification of biomass and polymeric wastes for a flexible end-use of the syngas: Focus on bio-methanol. Fuel 128 (**2014**). ISSN: 0016-2361- DOI: 10.1016/j.fuel.2014.02.070.

Giovanna. Ruoppolo*, Francesco Miccio, Paola Brachi, Antonio Picarelli, Riccardo Chirone, Fluidized Bed Gasification of Biomass and Biomass/Coal Pellets in Oxygen and Steam Atmosphere. Chemical Engineering Transactions 32 (**2013**). ISSN: 1974-9791- DOI: 10.3303/CET1332100.

Conference contributions not included in the thesis:

Francesco Miccio*, Roberto Solimene, Massimo Urciuolo, Paola Brachi, Michele Miccio, Fluidized bed combustion of a lignin based slurry, IConBM2016 2nd International Conference on BIOMASS 19-22 June 2016, Giardini Naxos-Taormina, Sicily, Italy, SUBMITTED.

Giovanna Ruoppolo*, Paola Brachi, Riccardo Chirone, Francesco Miccio, Antonio Picarelli, Co-gasification of plastic and biomass in fluidized bed reactor. Poster Presentation at: 1st International Congress on Advances In The Packaging Industry Product and Process, Naples (IT), 19-20 November 2015. Best Poster Awards (1st PRIZE).

Bartolomeo Cosenza, Michele Miccio*, Paola. Brachi. Continuity diagram analysis at open loop and closed loop to improve the operability of a bioreactor. Proceedings of the 14th International Conference on Instrumentation, Measurement, Circuits and Systems (IMCAS15), 27-29 June **2015** Salerno, Italy. ISSN: 1790-5117, ISBN: 978-1-61804-315-3.

Giovanna Ruoppolo*, Paola Brachi, Antonio Picarelli, Francesco Miccio, Riccardo Chirone, Primary catalysts for fluidized bed gasification of biomass and wastes. Proceedings of the XXI International Conference on Chemical Reactors "CHEMREACTOR-21", 22-25 Sept **2014**, Delft, Netherlands.

P. Brachi, R. Chirone, F. Miccio, M. Miccio, A. Picarelli, G. Ruoppolo*, Fluidized bed co-gasification of biomass and plastic wastes. Proceedings of the Joint Meeting: French and Italian Sections – IFRF and The Combustion Institute, 23-24 April **2014**, Pisa, Italy. ISBN:978-88-88104-16-4-DOI:10.4405/profic2014.D12.

Giovanna Ruoppolo, Riccardo. Chirone, Antonio Picarelli, Paola Brachi, Francesco Miccio, Michele Miccio, Fluidized bed co-gasification of industrial wastes for flexible end-use of syngas. Proceedings of the 14th International Waste Management and Landfill Symposium; 30 Sep – 4 Oct **2013**, Santa Margherita di Pula (CA), Italy. ISBN: 978-88-6265-028-1.

Giovanna Ruoppolo, Francesco Miccio, Paola Brachi, Antonio Picarelli*, Riccardo Chirone, Utilization of oxygen – steam moisture for FB gasification of fuel pellets, Proceedings of the XXXVI Meeting of the Italian Section of the Combustion Institute, **2013**, Procida, Italy. ISBN: 978-88-88104-15-7 - DOI: 10.4405/36proci2013.IX2

* Corresponding author

TABLE OF CONTENTS

LIST OF FIGURES

LIST OF TABLES

ABSTRACT

The purpose of this Ph.D. project was to investigate the potential of the torrefaction treatment for upgrading low-value agro-industrial residues into useable solid fuels to be employed as high-quality energy carriers.

The first phase of the project involved a screening of the agro-industrial residues available in Campania region (Italy) with good potentiality for energy applications. As a result of this analysis, tomato processing residues and olive mill residues, which have stood out as those in need of a more sustainable and environmental friendly disposal solution, were at first selected as biomass feedstocks for this Ph.D. project. However, practical difficulties encountered in the pre-treatment of the virgin olive husk (i.e., specifically in reducing the size of olives stone fragments which compose olive mill residues together with the olive pulp) led afterwards to discard such residue as a potential feedstock for the subsequent lab-scale torrefaction tests

The main chemical and physical properties (i.e., moisture content, elemental composition, calorific value, ash content, etc.) of virgin olive husk (OH) and tomato peels (TPs) were analyzed in order to evaluate their potential for energy recovery. A special focus was also devoted to the study of the thermal behavior of both residues by means of thermogravimetric analysis (TGA) coupled with mass spectrometry (MS) with the aim of studying the weight loss kinetics during the torrefaction of both the virgin olive husk and tomato peels as well as obtaining useful information about the qualitative composition of the evolved torgas.

Specifically, the kinetic analysis of thermal degradation of virgin olive husk, in the temperature range of interest for torrefaction, was performed by using non-isothermal thermogravimetric measurements at different heating rates, ranging from 2 to 40 °C/min. Modeling analysis of TGA data was performed by means of two selected integral isoconversional methods, i.e., the nonlinear Vyazovkin incremental approach, which is more rigorous but time-consuming, and the linear Ozawa–Flynn–Wall (OFW) method, which is computationally simpler but based on mathematical approximations. Results showed that the values of the activation energy of the thermal decomposition reaction derived from both models were very similar. This suggests that the OFW method, which is more user-friendly than the Vyazovkin procedure, is suitable for studying the weight loss kinetics upon the torrefaction of virgin olive husk. The reliability of the OFW method was further confirmed by the successful application of the derived kinetic parameters to reproduce two experimental TGA curves not included in the kinetic computations.

The kinetics of the thermal decomposition of tomato peels (TPs) under nitrogen atmosphere was studied by non-isothermal thermogravimetric

measurements in the heating rate range 2-40 °C/min. Due to the complexity of the thermal decomposition mechanism of TPs, which implies simultaneous multi-component degradation reactions, an analytical approach involving the deconvolution of the overlapping degradation steps from the overall differential thermogravimetric curves (DTG) and the subsequent application of model-free kinetic methods to the separated peaks was adopted. To this end, two different open-source Matlab functions employing a non-linear optimization algorithm to decompose a complex pattern of overlapping peaks into its component parts, were used. Different conventional statistical functions (i.e., Gaussian, Voigt, Pearson, Lorentzian, equal-width Gaussian and equal-width Lorentzian) were tested for deconvolution and the best fits were obtained by using a suitable combination of Gaussian and Lorentzian functions. The differential Friedman's isoconversional method was selected for the kinetic analysis of the deconvoluted DTG peaks. The reliability of the evaluated kinetic parameters was checked by reproducing a dynamic experimental curve recorded at a heating rate of 60 °C/min and not included in data used for kinetic computations. Theoretical and experimental data showed a good agreement in the conversion range 20-80%, suggesting that the computed kinetic parameters could be used for modeling torrefaction processes involving the investigated tomato processing residues.

An extensive experimental program was carried out in a new laboratory-scale batch experimental apparatus, which was purpose-designed and built for this Ph.D. project. The torrefaction section of the apparatus is represented by a batch fluidized bed reactor made up of a tubular glass column (inner diameter 100 mm, length 750 mm) surrounded by a glass jacket, which was kept under vacuum to ensure thermal insulation of the reactor while keeping the advantage of its transparency. This arrangement allowed visual monitoring of both the fluidization pattern and particles movement in the bed at any time and temperature tested for torrefaction.

An ancillary investigation on the cold fluidization and segregation behavior of two different sand and tomato peels binary mixture was preliminary carried out, by varying the biomass weight fraction in the range 2-9 %, in order to identify suitable operating conditions in terms of biomass particle size and maximum biomass batch loading (i.e., the mass fraction of biomass in the bed of sand beyond which the fluidization properties deteriorate) to be used during the fluidized torrefaction tests. Specifically, two different Geldart group B silica sands, in the 100-400 μm size range (FSS, fine silica sand) and in the 100-700 μm size range (CSS, coarse silica sand), were tested in cold flow experiments and then discriminated for their use as inert bed material to assist the biomass fluidization and also to maintain the desired hydrodynamics of the fluidized bed when biomass particles experience different degrees of devolatilization. As the coarse silica

sand proved to be poorer as fluidizing material compared to the fine sand, this latter was selected to be the inert bed component for fluidized bed torrefaction tests.

The effects of the main torrefaction process variables (i.e., temperature and reaction time) on both the key performance parameters (i.e., mass and energy yields) and the main properties of the solid product were investigated for tomato processing residues. Fluidized bed experimental runs were performed at 200, 240, and 285 °C and for holding times equal to 5, 15 and 30 min. Results showed that the thermochemical transformations that tomato peels underwent, as a results of the release of volatile matter arising from the thermal decomposition of its organic constituents, led to a significant improvement of their chemical and physical properties. In particular, it was observed that higher temperatures and longer holding times (with a more marked effect of the torrefaction temperature) determine an increasing in the calorific value (by a factor of 1.2 for the biomass torrefied at 285 °C and 30 min), a reduction of the O/C (up to approximately 40 % for the biomass torrefied at 285 °C and 30 min) and an improved hydrophobicity of the torrefied biomass with respect to the parent one, while maintaining the mass yield (approximately between 75 and 94 %, daf basis) and energy yield (approximately between 90 and 96 %, daf basis) at acceptable levels. These findings suggest tomato peels as a valuable and convenient candidate for the torrefaction treatment.

A limited set of torrefaction tests were also performed in a bench-scale fixed bed reactor which was purposely set-up in order to compare the performance of this configuration with respect to the fluidized bed one, under identical operating conditions. Results showed that at the laboratory-scale, where mass and heat transfer limitations are not negligible, the fluidized bed configuration is more suitable to obtain reliable and reproducible test results, good-quality of the torrefied solids and excellent process performance in terms of mass and energy yields.

INTRODUCTION

Millions of tons of biodegradable solid wastes are generated every year worldwide from agro-industry, in particular the food and beverage one (Singh nee' Nigam et al., 2009). Due to the high organic matter content (carbohydrates, proteins, fats, oils, etc.), these wastes, if not properly managed, not only pose increasing disposal and potentially severe pollution problems, but also represent a considerable loss of potentially valuable biomass and nutrients (Pelizer et al., 2007; de Araùjo Sousa and Correia, 2010; Ezejiofor et al., 2014;). In accordance with internationally agreed waste management strategies (Directive 2008/98/EC), waste treatments aimed at the conversion into useful forms of bio-energy and/or bio-fuels may represent an interesting alternative for a sustainable disposal of these residues.

The conversion of biomass into useful forms of bio-energy and/or bio-fuels encompasses a wide range of different biochemical, mechanical and thermo-chemical processes (Peter McKendry, 2002). Among these, the thermo-chemical processes (e.g., direct combustion, gasification and pyrolysis) are deemed as the most promising ones due to the higher efficiencies in terms of the lower reaction time required (a few seconds or minutes for thermo-chemical processes vs. several days, weeks or even longer for bio-chemical/biological processes) and the superior ability to convert/valorize most of the organic compounds (Zhang et al., 2010). For example, it is worth noting that lignin, a common primary component in biomass, is typically considered to be non-fermentable and thus cannot be completely decomposed via biological routes, whereas it is decomposable via the thermo-chemical processes (Williams et al. 2003; Zhang et al., 2010).

The concept of utilizing wastes from agro-industrial activities to produce energy and/or biofuels via the thermo-chemical route is not new. But, operational and logistical drawbacks related to intrinsic properties (e.g., low heating value, high moisture content, high heterogeneity, poor grindability, hygroscopic behavior, putrescible nature) have to date hampered development in this sector. However, over the last decade, new evidences from recent research (Bergman et al., 2005a; Bergman et al., 2005b; Uslu et al., 2008; Sadaka and Negi, 2009; Couhert et al., 2009; Chew and Doshi, 2011; Van der Stelt et al. 2011; Shah et al., 2012) have emerged suggesting that torrefaction, a relatively new thermal pretreatment of biomass, may became in the near future a viable option to overcome the above mentioned barriers and make low-value biomass feedstocks eligible for different energy-related applications thanks to its established ability convert any

lignocellulosic material into a solid with superior coal like properties (Kleinschmidt, 2011).

Torrefaction is a thermo-chemical treatment method where biomass is heated in an inert environment to a temperature ranging between 200 and 300 °C. Typically, it is characterized by low particle heating rate (i.e., less than 50 °C/min) and by a relatively long reactor residence time that, depending on feedstock, technology and temperature, ranges from 30 to 120 minutes (Bergman and Kiel, 2005; Nordin et al., 2013). Specifically, benefits accomplished by torrefaction for the treated biomass are: a.) higher heating value; b.) higher hydrophobicity or water-resistivity, so that thermally-treated biomasses do not regain moisture during storage (Kongkeaw and Patumsawad, 2011); c.) lower atomic O/C and H/C ratios, resulting in less smoke and water vapor formation, in addition to less energy loss during the combustion and gasification processes (Tumuluru et al., 2012); d.) improved reactivity (Bridgeman et al., 2008; Chew and Doshi, 2011), grindability (Arias et el., 2008) and fluidization behavior (Bergman et al., 2005b) and e.) strongly reduced biological activities (e.g., rotting, mould) making the torrefied biomass very stable in different storage environments (Tumuluru et al., 2011). Among the various applications being considered for the torrefied biomass, the most likely ones include co-firing with coal in pulverized coal fired power plants and cement kilns, small-to-medium scale dedicated biomass burners and gasification in entrained flow gasifiers that normally operate on pulverized coal (Koppejan et al. 2012).

Until now, most of the research and development (R&D) on torrefaction is largely based on clean and dry biomass resources such as waste wood (Chew and Doshi, 2011); this is due to both technical limitations of the currently available reactor technologies and economic considerations, which favor woody biomass (Kleinschmidt, 2011; Koppejan et al. 2012). Further, most utilities prefer clean woody biomass as co-firing fuel, because other residual biomasses are prone to negatively impact plant performance and are subject to stricter emission norms than woody biomass (Kleinschmidt, 2011). Hence, it is quite likely that the first commercial torrefaction installations will also operate on high-quality woody biomass. Nevertheless, due to the lower price and the better availability, the interest into waste streams and biomass residues as feedstock for torrefaction is increasing. Significant research is currently underway to explore the potential to produce high-grade solid biofuels from lignocellulosic agricultural and agro-industrial residues (Bridgeman et al., 2008; Uemura et al., 2011; Protasio et al., 2012; Wang et al., 2012; Lu and Chen, 2014; Toscano et al., 2015). Non-lignocellulosic biomass, such as food wastes, chicken litter and digested sludge (Poudel et al., 2015; Dhungana et al., 2012a) as well as municipal solid wastes (Yuan et al., 2015) have also received some attentions. As

regards non-woody biomass feedstocks, the main challenges are related to their high water content, which have a negative effect on the energy efficiency of the whole conversion process, and to other unfavorable physical-chemical characteristics (e.g., alkaline metals and chlorine), which may affect the integrity (e.g., fouling and corrosion) of the conversion plant devices and the composition of the volatiles (torgas) liberated during their treatment; substantial additional treatment of the feedstock as well as of torrefaction gases is therefore required (Koppejan et al. 2012). At present, it is yet uncertain if the additional cost associated with these factors may be compensated by the lower price of the input material. Moreover, due to the very dissimilar characteristics of such biomass feedstocks, the potential benefits arising from torrefaction pretreatment are hard to be generalized and must be evaluated on a case-by-case basis (Bergman and Kiel, 2005).

Further fundamental and applied R&D efforts are, therefore, required to examine if alternative non-woody biomass feedstocks, like for example agro-industrial residues, could benefit from torrefaction process just as conventional woody biomass does as well as to provide sufficient design data with respect to operating conditions (i.e., temperature, residence time, feed particle size and moisture content) and their relation to (1) relevant product properties (i.e., that are desirable for its end use), (2) key process indicators (such as process energy efficiency) and (3) the composition of the volatiles liberated during torrefaction. This latter being important with respect to how the gas can be utilized so that waste streams are prevented (Bergman et al., 2005a).

On the basis of the above-mentioned survey, the primary aim of this work was to provide a contribution to the "proof-of-concept" studies currently underway on the torrefaction process through a comprehensive investigation program focused on selected low-value agro-industrial residues, produced in Campania region (Italy). Specific research tasks involved in this Ph.D. research work include:

- to assess the availability and current uses of agro-industrial residues produced in Campania region (Italy) as a preliminary criterion for selecting biomass feedstocks to be used in this Ph.D. study;
- to investigate the thermal degradation behavior of the selected feedstocks by means of thermogravimetric analysis (TGA) coupled with mass spectrometry (MS) with the aim of studying the torrefaction weight loss kinetics during torrefaction as well as obtaining useful information about the qualitative composition of the evolved torgas;
- to investigate the effects of the main torrefaction process variables (i.e., temperature and reaction time) on both the key

performance parameters (i.e., mass and energy yields) and properties of the solid product (i.e., elemental composition, calorific value and hydrophobicity) as well as to develop mathematical models (i.e., multiple regression model) that can help predict their changes as a function of the torrefaction severity.

To achieve these objectives, an extensive experimental program was conceived and carried out in a new batch laboratory-scale experimental apparatus, which was purpose-designed and built for this Ph.D. project.

So far, a lot of the research on torrefaction has been performed at the micro-scale (powdered biomass) by using analytical instruments such as TGA (Park et al., 2013; Mafu et al., 2016), in which only few milligrams (e.g., 5-20 mg) are typically processed. These experiments usually provide good insight on the kinetics of torrefaction (Brachi et al., 2015a), but they do not give evidence of possible treatment heterogeneities in the torrefied materials, which typically occur on a testing scale larger than TGA (Di Blasi et al., 2012; Cavagnol et al., 2015), as induced by exothermic reactions and/or diffusional heat and mass limitations. Laboratory ovens and furnaces, which can process a larger amount of raw feedstocks, have also be profusely used in torrefaction research (Wu et al., 2012; Peng et al., 2013), but they could not reveal much information for scale-up and design considerations. Bench-scale apparatuses are certainly the most important early-stage tools for assessing and scaling new biofuels technologies: However, only a few studies have been performed on torrefaction on this investigation scale, generally as a fixed-bed reactor (Peng et al., 2013; Grigiante and Antolini, 2015). As regards torrefaction in fluidized beds, only two works have been published so far. Specifically, Li et al. (2012) were able to properly torrefy (without slugging and channeling) a bed made only of sawdust particles in the 0-350 μm size range, with the help of an inclined orifice distribution plate. Instead, Atienza-Martinez et al. (2013) torrefied dry sewage sludge (SWS) in the size range 250-500 μm in a bed consisting of torrefied SWS particles from previous experiments in order to reduce problems associated the start-up period. However, it is worth noting that, although the test configurations proposed by the abovementioned Authors enjoy the benefit of avoiding the separation of the torrefied product from heat carrier solids, the well-known difficulty to fluidize biomass particles alone (Cui and Grace, 2007) may restrict the use of such technology to a relatively narrow range of biomass feedstocks.

Anyway, the torrefaction of agro-industrial residues on a scale larger than TGA has received rather little attention. Regarding such feedstocks, the main

XX

challenge is related to their specific chemical composition rich of extractives, hemicellulose and lignin, which degrade exothermically (Di Blasi et al., 2014; Chen et al., 2015) and can lead to overheated zones mostly in torrefaction reactor where the heat transfer is low, with an increased risk for carbonization or even to a complete thermal runaway (Di Blasi et al., 2014; Cavagnol et al., 2015). These uncontrolled phenomena could significantly decrease the mass and the energy yields of the torrefaction process and generate strongly heterogeneous solid products at the exit of such a pre-treatment, making it a challenge to obtain reliable results on the effect of the main torrefaction parameters on both the solid product properties and process performance.

Therefore, in order to overcome the abovementioned limitations, a new sand-assisted torrefaction process based on fluidized bed (FB) technology has been proposed in this Ph.D project. Even though uncommon in torrefaction, fluidized bed technology, by guaranteeing that biomass particles undergo torrefaction in a well-mixed state under uniform temperature, could provide an even product quality that is generally difficult to attain in many other conventional laboratory scale systems (i.e., ovens and fixed beds reactors both directly and indirectly heated). Moreover, the large thermal inertia and the high heat transfer rate within a dense bed of sand make this technology particularly suitable to deal with the exothermicity associated with the thermal degradation of non-woody biomass (i.e., agricultural and agro-industrial residues), which tend to ignite or carbonize easily during torrefaction (Kleinschmidt, 2011).

On the other hand, however, the presence of particles which differ in one or more of their constitutive properties (i.e., shapes, sizes, density etc.) in a fluidized bed could give rise to some drawbacks. One of the most undesirable is the tendency of the particles to be segregated along the bed height (Beeckmans et al., 1985; Zhang et al., 2009a; Fotovat et al., 2014) as it may cause unstable fluidization patterns and thus reduce the heat and mass exchange rates (Daleffe et al., 2008). Therefore, a major concern for processes involving the fluidization of dissimilar components relies on setting the operating conditions in a way that the advantages associated with the mixing of the solid species can be exploited.

In spite of all the research reported in the literature (Cui and Grace, 2007), there is still little understanding on the fluidization dynamics of both the biomass and multicomponent particle beds. As a consequence, there are currently no general criteria that could be useful in setting process parameters suitable for the proper operation of fluidized beds involving biomass also in mixture with inert particles (Cui and Grace, 2007). Therefore, the design and operation of process involving biomass are

commonly based on conventional fluidization knowledge and methodologies, leading to trial and error ad hoc solutions (Zhang et al., 2008; Cui and Grace, 2007).

On the basis of the above-mentioned analysis, a complementary, but necessary aim of the present research work was to determine the suitable process parameters for the proper operation of the new lab-scale fluidized bed torrefier. Specific research tasks related to this aim included:

- to experimentally investigate by means of visual observation the mixing and segregation behavior of selected biomass-sand binary mixtures by varying the biomass particle size in cold flow experiments;
- to carry out a systematic experimental investigation on the effect of the biomass weight fraction on the characteristic velocities (i.e., complete fluidization velocities and minimum slugging velocity) of different binary mixtures in order to select the maximum biomass batch loading (i.e., the critical weight fraction of biomass in the mixtures beyond which the fluidization properties deteriorate) to be used during the subsequent torrefaction tests.

Finally, in order to provide a reference case to the "proof-of-concept" study based on the adoption of a fluidized bed, a new bench-scale fixed bed apparatus was also specifically built for this Ph.D. project. It was used to compare the performance of both the fixed and fluidized bed torrefaction concepts under identical operating conditions. This Ph.D. Dissertation is organized into four chapters.

Chapter I provides a general introduction to biomass feedstocks, which also includes a survey on the availability and current uses of agro-industrial residues in Campania region, Italy. The challenges and pretreatment needs in utilization of biomass fuels for energy applications are then presented together with an in-depth discussion on torrefaction, including its meaning, history, process details and definitions, fuel characteristics, research gaps and commercial challenges. A literary survey and a theoretical framework related to hydrodynamics and multiphase flow phenomena in fluidized beds involving biomass are also presented in this chapter.

Chapter II provides a detailed description of the raw materials and the protocols used in the experimental program as well as the instruments used for the characterization of feedstocks and inert bed materials; a description of the two lab-scale experimental apparatuses purposely-designed, built and optimized for the execution of torrefaction experiments is also provided.

In **Chapter III** the main results obtained from all of the above-mentioned experimental tests are presented and critically discussed.
Finally, conclusions and future developments are reported in **Chapter IV**

.

Theoretical Framework and Literature Review

I.1 Biomass resources

I.1.1 Biomass definition

The term biomass refers to non-fossilized and biodegradable organic material originating from plants, animals as well as microorganisms derived from biological sources. Biomass includes products, byproducts, residues and wastes from agriculture, forestry and related industries, as well as the non-fossilized and biodegradable organic fractions of industrial and municipal solid wastes. It also includes gases and liquids recovered from the decomposition of non-fossilized and biodegradable organic materials (UNFCCC, 2005; Demirbas, 2009), such as gases derived from landfilling (mainly methane).

I.1.2 Biomass resources: classification and potential energy recovery

Different classification are available for biomass resources. The most accepted one divides the biomasses into three primary source categories, according to their origin: i. natural or virgin biomass; ii. energy crops and iii. residual (dry and wet) biomass. (Figure I.1).

I.1.2.1 Virgin Biomass

Virgin biomass includes all naturally occurring terrestrial plants such as trees, bushes and grass. It occurs spontaneously in forest and grassland. Man has always used it to satisfy his personal need for firewood. A major challenge associated with this type of biomass is the necessary management of the resource acquisition and transport to the place of use that makes the exploitation of this biomass economically unviable for a large-scale utilization.
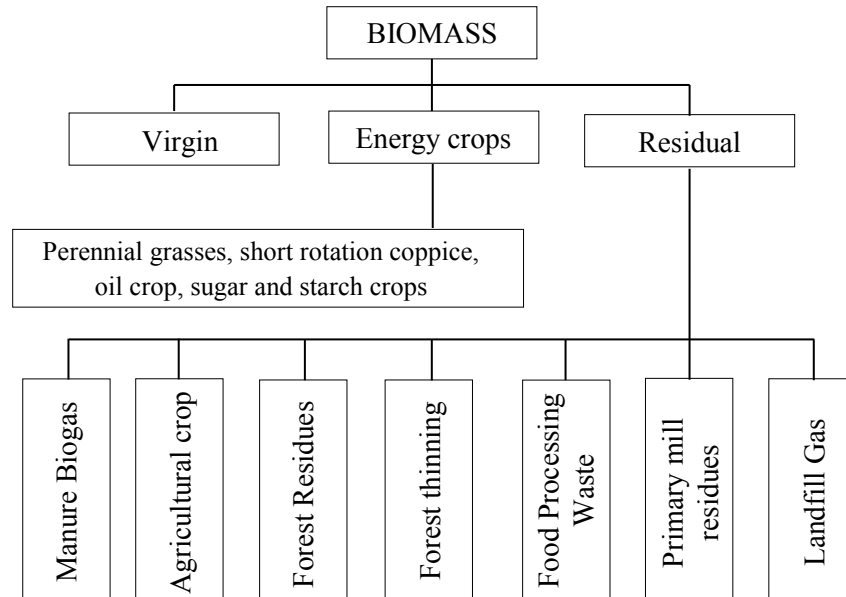
Figure I.1 *Biomass classification (adapted from Panwar et al.,2012).*

I.1.2.2 Energy Crops

Energy crops are perennial grasses and trees grown through traditional agricultural practices that are produced primarily to be used as feedstocks for energy generation (Spellman, 2011). Several energy crops have been studied throughout Europe: i. perennial grasses (e.g., miscanthus, switchgrass, giant reed, cardoon, etc.) and short rotation coppice for the production of lignocellulosic material; ii. oil crops (e.g., rapeseed and sunflower) for the production of biodiesel; iii. sugar and starch crops (beetroot, sugar cane, wheat, maize, etc.) for bioethanol production (Nikolaou et al.,. 2003). The advantages of using crops specifically grown for energy production is consistency in moisture content, heat content and processing characteristics. Disadvantages include relatively higher overall costs than many fossil fuels, higher-value alternative land uses that further drive up costs, added expenses associated with harvesting and processing, as well as farmers' and power plant owners' unfamiliarity with energy crops (BCHPC, 2007). Moreover, there are also great ethical problems associated with using such a kind of bioenergy. One key criticism is that energy crops can monopolize lands in competition with food production, causing global food prices to rise at the expense of the poorest people in the world. Another criticism is that a growing requirement for cultivating bioenergy crops may result in an increase in the activities of deforestation with a strong impact on the environment (DCE, 2012).

I.1.2.3 Residual Biomass

Residual biomasses (dry and wet) are generated by any human activities including agricultural and livestock activities, food processing and timber industry.

I.1.2.3.1 Forest residues

Forest residues are defined as the biomass material remaining in forests that have been harvested for timber, and are almost identical in composition to forest thinnings. Forestry residues include logging residues, excess small pole trees, and rough or rotten dead wood (Manahan et al., 2007). Generally, forest residues are either left in the forest or disposed of via open burning through forest management programs. Typically, they have an energy content of 11-12 MJ/kg (wet) and 19-20 MJ/kg (dry). The primary advantage of using forest residues for power generation is that an existing collection infrastructure is already set up to harvest wood in many areas. Companies that harvest wood already own equipment and transportation options that could be extended to gathering forest residues (BCHPC, 2007).

I.1.2.3.2 Forest thinning

Forest thinnings are defined as underbrush and saplings smaller than 2 inches in diameter, as well as fallen or dead trees. These substances are sometimes known as "ladder fuels" because they can accelerate a forest fire's vertical spread (Spellman, 2011). Forest thinnings typically have an energy content of 11-12 MJ/kg (as received) and 19-20 MJ/kg (dry basis). The high costs of harvesting, collecting and transporting loose forest thinnings represent an economic barrier to their recovery and utilization for energy. Typically, the wood waste from forest thinnings is disposed of through controlled burning (BCHPC, 2007).

I.1.2.3.3 Primary mill residues

Primary mill residues are waste wood from manufacturing operations that would otherwise be sent to a landfill. Manufacturing operations that produce mill residues usually include sawmills, pulp and paper companies, and other millwork companies involved in producing lumber, pulp, veneers, and other composite wood fiber materials. Primary mill residues are usually in the form of bark, chips, sander dust, edgings, sawdust, or slabs (Spellman, 2011). Due to the fact that primary mill residues are relatively homogeneous and concentrated at one source, the predominant part of residues generated are currently used as fuel or to produce other fiber products (Spellman, 2011). Because most primary mill residues are fairly dry after they have passed through a manufacturing process, they fall at the upper level of the

energy content range for wood (20 MJ/kg) (BCHPC 2007). Producing power from primary mill residues is highly advantageous for the wood products industries because they have a "free" (i.e., no additional cost) source of fuel with no transportation costs and a secure supply that they control by themselves. The cost of these residues is actually negative to most wood products industries because if the residues are not used on site, companies have to pay for disposal (BCHPC, 2007).

I.1.2.3.4 The crop residues

Crop residues are materials left in an agricultural field or orchard after the crop has been harvested. These residues include stalks and stubble (stems), leaves, and seed pods. The primary advantage of using such biomass resource for power generation reside in the chemical-physical characteristics, the consistency in terms of quantity, the distribution almost ubiquitous, and finally, the fact that their production does not threaten the world's food supply. The disadvantages are the crop seasonality, which creates an unsteady and unreliable fuel supply, and their competing uses (e.g., animal feed or animal bedding), which are sometimes established markets (BCHPC, 2007).

I.1.2.3.5 Wastewater treatment biogas

Wastewater treatment biogas is a by-product of the anaerobic (without oxygen) treatment of domestic/industrial wastewater sludge. Wastewater treatment biogas typically contains 55 to 65% methane, 30% CO_2 and other inert gases such as nitrogen, thus resulting in an energy content of approximately 22 to 24 MJ/Nm^3. Currently, most of wastewater treatment plants, employing anaerobic digestion, collect and use their biogas on site. Any excess biogas that cannot be used on site is generally flared (BCHPC, 2007).

I.1.2.3.6 Manure digester biogas

Manure digester biogas is produced at industrial livestock operations, also known as factory farm, when manure decomposes anaerobically (without oxygen) in a digester. Biogas from a manure digester consists of approximately 60 to 80% methane (Masse et al., 2011), depending on the type of animal and the manure collection system, plus other anaerobic digestion byproducts (i.e., CO_2 and trace amounts of hydrogen sulfide). This composition typically results in a heating value of approximately 20 to 30 MJ/Nm^3. Manure digester biogas represents a free-fuel for the factory farm, meaning there is no cost associated with its generation if an anaerobic digester is already in place. Capital costs, operation and maintenance costs, and costs associated with collection and gas treatment are critical factors in

evaluating the suitability for a biogas power project. In some instances, manure biogas systems could be too small for gas treatment to be economical (BCHPC 2007).

I.1.2.3.7 Landfill gas

Landfill gas (LFG) results from the anaerobic decomposition of organic wastes at MSW disposal facilities, commonly known as landfills. On dry basis, it consists of approximately equal amounts of CO_2 and CH_4 with trace amounts (< 1%) of other organic compounds (Qin et al., 2001). Small quantities of nitrogen, oxygen, and hydrogen, and trace of inorganic compounds, such as hydrogen sulfide (which has a strong odor), can also be found in LFG. Recovering and burning such gas to generate useful energy can virtually eliminate harmful emissions from a fuel that is otherwise wasted (Quig et al., 2006). Landfill gas, with a calorific value in the range of 13-22 MJ/Nm^3 (BCHPC 2007), constitutes a high-value fuel for gas engines and internal combustion engines (Bove and Lunghi, 2006; McKendry, 2002).

I.1.2.3.8 Agro-industrial residues

Agro-industrial residues, which encompass a wide array of materials derived from the industrial processing of raw agricultural products, are among the greatest sources of biomass in the world (Lima et al., 2014). Since these are rich in organic constituents, they represent one of the most energy-rich resources on the planet (Singh nee' Nigam et al., 2009), however, still largely untapped. Agro-processing wastes are actually difficult to utilize as a fuel source due to the varying characteristics and properties of the different waste streams. As such, most of them are currently disposed as industrial wastes and transferred to a local treatment plant (BCHPC, 2007). Therefore, an intense work is underway in the agro-industry to evaluate the energy resource these wastes represent, and to develop processing methods that would allow for more effective utilization of this biomass resource, which otherwise represent not only a considerable loss of potentially valuable biomass and nutrient, but also an added cost for manufacturing companies.

I.2 The agro-industrial sector in the Campania region (Italy)

The agro-food industry is one of the main pillars of manufacturing of Campania region. This justify the interest for identify new options for the disposal and the recovery of residues generated by this sector, as investigated in this Ph.D. project.

Campania produces over 50 % of Italy's nuts and is also the leader in the production of tomatoes, which reaches 1.5 million tons a year (Eurostat,

2009). Olive trees cover over 74,604 hectares of the agricultural land and contribute by € 620.6 million to the added value of agriculture, together with the production of fruit. Animal breeding is widespread (it was done in 70,278 farms in 2000) and the milk produced is used to process typical products, such as "mozzarella"(Eurostat, 2009). Wine production has also increased in the last years, together with the quality of the wine (Bettini, 2014). Therefore, potential sources of residual biomass in Campania region could be:

- Residues from the oil industry: virgin and exhausted olive husk;
- Residues of the alcohol industry: fresh and exhausted grape pomace;
- Residues of the canning industry: kernels of fresh fruit, dried fruit shells, tomato seeds and/or skins.

I.2.1 Availability and uses of agro-industrial residues in Campania

I.2.1.1 Methodology for estimating the amount of residues

The scientific basis for estimations of the sustainable potential of waste and residues is currently still very limited (Terrapon-Pfaff et al., 2012). However, even though type and amount of agricultural products available varies from crop to crop depending on the plant structure, seasonal availability, harvesting methods, irrigation practices, soil quality and other factors, the amount of agro-industrial residues produced is directly related to the corresponding crop production (Terrapon-Pfaff et al., 2012). Therefore, if the crop production quantities at a particular time are known, it is possible to simply estimate the amounts of residues produced using the residue-to-product ratio (Koopmans and Koppejan, 1998) in the following general equation:

$$R = Cp \cdot RPR \tag{I.1}$$

where "R" is the total available agricultural residual biomass in kiloton per year, "Cp" the amount of crop production in kiloton per year and "RPR" the residue-to-product ratio in kiloton of residues per kiloton of product (Terrapon-Pfaff et al., 2012). This method has been widely applied to estimate the potential availability of agricultural residues for energy generation (Rosillo-Calle, 2007). Although this approach has its limitations as it does not include future developments and investments in the agricultural and agro-food sector, it is suitable to estimate the current country-specific energy potential of residues (Terrapon-Pfaff et al., 2012).

Accordingly, in the present work, eq.(I.1) was employed to estimate the current availability of agro-industrial residues in the Campania region relying on data made available by the Italian National Institute of Statistics

(Istituto Nazionale di Statistica; ISTAT), as regards Cp-values, and by the main professional and industrial associations, as regards RPR-values.

I.2.1.2 Olive mill residues: availability and current uses

Typically, three different types of residues are generated from olive mill: i. virgin olive husk (OH), ii. olive mill wastewater (OMWW) and iii. olive sludge or pomace. OH is a solid waste containing the stone, the pulp and the tegument of the olive. OMWW is made up of the water contents of the olive and frequently of some additional fresh water added in the process. It presents high biological and chemical pollutant load and it has been traditionally used as agricultural amendment. Finally, the sludge is a byproduct similar in appearance to a mixture of OH and OMWW (Gómez et al., 2010).

The types and quantities of residues obtained from olive mills depend greatly on the oil extraction system installed at the facility (Gómez et al., 2010). There are currently three different extraction technologies commonly used in the Mediterranean basin (Figure I.2), each one presenting different degrees of regional penetrations (Gómez et al., 2010). These are the traditional batch pressing system, the three-phase system and the two-phase system. The press is the traditionally used system. It consists in the crushing of the ground paste (from milling step) by means of hydraulic devices in order to extract the oil mix (mixture of oil and water). The mixture is then poured into a vat or holding tank. This is allowed to rest so that gravity and different densities come into play separating the oil from the water (REACM, 2008). In this process, three main output material flows are generated: olive oil, virgin olive husk (OH) and olive mill wastewater (OMWW). From the 1970s, presses have been increasingly replaced by continuous systems, even though they are still used in small production facilities. Continuous systems use centrifuges for the separation of the main material flows permitting lower operating costs and higher performance and production rates (Gómez et al., 2010). For few decades the most successful one was the three-phase system, which is based on the use of 3-phase decanter. Typically, 1 liter of water is added per kg of ground paste (from crushing/milling phase); it is then added to a horizontal centrifugal machine (i.e., H-centrifugation), where the solid is separated from the oil must. The must is then passed on to a vertical centrifugal machine (i.e., V-centrifugation), where the oil is separated from the vegetable water (REACM, 2008). The two-phase system was developed in the early 1990s as an evolution of the three-phase system with the intent to reduce the amount of wastes generated, especially of OMWW given their highly polluting nature (Gómez et al., 2010). The process is based on the use of a 2-phase decanter. This system mainly consists in a modification of the horizontal three phase one so that only two phases result (i.e., oil and sludge); namely instead of adding water for the horizontal centrifugation, the vegetable water

is recycled (REACM, 2008). This results in less polluting production, higher processing capacity and slightly higher quality of the olive oil.

Olives

```
                          Olives
                            ↓
                        ┌─────────┐
                        │ Washing │
                        └─────────┘
```
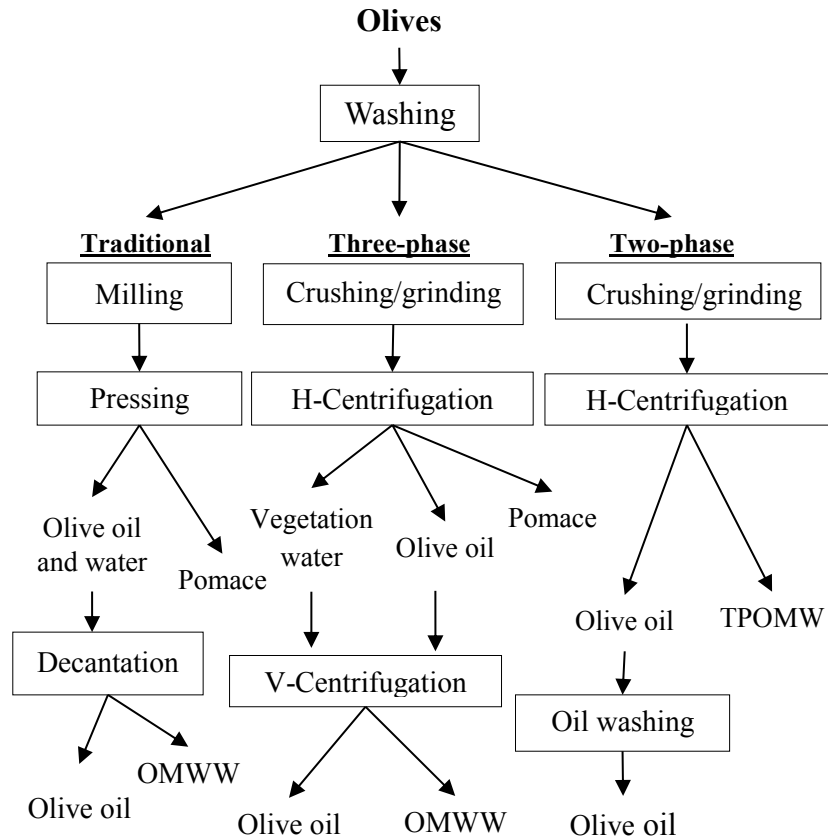

Figure I.2 *Simplified flow chart of industrial-scale olive oil extraction processes; tradition press-cake system, three-phase decanter system and two-phase centrifugation system. TPOMW stands for two-phase olive-mill waste (adapted from Morillo et al., 2009).*

Typically, the virgin olive husk (OH) has a moisture content ranging from 45-60% in 3-phase centrifugal systems, to 50-70% in continuous systems in two stages, to 25-30% in the conventional pressing system (REACM, 2008). Traditionally, it has been processed in seed-oil factories, in order to extract the residual olive oil. An easy-to-burn dry residue was also obtained, namely the so called exhausted olive husk, which accounts for 45-55% of virgin OH in input and has a moisture content of approximately 8-12% (Rossini, 2013). However, the declining market request for such a low-quality product and, at the same time, both the more limited storage life and the higher transportation costs of the virgin olive husk from continuous

processing systems, are currently raising the problem of olive husk disposal (Caputo et al., 2003).

Due to lack of consistent data on the productive capacity of the mills operating in the Campania region as well as the amount of olives actually processed for the oil production, in this Ph.D. study, the estimation of the olive mill residues was carried out indirectly by employing eq.(I.1). Table I.1 shows the values considered for the distribution of byproducts for the different extraction systems, as reported by Gomez et al.,(2010). In particular, the lowest value among the "residue-to-product" ratios shown in Table I.1 was chosen, in this research, as RPR-value for estimating the production of olive husk (OH) residues. This was done both to orientate the estimation towards precautionary values and in reference to the fact that the olive oil production in the Campania region is mostly based on the traditional press method (ENAMA, 2011).

Table I.1 *Percentage of byproducts as a function of the extraction technology* (adapted from Gomez et al., 2010)

Extraction system	Byproduct	Ratio byproduct/olives (%wt.)
Presses	Oil	20
	OH	40
	OMWW	40
Three-phase[*]	Oil	20
	OH	50
	OMWW	120
Two-phase	Oil	20
	Sludge	80

[*] The breakdown for the three-phase system exceeds 100 %wt. because some water is added in the process for the washing of the raw material.

Table I.2 *Harvested olives for oil production in Campania region, into kilotons per year (source: reference period 2006-2012)*

Province	2006	2007	2008	2009	2010	2011	2012	Average
Caserta	28	29	29	30	30	30	30	29
Benevento	32	34	49	49	42	44	43	42
Napoli	10	11	11	11	10	11	13	10
Avellino	21	18	26	22	22	24	19	21
Salerno	95	124	141	141	141	136	157	134
Campania	186	216	256	253	245	245	262	236

Therefore, on the base of the data on the regional production of olives intended for industrial processing (Table I.2), which are available on the

ISTAT website, it was estimated that approximately 95 kilotons of virgin olive husk per year are produced in the Campania region (approximately 40 %wt. of the processed olives), which potentially correspond to approximately 47 kilotons of exhausted olive husk (approximately 50 % of virgin olive husk), as shown in Table I.3.

Table I.3 *Estimated annual production of residues from the olive oil production in Campania. Data into kton per year, as received basis (average 2006-2012)*

Province	Virgin Olive Husk	Exhausted Olive Husk
Caserta	12	6
Benevento	17	8
Napoli	4	2
Avellino	8	4
Salerno	54	27
Campania	95	47

I.2.1.3 Winery residues: availability and current uses

Figure I.3 shows the process flow sheet for the generation of winery residues and wastewater from the winery and distillery industries. The main wastes from the viticulture activities are the vine stalks generated during the pruning of the grapevine. The primary by-product from the winery production is the grape marc, which comprises grape stalks, seeds and skins left after the crushing, draining and pressing stages of wine production (Jin and Kelly, 2009). Grape marc is typically processed to obtain additional products such as alcohol (ethyl alcohol, grappa, etc.) and tartaric acid (used by the food industry, pharmaceutical and by the same wine industry for the correction of the acidity of the wines), which results in a new lignocellulosic by-product, spent grape marc. This latter is traditionally used in the preparation of feed for animals, for the extraction of grape-seed oil or for the production of process heat and/or electricity directly through combustion on site close to the same distillation plant. Any surplus may be taken in composting. The wine lees are accumulated in the bottom of grape-juice or wine fermentation tanks. The distillation of the alcohol from low-quality wine, wine lees and grape marc also produces a large quantity of a viscous and acidic wastewater known as vinasses (Jin and Kelly, 2009). In many winery industries, an anaerobic depuration process is operated after the distillation to treat the winery effluents, i.e., vinasses and winery waste water, therefore generating waste bio-solids.

In the absence of consistent data on the productive capacity of winery and distillery industries operating in the Campania region as well as the amount

of grape actually processed for the winery production, in this Ph.D. study, the estimation of the winery residues was carried out indirectly by employing eq.(I.1). The RPR-values to be used for the estimation of the different by-products and residues from the winery production were taken from a survey carried out by ENAMA (2011), which is an Italian association ("Ente NAzionale per la Meccanizzazione Agricola") promoted by the Italian Ministry for Agricultural and Forestry Policies.
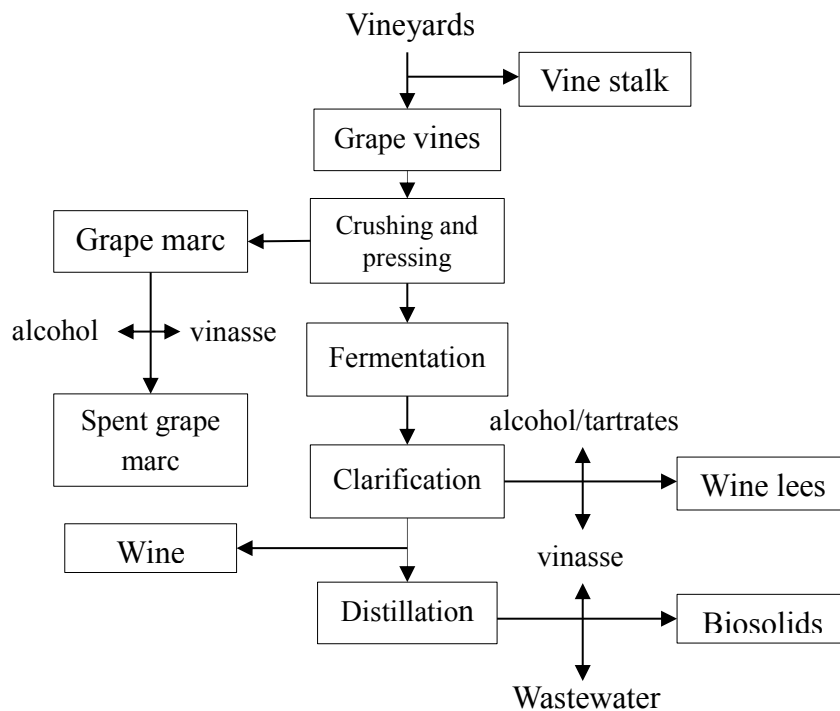
Figure I.3 *Sketch flow sheet showing the generation of by-products, residues and wastewater from the wine and distillation industries (adapted from Jin and Kelly, 2009).*

Specifically, as reported in the above survey, it results that approximately 74 %wt. of wine, 13 %wt. of grape marc (seeds, pulp and skin), 2.2 %wt. of stalks together with small amount of other wastes are obtained by processing wine grape. Only 15 %wt. of the produced grape marc is immediately recovered, while the remaining fraction is destined for distillation. Finally, about 42 %wt. of the fraction fed to distillation becomes spent grape marc. Instead, approximately 2/3 of stalks are discarded, while the remaining fraction is destined for distillation and produces no or negligible waste (ENAMA, 2011). Accordingly, on the base of data on the regional production of wine grape (Table I.4), available in the ISTAT database (reference period 2006-2012), it was estimated that approximately 5.38

kilotons of grape marc per year, 3.86 kilotons of stalks per year and 11.70 kilotons of spent grape marc per year are produced in the Campania region, on the as-received basis, as shown in Table I.5.

Table I.4 *Harvested wine grape production in Campania, into kton per year (source: ISTAT data, reference period 2006-2012)*

Province	2006	2007	2008	2009	2010	2011	2012	Average
Caserta	31	27	27	27	27	27	22	27
Benevento	135	117	111	117	117	109	111	117
Napoli	23	22	26	27	25	25	22	24
Avellino	52	44	46	43	47	47	39	45
Salerno	48	38	47	45	48	48	29	43
Campania	289	248	257	259	264	256	223	256

Table I.5 *Estimated annual production of residues from winemaking and distillation processes in Campania. Data into kton per year, as received basis (average 2006-2012)*

Province	Grape Marc	Stalks	Spent grape marc	Total Amount
Caserta	0.57	0.41	1.24	2.22
Benevento	2.46	1.76	5.38	9.60
Napoli	0.50	0.36	1.10	1.96
Avellino	0.95	0.68	2.07	3.70
Salerno	0.90	0.65	1.98	3.53
Campania	5.38	3.86	11.77	21.01

I.2.1.4 Canning industry residues

I.2.1.4.1 Fresh fruit processing residues

The main residue from the production of fruit juices, jams and canned fruit is represented by the kernels. Since these residues are relatively homogeneous and concentrated at one source, most of them are currently used as an energy source for the production of process heat, especially in large companies. Typically, they have an energy content of 18-20 MJ/kg, dry basis.

Due to lack of reliable and consistent data on the productive capacity of fruit processing industries operating in the Campania region as well as the amount of fresh fruit actually processed, in this Ph.D. Thesis, the estimation of the main residues (i.e., nectarines, apricots and peaches) from local fruit processing facilities was carried out indirectly by employing eq.(I.1). To this aim, in keeping with ENAMA (2011), a residue-to-product ratio (i.e., RPR-value) of 8 %wt. was assumed, regardless of processed fruit.

Typically, approximately 25 %wt. of the total amount of peach and nectarines harvested is intended for food processing sector while only 15% wt. in the case of nectarine (ENAMA, 2011). Accordingly, on the basis of data on the regional production of these fresh fruits (Table I.6-8), available in the INSTAT database (reference period 2006-2012), it was estimated that approximately 8 kilotons of apricot kernel per year, 61 kilotons of peach kernel per year and 85 kilotons of nectarine per year are generated in the Campania, as shown in Table I.9.

Table I.6 *Harvested apricots in Campania. Data into kton (source: ISTAT data, reference period 2007-2013)*

	2007	2008	2009	2010	2011	2012	2013	Average
Caserta	105	105	104	107	132	137	139	118
Benevento	3	9	9	10	10	11	5	8
Napoli	493	350	391	498	536	464	332	438
Avellino	8	8	8	9	9	10	6	8
Salerno	67	80	74	81	122	103	77	86
Campania	676	552	586	705	809	725	559	659

Table I.7 *Harvested peaches in Campania. Data into kton (source: ISTAT data, reference period 2007-2013)*

Province	2007	2008	2009	2010	2011	2012	2013	Average
Caserta	2339	2045	2317	2229	2314	2362	2391	2285
Benevento	17	20	21	22	23	25	25	22
Napoli	408	527	508	515	519	453	445	482
Avellino	5	6	7	6	6	5	2	5
Salerno	335	310	302	289	280	253	137	272
Campania	3104	2908	3155	3061	3142	3098	3000	3067

Table I.8 *Harvested nectarines in Campania. Data into kton (source: ISTAT data, reference period 2007-2013)*

	2007	2008	2009	2010	2011	2012	2013	Average
Caserta	490	481	507	452	503	524	570	504
Benevento	4	5	6	7	8	9	9	7
Napoli	100	126	125	120	124	95	91	112
Avellino	-	-	-	-	-	-	-	-
Salerno	190	190	181	182	165	155	72	162
Campania	784	802	819	761	800	783	742	784

Table I.9 *Estimated annual production of residues from the processing of fresh fruit in Campania. Data into kton per year, as received (average 2007-2013)*

	Apricot Kernel	Peach Kernel	Nectarine Kernel	Total Amount	Total* Amount (dry basis)
Caserta	1.4	45.7	10.1	57.2	51.5
Benevento	0.1	0.4	0.1	0.7	0.6
Napoli	5.3	9.6	2.2	17.1	15.4
Avellino	0.1	0.1	-	0.2	0.2
Salerno	1.0	5.4	3.2	9.7	8.7
Campania	7.9	61.3	15.7	84.9	76.4
* calculated on a 90% dry-matter basis (ENAMA, 2011).					

I.2.1.4.2 Nuts processing residues

The main by-product resulting from the industrial processing of nuts are the shells. Due to their low moisture content (approximately 10 %wt.) and lignocellulosic nature, these residues represent a biomass source particularly suitable for use in direct combustion. Accordingly, most of them are currently used for the on-site generation of thermal energy (heat process) as well as for the production of electricity in some plants.

Table I.10 *Estimated annual production of residues from the processing of nuts in Campania region, into kton per year.*

Dried fruit shells	(as received)	(dry basis)
Hazelnuts	64	57
Almonds	75	68
Walnuts	16	14
Total Amount (Italy)	155	139
Total Amount (Campania)	16	14

In the absence of data on the productive capacity of the industries operating in the Campania region as well as the amount of dried fruit actually processed or harvested, in this Ph.D. Thesis, the assessment of the residues generated from the local processing facilities relies on data and information available in a survey carried out by ENAMA (2011). In more details, this survey shows that the amounts of nuts annually intended, in Italy, for processing include approximately: i. 110.000 tons of hazelnuts with a yearly production of residues of 54.000 t; ii. 100.000 tons of almonds with a waste production of 75.000 t per year and iii. 31.500 tons of walnuts with an annual waste generation of 16.000 t (see Table I.10). Approximately 10.18 %wt. of the total amount of the shell residues generated in Italy comes

from the Campania region (ENAMA, 2011). Accordingly, it was estimated that approximately 16 kilotons of nut shells per year, corresponding to 14 kton per year on dry basis, are generated in the Campania, as shown in Table I.10.

I.2.1.4.3 Tomato processing residues

The tomato (Lycopersicon esculentum Mill.) is the second most-consumed vegetable worldwide, next to the potato (FAO, 2011). While the most of tomatoes are sold fresh, a little more than one third of the production is processed to make canned tomatoes, tomato juice, tomato paste or puree, sauces and ketchup (Heuzé et al., 2015). During tomato processing, two kinds of solid wastes (Figure I.4), which represent approximately 3 to 5 %wt. of the whole tomato, are typically generated: i. tomato skins (peels), which are the by-product of the peeling of tomatoes used for canning, and ii. tomato pomace, which is a mixture of tomato peels, crushed seeds and small amounts of pulp that remain after processing (Heuzé et al., 2015). Typically, wet pomace has the following composition: i. 33 %wt. seed; ii. 27 %wt. peel and iii. 40 %wt. pulp (Rossini et al., 2013). The dried pomace instead contains 44 %wt. seed and 56 %wt. pulp and peel (Sogi et al., 1998).

Since the production of these wastes is seasonal and linked to the harvest period, mainly concentrated in 2-3 months of the late warm-season, the daily production rate of these residues is very high and, consequently, its management causes many problems to the manufacturing companies (Mangut et al., 2006). Tomato processing residues are currently disposed of as a solid waste or used, to a limited extent, for animal feeding (Zuorro et al., 2014). The Italian legislation, for instance, allows for such residues to be recycled directly to the agriculture as long as they comply with the legislative requirements (Canali et al., 2014). However, although direct disposal on the soil is an inexpensive way of its utilization, with compensation of plants nutrients, it can also be a source of water pollution and odors, as well as it provides a breading place for a variety of pests, e.g., flies and mosquitoes. Moreover, methane and carbon dioxide emitted as a result of microbial activity under uncontrolled anaerobic conditions at the dumping site, are released into the atmosphere and contribute to the greenhouse effect (Mangut et al., 2006). Therefore, an intense work is underway to evaluate the energy resource these wastes represent (Celma et al., 2012; Rossini et al., 2013) as well as to develop new processing methods (Brachi et al., 2015b; Toscano et al., 2015; Sabio et al., 2015; Mangut et al., 2006) that would allow for more effective utilization of these residues, which otherwise represent not only a considerable loss of potentially valuable biomass and nutrient, but also an added cost for manufacturing companies.

Due to lack of reliable and consistent data on the productive capacity of the tomato processing industries operating in the Campania region as well as the amount of tomatoes actually processed, in the present Ph.D. study, the estimation of the residues from the local processing facilities was carried out indirectly by employing eq.(I.1). In particular, in the present investigation, the highest value in the aforementioned range 3 to 5 %wt., was chosen as RPR-value for estimating tomato processing residues. This was done to orientate the estimation towards precautionary values, which take into account the fact that in the Campania region, in addition to the locally grown tomatoes, large quantities coming from other regions are also processed.

Table I.11 *Harvested tomatoes for industrial application in Campania. Data into kton per year (source: ISTAT data, reference period 2007-2012)*

	2007	2008	2009	2010	2011	2012	Average
Caserta	130	122	117	118	115	115	120
Benevento	29	25	21	22	22	15	22
Napoli	38	36	24	32	33	35	33
Avellino	23	29	23	25	24	18	24
Salerno	66	78	76	11	88	62	64
Campania	286	290	261	208	282	245	262

Therefore, on the basis of the data on the regional production of tomato intended for industrial processing (Table I.11), which are available on the ISTAT website (reference period 2007-2012), it was estimated that approximately 13100 tons of tomato residues per year are produced in the Campania region, as shown in Table I.12. Finally, by assuming for these residues a moisture content of approximately 70% (Assi and King, 2008), an annual availability of around 3900 tons of dry tomato residues was estimated.

Table I.12 *Estimated annual production of residues from the processing of tomatoes in Campania. Data in kton per year (average 2007-2012)*

Province	Tomato Pomace (as received)	Tomato Pomace (dry basis)
Caserta	6.0	1.8
Benevento	1.1	0.3
Napoli	1.7	0.5
Avellino	1.2	0.4
Salerno	3.2	1.0
Campania	13.1	3.9
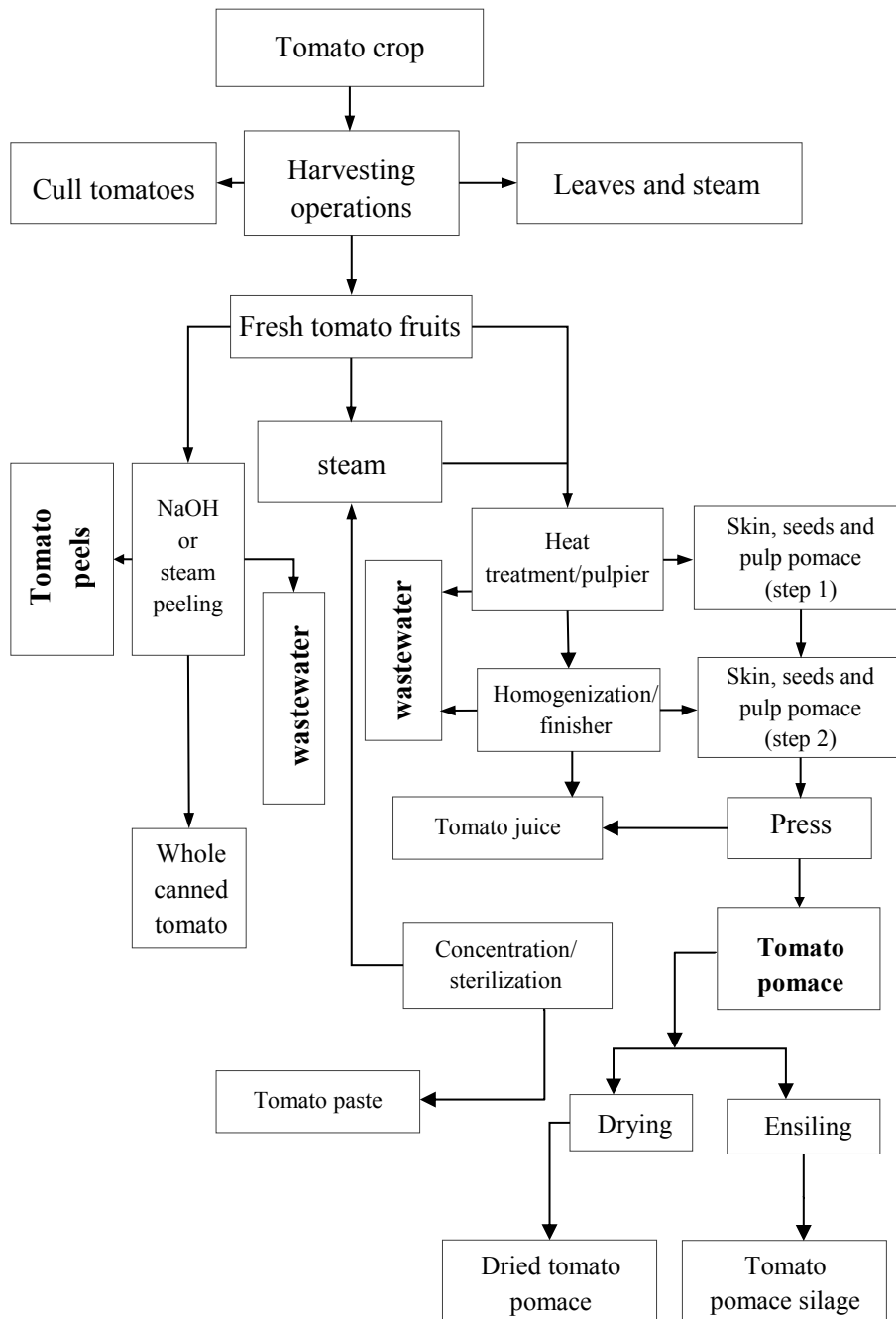
Figure I.4 *Simplified flow chart of industrial-scale tomato processing (adapted from Heuzé et al., 2015).*

I.2.2 Rationale for the feedstock selection

Based on the above-analysis concerning the availability and the current use of agro-industrial residues in Campania region, the need for more sustainable environmentally friendly disposal solutions arose, mostly with regard to tomato processing and olive mill residues. Accordingly, these residues, although not the most abundant ones in Campania, have been selected in the present Ph.D. study as potential feedstocks for the preparation of high-quality solid biofuels by means of torrefaction pre-treatment.

I.3 Classification of biomass according to its composition

Although there are many types of biomass, and their compositions are quite different, most of them have some primary components in common such as carbohydrate polymers (i.e., cellulose, hemicellulose and starches), aromatic polymer (lignin), simple sugars, fats and proteins, along with small amounts of minerals as sodium, phosphorous, potassium, calcium and iron and a fraction of water. Based on the chemical composition, biomass feedstocks are typically classified into four distinct categories (Meléndez et al., 2012), as follows :

i.   *Biomass feedstocks with a high sugar and starch content*. Normally these are agricultural crops such as beetroot, sugar cane, wheat, maize, etc. They also include residual by-products and discharges from industrial processes (e.g., the food and beverage industry), which contain high concentrations of residual sugars. Processing of these feedstocks normally involves biochemical treatments to produce first-generation bioethanol;

ii.   *Oleaginous biomass feedstocks*. This category includes agricultural crops that are rich in lipids (e.g., rapeseed, palm, soya, sunflowers, etc.) and industrially produced residual oils (waste vegetable oil), these latter being feedstocks for the production of first-generation biodiesel by transesterification.

iii. *Lignocellulosic biomass feedstocks*. These include all types of material that contains three main biochemical components, i.e., cellulose, hemicellulose and lignin. Included in this category are forest products such as white wood logs and chips as well as all forestry and agricultural residues from both harvesting and secondary processing operation; purpose-grown herbaceous and woody energy crops such as willows, poplars and switchgrass; and any green residues from urban communities and industries (grass clippings, tree limbs, woodchips, leaves and paper waste). Because of their low moisture content or easiness of water

removal, high energy content and great abundance, these feedstocks are preferred for thermochemical processing, although second-generation biorefinery could process them through biochemical routes.

iv. *Biodegradable waste feedstocks.* Typically, this category consists of animal wastes, industrial residues (i.e., wastewater treatment sludge) and municipal solid wastes containing large amount of organic material and high amount of moisture that render them unsuitable or uneconomical for thermal treatments. In an industrial process, normally anaerobic digestion is used to produce both "biogas" and a solid residue or by-product, which is used as fertilizer.

Olive mill residues and tomato processing residues investigated in this Ph.D. research work can both be classified as lignocellulosic biomass, so this type will be described in more detail in the following section.

I.3.1 Composition, structure and properties of lignocellulosic biomass

As mentioned above, lignocellulosic biomass is a class of biomass that consists of three major compounds, i.e., cellulose, hemicellulose and lignin (Figure I.5). It also includes moisture, organic extractives and inorganic minerals (which upon thermal decomposition transforms into ash).

Cellulose is a major structural component of plant cell walls (Figure I.5), which is responsible for mechanical strength. It is a high molecular weight linear homopolysaccharide composed of β-D-glucopyranose units linked together by (1→4)-glycosidic bonds. The long-chain cellulose polymers are linked together by hydrogen and van der Walls bonds, which cause the cellulose to be packed into microfibrils (Mussatto and Teixeira, 2010). Both crystalline and amorphous structures are contained in cellulose and can be expressed by $(C_6H_{10}O_5)_m$ where subscript m is the degree of polymerization (Chen et al., 2015).

Hemicellulose is a term used to refer to a wide variety of branched heteropolysaccharides consisting of five different sugar building units including xylose, glucose, mannose, galactose and arabinose together with other components such as acetic, glucuronic and ferulic acids (Mussatto and Teixeira, 2010). It is an amorphous polymer and this is attributed to the low degree of polymerization (DP < 200) and the branch structure. Its basic structures can be represented by $(C_5H_8O_4)_m$. Hemicellulose acts as a supporting material in the cell walls in the same way as cellulose.

Hemicellulose binds tightly with non-covalent attractions to the surface of each cellulose micro-fibril (Anwar et al., 2014), as shown in Figure I.5.
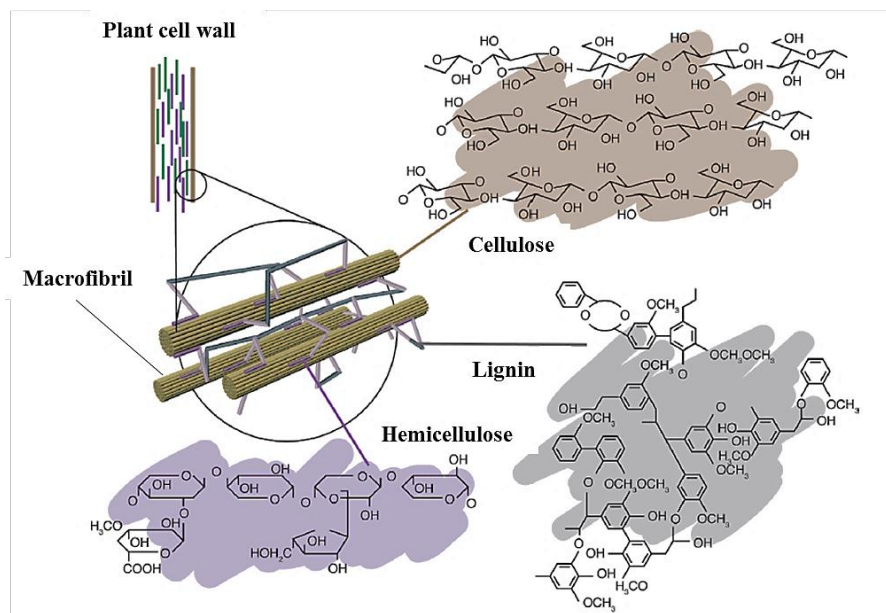
Figure I.5 *Plant Cell wall and lignocellulosic biomass composition (source: Tumuluru et al., 2011).*

Lignin is a three-dimensional, highly branched and polyphenolic substance that consists of an irregular array of variously bonded "hydroxy-" and "methoxy-" substituted phenylpropane units. Its chemical formula is represented by $[C_9H_{10}O_3 \cdot (OCH_3)_{0.9-1.7}]_m$ (Chen et al., 2015). Lignin is closely bound to cellulose and hemicellulose (Figure I.5) and its function is to provide rigidity and cohesion to the material cell wall, to confer water impermeability to xylem vessels, which are involved in the movement of water through a plant from its roots to its leaves, and to form a physic–chemical barrier against microbial attack (Mussatto and Teixeira, 2010).

Ash is the general term used to describe the inorganic matter in a fuel. In biomass fuels, the ash content may originate from the biomass itself, e.g. materials that the plant absorbed from the water or the soil during its growth, or from the supply chain, e.g. soil collected along with biomass. Ash content of different biomass fuels can vary significantly. Generally, the ash content of herbaceous biomass is higher than that of woody biomass. Specifically, while an ash content less than 1% wt. (on dry basis) is typically detected for wood, different herbaceous biomass types have reported values ranging from less than 2 %wt. up to 8-10 %wt. or even up to 25 %wt. for rice husks (BISYPLAN, 2012).

Extractives are a broad class of non-structural compounds found in all types of biomass. The composition of extractives varies with both biomass species (wood, herbaceous, agricultural residues) and its age before harvesting. They typically includes proteins, waxes, fats, inorganic salts, phytosterols, resin and non-volatile hydrocarbons, which play various physiological roles in the biomass feedstocks. They also provide plants with odor, color and durability and can be separated from biomass by successive treatment with polar and non-polar solvents and recovered by evaporation of the solution.

Moisture. Due to the water's role in transpiration, photosynthesis and fluid transport, raw biomass contains characteristically high amount of moisture. Moisture can be divided into free (also called external or imbibition) and inherent (also called bound or saturation) moisture. The former is defined as moisture above the fiber saturation point and generally resides outside the cell walls in cavities of conductive (Bates, 2012). The inherent moisture resides within the cell wall and is a function of relative humidity and air temperature (Basu, 2010).

Due to the different composition and structure, hemicellulose, cellulose and lignin typically show different thermal stability and reactivity. Hemicelluloses are usually less thermostable than cellulose and have a thermal decomposition temperature (TDT) in a range of 220 to 315° C. The crystalline structure of cellulose resists to thermal depolymerization better than unstructured hemicelluloses. It typically decomposes at temperatures between 315 and 400 °C. Lignin is featured by gradual thermal decomposition over a wide temperature range from 160 to 900 °C (Chen et al., 2015). Hemicelluloses generally evolve as light volatiles, producing less tars and char compared to cellulose. Lignin is difficult to dehydrate and thus converts to more char that cellulose or hemicelluloses. The thermal decomposition of hemicellulose and lignin is exothermic in nature and a higher content of such components in biomass led to the higher exothermicity in a biomass decomposition process (Di Blasi et al., 2014). In contrast, the thermal degradation of cellulose is endothermic. However, cellulose thermal degradation could be driven in the exothermic direction by the charring process (i.e., exothermic formation of secondary char), which competes with tar formation (Chen et al., 2015; Di Blasi et al., 2014). The main properties of cellulose, hemicellulose, and lignin are also summarized in Table I.13.

The amounts of carbohydrate polymers (i.e., cellulose and hemicellulose) and lignin (i.e., aromatic polymer) vary from one plant species to another. In addition, the weight fraction of each component in a single plant may also vary with age, stage of growth, and other conditions.

Table I.13 *Summary of the properties of cellulose, hemicellulose, and lignin in biomass (adapted from Chen et al., 2015)*

	Cellulose	Hemicellulose	Lignin
Structure	linear	branched	three-dimensional
Formula	$(C_6H_{10}O_5)_m$[a]	$(C_5H_8O_4)_m$	$[C_9H_{10}O_3 \cdot (OCH_3)_{0.9\text{-}1.7}]_m$
O/C ratio	0.83	0.80	0.47–0.36
H/C ratio	1.67	1.60	1.19–1.53
TDT[b] (°C)	315–400	220–315	160–900
Component	glucose	xylose, glucose, mannose, galactose, arabinose, etc.	phenylpropane
Thermal behavior	endothermic[c]	exothermic	exothermic

[a]m: degree of polymerization; [b]TDT: thermal decomposition temperature; [c]exothermic if char formation is significant.

Table I.14 shows the typical chemical compositions of some lignocellulose wastes, as reported by Anwar et al., (2014). Data demonstrate that, in most cases, cellulose is the dominant structural polysaccharide of plant cell walls, followed by hemicellulose and lignin.

Table I.14 *Chemical compositions of some lignocellulose wastes (adapted from Anwar et al., 2014)*

Lignocellulosic material	Cellulose (%)	Hemicellulose (%)	Lignin (%)
Sugar cane bagasse	42	25	20
Sweet sorghum	45	27	21
Hardwood	40-55	24-40	18-25
Softwood	45-50	25-35	25-35
Corn cobs	45	35	15
Corn stover	38	26	19
Rice straw	32.1	24	18
Nut shells	25-30	25-30	30-40
Newspaper	40-55	25-40	18-30
Grasses	25-40	25-50	10-30
Wheat straw	29-35	26-32	16-21
Banana waste	13.2	14.8	14
Bagasse	54.87	16.52	23.33
Sponge gourd fibers	66.59	17.44	15.46

I.4 Biomass conversion technologies

The conversion of biomass into useful forms of bio-energy and/or bio-fuels encompasses a wide range of different biochemical, mechanical and thermo-chemical processes, as illustrated schematically in Figure I.6. Factors that influence the choice of conversion route are: i. the type and quantity of biomass feedstock; ii. the desired form of the biofuel/bioenergy, i.e. end-use requirements; iii. environmental standards; iv. economic conditions; and v. project specific factors (McKendry, 2002). Generally, thermo-chemical processes (e.g., direct combustion, gasification and pyrolysis) have higher efficiencies than bio-chemical/biological processes in terms of the lower reaction time required (a few seconds or minutes for thermo-chemical processes vs. several days, weeks or even longer for bio-chemical/biological processes) and the superior ability to process/valorize most of the biomass organic compounds (Zhang et al., 2010). In this respect, it should be noted that lignin, a major component of lignocellulosic biomass, is typically considered to be non-fermentable and thus cannot be completely decomposed via biological approaches, whereas it is decomposable *via* the thermo-chemical pathways (Zhang et al., 2010; Williams et al. 2003).

I.4.1 Bio-chemical conversion

Bio-chemical conversion routes include two main processes, i.e., fermentation and anaerobic digestion (AD), together with a less-used process based on mechanical extraction/chemical conversion (Figure I.6).

I.4.1.1 Fermentation

Fermentation of both sugar (e.g. sugar cane, sugar beet) and starch (e.g. maize, wheat) crops to produce ethanol is a fully commercial process in various countries (Basu, 2013). On the other hand, there are currently no commercial processes for lignocellulosic biomass feedstocks (see "*Section I.3*"). In fermentation of sugar- and starch-based biomass, the feedstock is typically ground down and the starch converted by enzymes to sugars, with yeast then converting the sugars to ethanol. The solid residue from the fermentation process can be used as cattle-feed and in the case of sugar cane, the bagasse can be used as a fuel for boilers or for subsequent gasification (McKendry, 2002). The conversion of lignocellulosic biomass is instead more complex and expensive. Due to the presence of longer-chain polysaccharide molecule which are hard to break down into fermentable sugars, lignocellulosic feedstock requires hydrolysis pretreatments (e.g., acid, enzymatic or hydrothermal) before the resulting sugars can be fermented to ethanol. Such hydrolysis techniques are currently at a pre-pilot development stage (McKendry, 2002).
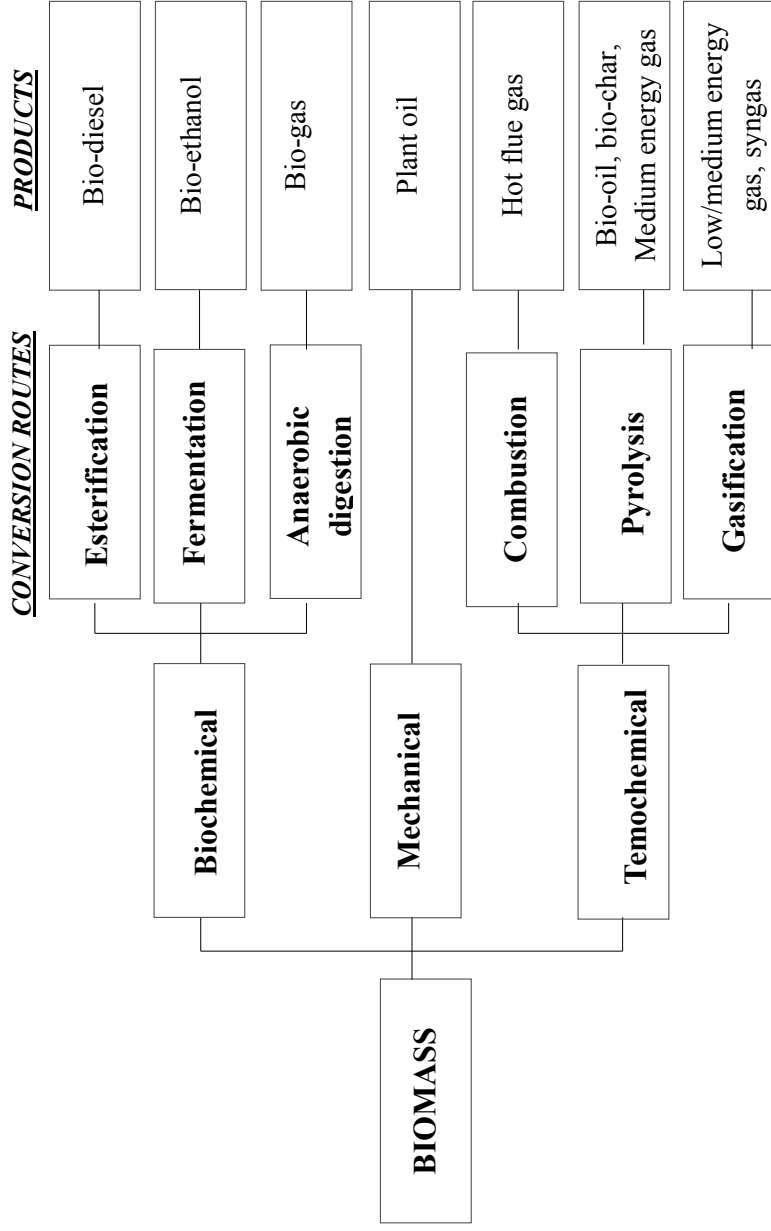
Figure I.6 *Summary of biomass conversion routes (adapted from Chew and Doshi, 2011).*

I.4.1.2 Anaerobic digestion

Anaerobic digestion (AD) is a commercially proven technology and is widely used for treating high moisture content (i.e. 80–90 %wt.) organic wastes. During the process, that occur in the absence of free molecular oxygen, the biomass feedstocks is converted by bacteria into a gas, designated as biogas, which is basically a mixture of methane (CH_4) and carbon dioxide (CO_2) along with water vapor and traces of ammonia and hydrogen sulfide (see "*Sections I.1.2.3.5 - I.1.2.3.57*"). Biogas can be used directly in gas engines and gas turbines but it can be also upgraded to higher quality (i.e. natural gas quality), by the removal of CO_2. (McKendry, 2002).

I.4.1.3 Mechanical extraction

Extraction is a mechanical conversion process used to produce oils intended for energy recovery, from the seeds of various biomass crops, such as oilseed rape, cotton and groundnuts. The process also produces a residual solid or 'cake', which is suitable for animal fodder (McKendry, 2002). Due to the high viscosity (up to 20 times greater than diesel) vegetal oils are not suitable for direct use in engines. Therefore, they are generally either subject to the trans-esterification process for the production of biodiesel or blended with diesel to reduce its viscosity.

I.4.2 Thermochemical conversion

Thermo-chemical conversion processes mainly include direct combustion, pyrolysis and gasification. As shown in Figure I.6, the chemical energy in biomass can be released directly as heat *via* combustion/co-firing, or it can be also transformed into solid (e.g., charcoal), liquid (e.g., bio-oils), or gaseous (e.g., synthetic gas and short for syngas) fuels with various utilization purposes, *via* pyrolysis or gasification.

I.4.2.1 Combustion

Direct combustion is the best established and most commonly used technology for converting biomass into heat. During combustion, biomass fuel is burnt in excess air to produce heat. The first stage of combustion involves the evolution of combustible volatiles from the biomass, which burn as flames. The residual material, in the form of charcoal, is burnt in a forced air supply to give more heat. The combustion of volatiles gases contributes to more than 70% of the overall heat generation (Zhang et al., 2010). Combustion of biomass typically produces hot gases at temperatures around 800 – 1000 °C. The hot flue gases are sometimes used directly for product drying, but more usually they are passed through a heat exchanger to produce hot air, hot water or steam as well as electricity with a steam

turbine. It is possible to burn any type of biomass but in practice combustion is feasible only for biomass with a moisture content < 50 %wt., unless the biomass is pre-dried (McKendry, 2002). Biomass is used either as a stand-alone fuel or as a supplemented to fossil fuels in a boiler. This latter option is becoming increasingly common as the faster and least-expensive means for decreasing the emission of carbon dioxide from existing fossil fuel plant (Basu, 2013). Some options for co-utilization of biomass with coal are, for example: i. co-combustion or direct firing where the biomass is directly fed to the boiler furnace and ii. indirect co-firing which is a process whereby biomass is gasified and the product gas is fed to the boiler furnace. Co-combustion of biomass in coal-fired power plants is an especially attractive option because of the high conversion efficiency of these plants. However, the combustion of biomass on a large scale is still considered to be a complex process with technical challenges associated with the biomass fuel characteristics (i.e., risk of alkali deposition and plant corrosion), types of combustors and the challenges of co-firing processes (Zhang et al., 2010).

I.4.2.2 Pyrolysis

Pyrolysis of biomass is a promising route for the production of solid (charcoal), liquid (bio-oil or bio-crude) and gaseous products as possible alternate sources of energy (Balat et al., 2009) by heating the biomass in the absence of oxygen at a temperature ranging between 300-600 °C. Depending on the reaction temperatures and residence time, pyrolysis processes can be classified as fast, intermediate and slow. Table I.15 lists the reaction conditions and the product yields of the different pyrolysis processes, in comparison with gasification (Zhang et al., 2010).

Table I.15 *Typical product yields (dry basis) of pyrolysis compared with those of gasification (adapted from Zhang et al., 2010).*

Mode	Conditions	Liquid	Char	Gas
Fast	Moderate temperature (~ 500 °C), short hot vapor residence time ~ 1 second	75 %	12 %	13 %
Intermediate	Moderate temperature (~ 500 °C), moderate hot vapor residence time ~ 20 seconds	50 %	20 %	30 %
Slow (carbonization)	Low temperature (~ 400 °C), very long solid residence time	30 %	35 %	35 %
Gasification	High temperature (~ 800 °C), long solid and vapor residence time	5 %	10 %	85%

Among them, fast pyrolysis has aroused great attention and interests in recent years. The liquid bio-oil produced by fast pyrolysis has the considerable advantage of being a storable and transportable energy source, and it is a potential source of valuable chemicals, these latter being characterized by a much higher added value with respect liquid fuels (Balat et al., 2009). Problems associated with the conversion process and the subsequent use of the oil (i.e., poor thermal stability and corrosively), still need to be overcome. Upgrading bio-oils by lowering the oxygen content and removing alkalis by means of hydrogenation and catalytic cracking may be required for certain applications (McKendry, 2002). Possible treatments and upgrading options for bio-oil are simply shown in Figure I.7.
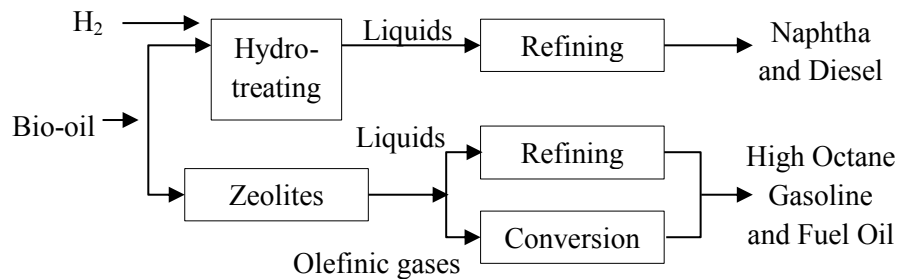
Figure I.7 *Treatment and upgrading options for bio-oil (adapted from* McKendry, 2002*).*

I.4.2.3 Gasification

Gasification is a partial oxidation process in which carbonaceous substances (e.g., biomass, coal and plastics) are converted into gas in presence of a gasifying agent (i.e., air, steam, oxygen, CO_2 or a mixture of these). It typically takes place at temperatures between 500 and 1400 °C and at a range of pressure that runs from atmospheric pressure to 33 bar (Morrin et al., 2012). The producer gas generated from gasification processes can be used in various applications including: i. the combined heat and power (CHP) generation in gas engines, turbines, fuel cells (FCs); ii. the production of gaseous fuels (e.g., hydrogen, substitute natural gas (SNG)); iii. the synthesis of liquid fuels (or biofuel if biosyngas is concerned) *via* Fisher-Tropsch process and iv. the production of chemicals such as methanol, dimethyl ether, ammonia and oxo-alcohols (Brachi et al., 2014). A detailed overview of main processes for the production of both chemicals and fuels starting from syngas may be found in literature (Wender, 1996). Typically, the gas composition specifications are different for the specific applications. The composition of the producer gas is very dependent on the type of gasification process, especially the gasification agent (steam and/or

air/oxygen) and the gasification temperature (Brachi et al., 2014). Based on the above critical gasification process variables, two main types of gas can be distinguished, i.e. "biosyngas" and "product gas", as illustrate in Figure I.8. *Product gas* is produced by low temperature gasification (below 1000 °C) and contains CO, H_2, CH_4, C_xH_y light aliphatic hydrocarbons, benzene, toluene and condensable hydrocarbons or tars (besides CO_2 and H_2O). The syngas components, H_2 and CO, typically contain only about 50 % of the energy in the gas. While the remainder is contained in CH_4 and higher (aromatic) hydrocarbons (Boerrigter and Drift, 2005). *Biosyngas* is produced by high temperature (above 1200 °C) or catalytic gasification. Under these conditions the feedstock is completely converted into H_2 and CO (besides CO_2 and H_2O). Biosyngas is chemically similar to syngas derived from fossil sources and can replace its fossil equivalent in all applications. Biosyngas can also be generated by the thermal cracking or catalytic reforming from of the product gas (Boerrigter and Rauch, 2006). Typically, both gases need additional gas cleaning and conditioning to meet the requirements for the final application (e.g. synthesis or energy production). An overview of the main gas specifications for synthesis and energy related applications are shown in Table I.16 and Table I.17, respectively.

Table I.16 *Overview of main gas composition specification for selected application (adapted from Boerrigter and Rauch, 2006)*

Synthesis	H_2 for refinery	Ammonia	Methanol	Fischer-Tropsch	Oxo alcohols
H_2	> 98 %vol.	75 %vol.	71 %vol.	60 %vol.	60 %vol.
CO	<10-50 ppmv	$CO+CO_2$ < 20 ppmv	19 %vol.	30 %vol.	40 %vol.
CO_2	<10-50 ppmv		4-8 %vol.		
N_2		25 %vol.			
Inert	N_2, Ar, CH_4 balance	Ar, CH_4 as low as possible	N_2, Ar, CH_4 as low as possible	CO_2, N_2, Ar, CH_4 low	
H_2/N_2		~ 3			
H_2/CO				0.6-2	1-1.5
$H_2/(2CO+3CO_2)$			1.3-1.4		
Process temperature (°C)		350-550	300-400	200 -350	85-200
Process Pressure (bar)	> 50	100-250	50-300	25-60	15-350
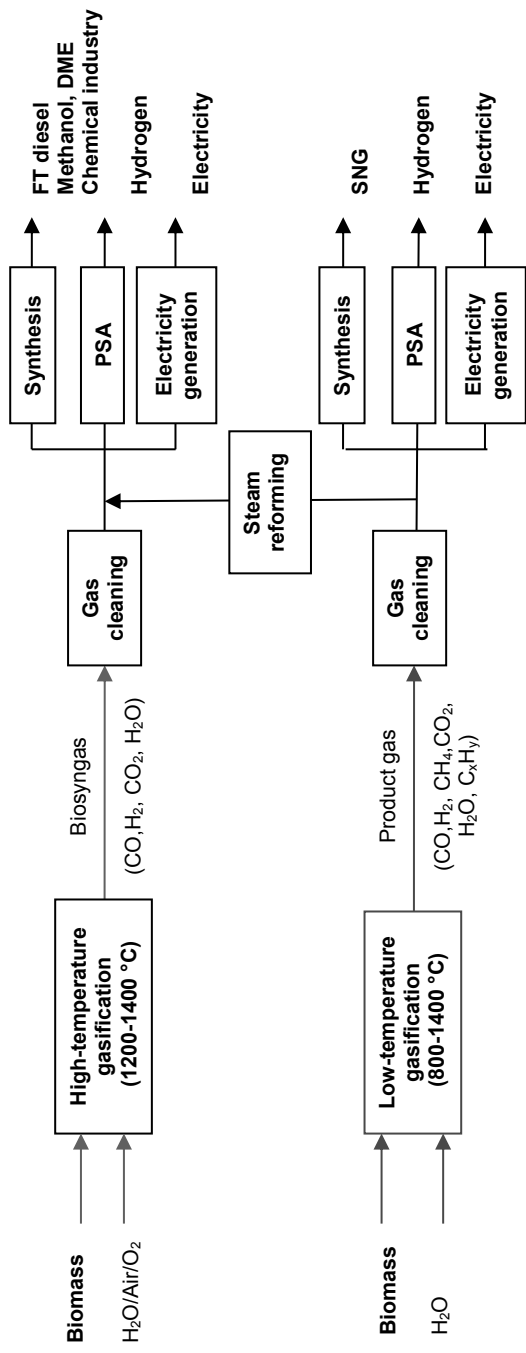
Figure I.8 *Difference between biosyngas and product gas and their typical applications (source: Brachi et al., 2014).*

A considerable amount of published research (Bridgwater, 1995; Franco et al.,2003; van der Stelt et al., 2011; Ruoppolo et al., 2013; Brachi et al., 2014) describe gasification as the most promising route for biomass conversion in order to displace the use of fossil fuels and to reduce CO_2 emission, most likely as a result of its feedstock flexibility and its potential to produce a wide range of fuels and chemicals in addition to energy. However, challenges still remain in the gasification process, particularly with respect to the tar reduction, ash behavior, gas cleaning, relative independence of process with regard to the nature of biomass, etc. (Franco et al., 2003), which are likely to preclude its long-term commercial viability. (Kumar et al., 2009).

Table I.17 *Overview of main product gas specifications for selected energy application (adapted from Arena and Mastellone, 2008)*

Parameter	Boiler	I.C. engines	Gas turbine
LHV, MJ/Nm^3	no restrictions	≥ 4	≥ 4
TAR, mg/Nm^3	no restrictions	≤ 100	≤ 10
Alkali metals (Na, K), ppmw	no restrictions	≤ 50	≤ 2.4
Heavy metals (Pb, Hg, V), ppmw	no restrictions	0.025-0.1	0.025-0.1
H$_2$S, ppmv	no restrictions	≤ 20	≤ 20

I.5 Biomass pretreatments: focus on torrefaction

I.5.1 Thermochemical conversion of lignocellulosic biomass: targets and challenge

Lignocellulosic biomasses have the potential to compete with fossil fuels as they share similar thermochemical conversion process. However, significant limitation to the deployment of biomass-based energy systems exists, which is closely related to the difficulty in working with biomass compared to conventional fossil fuels. Fossil fuels are standardized, high-energy products, which come in convenient forms that can be used by a variety of mature energy conversion systems. The benefits of fossil fuels have made them almost the exclusive source of energy for most industrial facilities in the world (Tallaksen, 2011). Conversely, biomass fuels, being of biological origin, are easily subjected to biodegradation (e.g., fungal attack) and are often bulky, have a high moisture content, a low energy density (higher load of biomass is required to generate the same amount of energy when compared to fossil fuels) and are usually of variable and even unpredictable quality (Chew and Doshi, 2011). The vulnerability of biomass to degradation along with the decentralized sites of most biomass sources

also reduces the competitiveness of biomass compared to fossil fuels (Chew and Doshi, 2011).

Therefore, one of the most challenging aspects for developing biomass energy projects is to overcome the operational and logistical limitations related to the use of biomass by successfully preprocessing it. Various pretreatments are often used to modify the size, the shape, the density or the moisture content of biomass in order to match the feedstock specifications for a particular energy conversion process. A major concern in preprocessing biomass relies on the cost associated with these treatment. On the other hand, fossil fuels are becoming day by day more expensive, as their supply becomes limited, and the associated environmental issues more and more serious (Tallaksen, 2011).

I.5.2 Pretreatment technologies for the thermochemical pathway

In view of the problems associated with the undesirable characteristics of raw biomasses, pre-treatment offers a promising solution to enhance process efficiency prior to the main energy conversion step (Chew and Doshi, 2011). The available biomass pretreatment processes are various. Table I.18 gives an overview of the current technologies available for both biochemical and thermochemical conversion pathways. They are organized in four main categories: physical, thermal, chemical and biological pretreatment technologies.

Table I.18 *Biomass pretreatment technologies (adapted from Berg, 2013)*

Thermal	Physical	Chemical	Biological
Steam Treatment	Drying	Acid Catalyst	Bacteria
Steam Explosion	Sizing/Milling	Alkaline Catalyst	Fungi
Liquid Hot Explosion	Densification	Oxidative Catalyst	
Torrefaction	Irradiation		

Physical pretreatment technologies include biomass drying, milling and irradiation. Thermal pretreatment technologies include steam pretreatment, steam explosion, liquid hot water pretreatment and torrefaction. Chemical pretreatment technologies include the use of acid, alkaline or oxidative catalysts. Biological pretreatment technologies include the use of certain types of bacteria or fungi. Thermal, chemical and biological pretreatments are usually applied to bio-chemical conversion (e.g., anaerobic digestion) process, the only exception is torrefaction, which is solely applied to thermochemical conversion process (Berg, 2013), including combustion (Bergman et al., 2005a), gasification (Prins et al., 2006; Bergman et al., 2005) and pyrolysis (Zheng et al., 2012; Ren et al., 2013).

In this section the main features of biomass pretreatment technologies are summarized schematically in Tables I.19-20, just as reported by Berg (2013). Specifically, for biochemical routes the lignin removal, hemicellulose removal and the production of eventual inhibitors are emphasized in the evaluation since a major challenge associated with the anaerobic digestion of lignocellulosic material is making the cellulose available for the anaerobic microorganisms (Berg, 2013). For thermochemical routes, the moisture content, energy density and thermal instability are taken into account (Berg, 2013). Environmental and economic feasibility is emphasized in both cases (Berg, 2013). However, since this Ph.D. research work focuses on evaluating the potential of torrefaction treatment for upgrading low-value agro-industrial residues into high-quality energy carriers, only this pre-treatment technology will be described in details. However, a brief description will also be presented for the other pretreatment technologies that are especially relevant for the thermochemical conversion pathway.

Table I.19 *Pretreatment technologies for thermochemical conversion pathway* (*adapted from Berg, 2013*)

Pretreatment	Moisture Content	Energy Density	Thermal Instability	Environmental Feasibility	Economic Feasibility
Natural drying	Good	No	No	High	Medium
Artificial drying	Good	No	No	High	High
Milling	No	Medium	No	High	Medium
Pelletizing	Medium	Good	Medium	High	Low
Torrefaction	Good	Good	Good	High	Low

I.5.2.1 Drying

Drying is a typical pretreatment technology for thermochemical conversion pathway of biomasses. Drying can be both natural and artificial. Artificial drying involves the use of a source of heat such as steam or process heat or fan equipment or even sun light. Natural drying occurs naturally by moisture diffusion to the surrounding. Artificial drying offers better control than natural drying, resulting in greater product uniformity and quality. The natural drying involves no energy-requiring equipment and is thus slightly more economically feasible than artificial dying method (Berg, 2013). However, there are some negative aspects associated with natural drying, such as biological decomposition due to microbial activity and the

attack of insect pests (Spinelli et al., 2007). These two factors cause substantial weight losses of biomass, due to the degradation of the dry substance. The weight fraction of biomass lost due to biological degradation may be high, and therefore not convenient, in particular, with wet biomass and in the early months of storage. Drying acts on the biomass moisture content, but does not affect energy density and the thermal properties of the fuel.

I.5.1.2 Size reduction

Sizing/Milling refers to the process of reducing the size of the biomass with the aim to improve the conversion efficiency. Milling is a pretreatment relevant for both thermochemical and thermochemical pathways. Biomass can be rarely fed into the conversion plant without being preliminary subjected to a grinding operation. Inconsistent biomass particle size may cause unreacted materials to pass through the conversion process and reduce efficiency (EverGreen Renewable, 2009).

Table I.20 *Pretreatment technologies evaluated for the biochemical conversion pathway (adapted from Berg, 2013)*

	Pretreatment	Lignin removal	Hemicel. removal	Inhibitors formation	Toxics emission	Economic Feasibility
Physical	Milling	Poor	Medium	Low	Low	Medium
Physical	Irradiation	Good	Poor	Medium	Low	Poor
Thermal	Steam Pretreatment	Poor	Good	Medium	Low	Good
Thermal	Steam Explosion	Medium	Good	High	Low	Medium
Thermal	Liquid Hot Water	Medium	Medium	Low	Low	Good
Chemical	Acid Catalysts	Medium	Medium	High	Medium	Medium
Chemical	Alkaline Catalysts	Good	Medium	Medium	Medium	Medium
Chemical	Oxidative Catalysts	Good	Good	High	Low	Good
Bio	Biological	Good	Good	Medium	Low	Medium

I.5.1.3 Densification

Generally, densification improves the initial bulk density of biomass from 40-200 kg/m^3 to a final density of 300-800 kg/m^3. Densification techniques can be categorized into two main categories: i. pressure agglomeration and ii. tumble agglomeration (Lim et al., 2012). Pressure agglomeration involves the mechanical compression of biomass materials *via* extruding, pelleting or briquetting, whereas in tumble agglomeration binding agent are required (Kaliyan and Morey, 2009). To produce good quality product, generalized optimum densification conditions can serve as reference, coupled with good design of machine (Chiu and Lu, 2009). Densified biomass can minimize the cost of handling, storage and transportation. Researches also indicate that a homogenously densified biomass fuel, such as biomass pellet, is a key component in realizing full automatic operation and complete conversion in furnaces (Oberberg and Thek, 2004).

I.5.1.4 Torrefaction

I.5.1.4.1 Torrefaction mechanism overview

Torrefaction is a relatively new thermal pretreatment of biomass that, over the past 10 years, has been recognized as a technically feasible method for converting any lignocellulosic material into a high-energy-density, hydrophobic, compactable, easily-grindable and biochemically stable coal-like solid, which is suitable for commercial and residential combustion and gasification applications (Tumuluru et al., 2010). Torrefied biomass can be produced from a great variety of biomass while yielding similar product properties; this would allow the biomass to become a commodity fuel, through standardization. As such this process has stood out as one of the most promising technological option to increase the efficiency and reduce the cost of overall biomass-to-energy chains, thus attracting significant interest and financial resources for further technological development and commercialization. Although torrefaction is not yet commercially available, the sheer volume of scientific studies, engineering initiatives, and considerable companies and investors currently involved leaves little doubt that this technology will find its way into the biomass-to-energy value chain by the end of this decade (Deutmeyer et al., 2012).

Basically, torrefaction is a thermo-chemical treatment method where biomass is heated in an inert environment to a temperature ranging between 200 °C and 300 °C. Low particle heating rates (typically less than 50 °C/min) and relatively long residence times, typically ranging between 30 and 120 min (Nordin et al., 2013; Bergman and Kiel, 2005), have been initially suggested and studied for torrefaction in order to ensure a high yield of the solid product (Deng et al., 2009). However, recent studies have shown that higher particle heating rates (Li et al., 2012; Atienza-Martìnez et al.,

2013) and quite short reaction times, in the range 8-20 min (Prins et al., 2006; Ren et al., 2012; Medic et al., 2012; Brachi et al., 2015b), may also allow maximizing the benefits of torrefaction while maintaining suitable mass and energy yields. For instance, Repellin et al. (2010) recommend solid residence times lower than 20 min since the anhydrous weight loss occurs primarily during the first 20 min. Besides, these authors also point out that short residence time are more suitable for industrial applications.
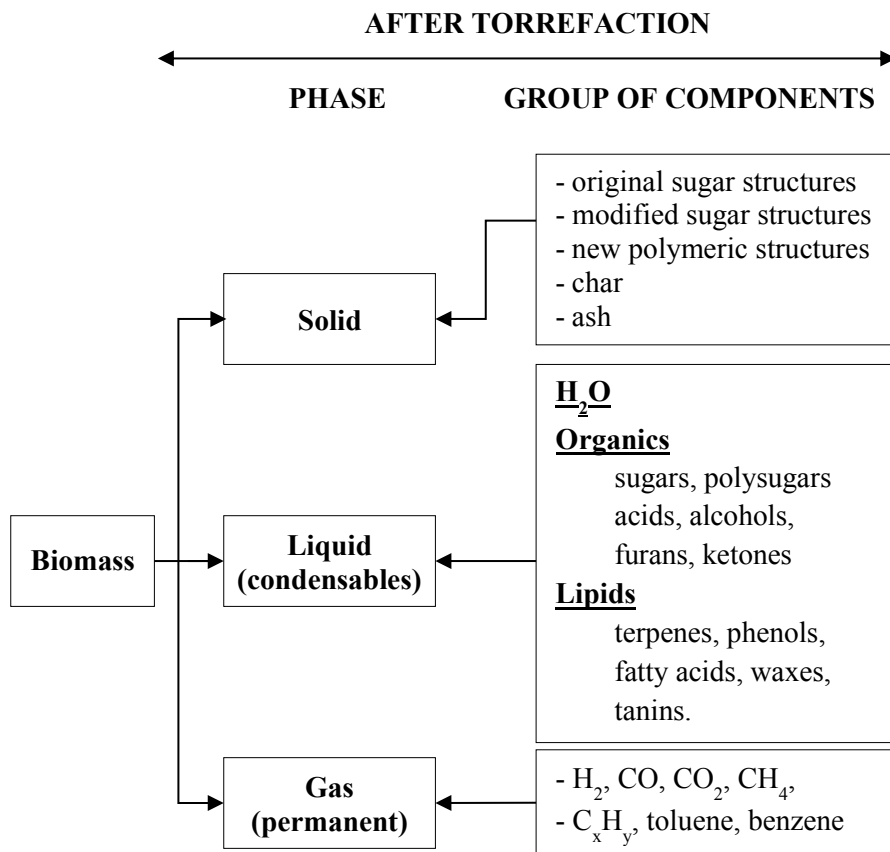
Figure I.9 *Products formed during torrefaction of woody biomass (adapted from Bergman et al., 2005a).*

Under these conditions, the properties of biomass (i.e., grindability, hydrophobicity, resistance against microbial degradation, energy density, etc.) are improved through the removal of a portion of its volatile matter in the form of both light gas (manly CO, CO_2, CH_4 and traces of H_2) and other condensable compounds (including water, organics and lipids). The final product is the remaining solid, which is often referred to as torrefied biomass or char. Figure I.9 gives an overview of the main torrefaction products,

classified based on their state at room temperature. This classification was developed by Bergman et al. (2005a) based on results from woody biomass torrefaction tests.

The removal of volatiles through different decomposition reactions is the basic principle behind the torrefaction process. But, essentially, a high torrefaction degree (as represented by the weight loss) was found not necessary to produce high-quality solid products since, as a rule, physicochemical properties of the biomass improve tremendously in the first 5-30 % anhydrous weight loss (Shag et al., 2013). Hence, most of the volatiles remain in the biomass when torrefaction is applied efficiently. Conversely, during the process of charcoal production (i.e., carbonization) from biomass, most of the volatiles are lost, which also means an unnecessary loss of energy. From a technical perspective, this also means that every form of carbonization must be avoided during torrefaction, because it leads to suboptimal efficiency (Kleinschmidt, 2011).

Torrefaction Gases

| 0.3M | 0.1E |

Biomass

| 1M | 1E |

Torrefaction 250 -300 °C

Torrefied Biomass

| 0.7M | 0.9E |
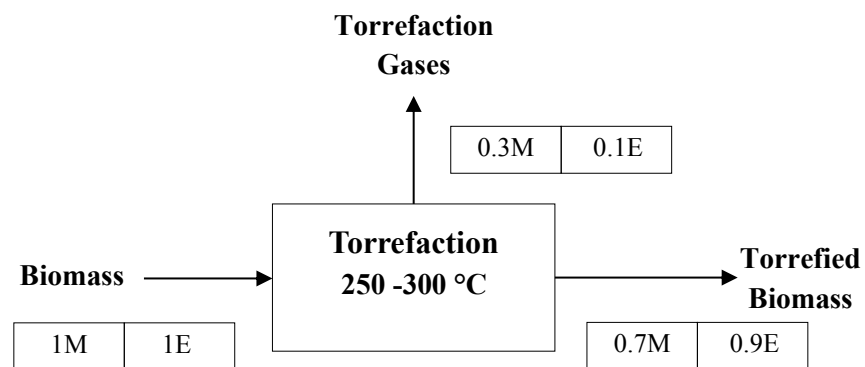
Figure I.10 *Typical mass and energy balance for woody biomass torrefaction. Symbol: E=energy unit, M = mass unit (adapted from Bergman et al., 2005a).*

Figure I.10 provides a typical mass and energy balance for woody biomass torrefaction. In general, approximately 70 %wt. of the mass is retained as a solid product, containing 90 % of the initial biomass energy content. The other 30 %wt. is converted into condensable and non-condensable products (Tumuluru et al., 2011), which contain only 10 % of the raw biomass energy content. Therefore, a considerable energy densification, typically up to a factor of 1.3, can be achieved through torrefaction treatment. This is in contrast with the classical pyrolysis process, which is characterized by an energy yield of 55-65% in advanced configuration concepts down to 20 % in the traditional ones (Pentananunt et al., 1990). This example points out one of the fundamental advantages of the process, which is the high transition of the chemical energy from the raw feedstock to the torrefied product, whilst fuel properties are improved

(Bergman et al., 2005a). Basically, the energy gain versus mass loss during torrefaction is ascribed to the fact that the latter predominantly arises from the release of volatiles more rich in oxygen than carbon (e.g. H_2O, CO_2, CH_3OH, CH_3COOH), as shown in Figure I.9.

It is worth noting that, the mass and energy yields of the torrefied biomass is strongly dependent on both the biomass type and the torrefaction reaction time and temperature. Specifically, at the same operating conditions, mass and energy yields will vary for different biomass as the polymeric composition and reactivity may differ (see "*Section I.3.1*"). Mass and energy yields may also differ as a result of differences in the extractive or lipids between different biomass. Lipids and extractives are believed to be not involved in torrefaction decomposition reactions, but rather driven off the biomass by evaporation (Bergman and Kiel, 2005). Typically, non-woody biomass has a wider spread in mass yield (from 24 to 95 % of its original weight) and energy yield (from 29 to 98 %) compared to woody biomass due to its higher hemicellulose and extractive content (Chew and Doshi, 2011). Therefore, this suggests that not all types of non-woody biomass are a suitable feedstock for torrefaction (Chen et al., 2015), with respect to the process energy efficiency. Anyhow, due to the very dissimilar characteristics of biomass feedstocks the potential benefits arising from torrefaction pretreatment are hard to be generalized and must be evaluated
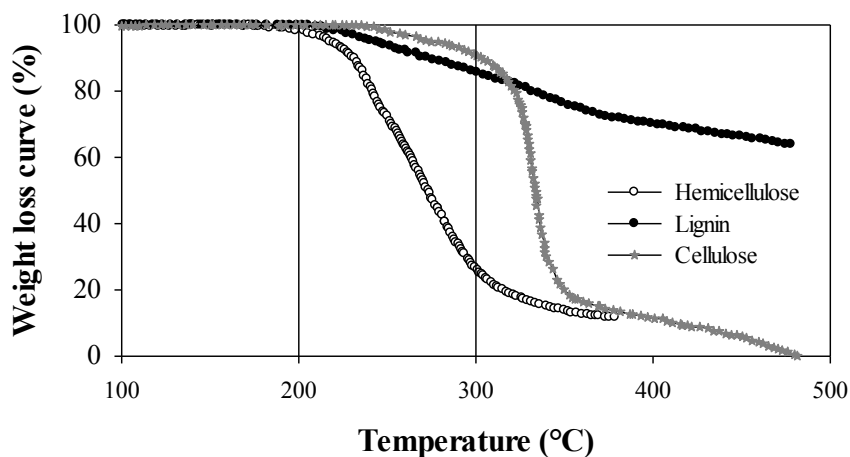
Figure I.11 *Thermogravimetric pattern of cotton wood polymeric constituents (i.e., lignin, hemicellulose and cellulose) in inert atmosphere (adapted from Basu, 2013).*

Among the basic polymeric constituents of biomass, hemicellulose is the most reactive, followed by lignin, whereas cellulose is the most thermostable

(see "*Section I.3.1*"). In addition, the reactivity of hemicellulose deeply depends on its composition and molecular structure, which may vary greatly/significantly among different biomass types. Typically, the xylan-based hemicellulose is the most reactive within the torrefaction temperature, which degrades faster than any other solid component of the biomass. Accordingly during torrefaction, mass loss predominantly comes from the decomposition of particularly hemicellulose and some of lignin, as shown in Figure I.11. Lignin decomposition proceeds slower, but shows a gradual increase of decomposition rate starting from a temperature of about 200 °C or even lower. It is worth noting that the thermal decomposition behavior of the individual polymers of wood (and in general biomass) may be different due to their strongly interacted structure in wood itself. For example, although only a small portion of the cellulose degrades within the torrefaction temperature range (200-300 °C), the water vapor and the acids released from hemicellulose may also enhance the degradation of cellulose (Nhuchhen et al., 2014).

I.5.1.4.2 Origin and current state of torrefaction technology

Torrefaction has a long history as a thermal treatment process. The early technical development of torrefaction started for the coffee production process in the late 1800s. With respect to bioenergy, torrefaction was first studied in the 1930s in France, where a research was done on its application to produce a gasifier fuel (Bioenergy, 2000). During most part of the early and middle part of the 20th century, only sporadic work on torrefaction for energy conversion were performed (Nordin et al., 2013). The interest in torrefaction process has increased significantly only in the last decade. A quick survey at http://www.sciencedirect.com shows that the annual number of the scientific papers published on torrefaction has increased from 1in 2004 to 5 in 2005, 11 in 2006, 5 in 2007, 24 in 2008, 15 in 2009, 32 in 2010, 52 in 2011, 88 in 2012, 167 in 2013, 175 in 2014, 237 in 2015.

Around the world, there are currently several universities, research institutes and companies that are studying the main torrefaction concepts at the pilot scale and/or in a demonstration plant. These include both *indirectly heated reactors*, such as rotary drum and screw type and *directly heated reactors* such as fixed bed reactor, multiple-hearth furnace, TORoidal BED reactor, fluidized bed and belt reactor, compact moving bed and fluidized moving bed concepts. The major advantages and disadvantages for both indirectly and directly heated reactors are summarized in Table I.21 and I.22, respectively. A detailed overview of the main torrefaction technologies may be found in literature (Cremer et al., 2012; Koppejan et al., 2012; Junsatien et al., 2013; Nhuchhen et al., 2014).

In general, these technologies have been designed and tested on processing woody biomass. Preliminary pilot plants testing with different biomass types have already highlighted that the feedstock flexibility of the current generation of torrefaction technology is still rather limited (Kleinschmidt, 2011).

Table I.21 *Advantages and limitations of different indirectly heated reactors (adapted from Nhuchhen et al., 2014)*

Reactor Type	Advantages	Limitations
Rotary drum	• Proven relatively simple equipment • Low pressure drop • Possibility of both direct and indirect heating • Wide range of size and types of biomass • Proven technology for biomass drying	• Lower heat transfer (especially in indirect heating) → long residence time • Difficult to measure and control temperature • Less plug flow compared with other reactors • Bigger system size • Necessary proper drum sealing • Difficult in scaling up the system • Increase of dust (friction)
Screw type	• Possibility for plug flow • Mature technology for torrefaction	• Indirect heating only • Higher possibility of hot spots • Lower heat transfer rate • Scale up problem • Requiring shaft sealing
Microwave reactor	• Shorter heating time • Accepts any size particle • Compact design	• Electricity to produce microwave isn't efficient • Non-uniform heating (mostly internal, very little external)

Moreover. only a few of them, including rotating drum reactors, are able to handle a large spectrum of particle sizes. In fact, some technologies are capable of processing feedstock of small particle size, such as sawdust, while other technologies are able to process large particles. This means that selection of technology needs to be done based on the characteristics of the feedstock, or alternatively, the feedstock needs to be pre-processed before torrefaction (Koppejan et al., 2012). Anyhow, regardless of the particular reactor technology, it appears that feedstocks with small particles size distribution are recommended to achieve an optimized torrefaction efficiency and product quality (Lam et al., 2013).

Apart from the reactor technology and the related performances, the viability of the torrefaction process also depends on the heat integration

design. Although heat can be integrated in various ways (Håkansson et al., 2010), all torrefaction developers apply the same basic design in which volatiles are combusted in an afterburner and the flue gas is used to directly or indirectly heat the pre-drying step and the torrefaction reactor (Kleinschmidt, 2011).

Table I.22 *Advantages and limitations of different directly heated reactors (adapted from Nhuchhen et al., 2014)*

Reactor	Advantages	Limitations
Moving bed	• Simpler reactor and its construction (low cost) • Very good heat transfer • High bed density	• Difficult temperature control • No mixing, hot spot • High pressure drop over the bed
Multiple heart furnace	• Proven equipment design • Higher possibility of scale up • Close to plug flow • Good temperature and residence time control • Possibility of adding fines	• Lower heat transfer rate compared with other direct reactors • Limited volumetric capacity • Relatively large reactors • Require shaft sealing
Fluidized bed	• Excellent heat transfer rate • Easily scalable	• Require smaller particle size • Necessary to have additional gas equipment to supply fluidizing fluids • Possibility of attrition (fines formation) • Difficult to get plug flow
Belt reactor	• Close to plug flow	• Difficult to measure and control temperature • Difficult in scaling up • Potential clogging of the porous belt from tars or small particles
TORoidal BED reactor	• Low pressure drop • Short residence time (around 80 s)→ small reactor size	• Risk of carbonization
Fixed Bed reactor	• Possibility of both direct and indirect heating • Simpler reactor and its construction (low cost)	• Cannot be operated continuously • Difficult to control temperature • No mixing, hot spot • High pressure drop over the bed

I.5.1.4.3 Feedstock flexibility

In a recent past, most of the research and development projects on torrefaction have been largely based on rather clean and dry biomass feedstocks such as waste wood (Chew and Doshi, 2011); this is due to both technical limitations of the currently available reactor technologies and economic considerations, which favor woody biomass. Furthermore, most utilities prefer clean woody biomass as co-firing fuel, because agro-food

industrial wastes are prone to negatively impact plant performance and are subject to stricter emission norms (Kleinschmidt, 2011). This preference might change in future in case torrefied wastes exhibit significant price benefits and prove to result in acceptable combustion plant performance.

Nowadays significant research is under way to explore the potential to produce high-grade solid biofuels from lignocellulosic agricultural (Protásio et al., 2012; Wang et al., 2012; Lu and Chen, 2014) and agro-industrial residues (Brachi et al., 2015b; Toscano et al., 2015; Cellatoğlu and İlkan, 2015). As regards such non-woody biomass feedstocks, the main challenges are related to their high water content, which impairs the energy efficiency of the whole conversion process, and to other unfavorable physical-chemical characteristics (e.g., alkaline metals and chlorine), which may affect the integrity (e.g., fouling and corrosion) of the conversion plant devices and the composition of the volatiles (torgas) liberated during torrefaction as well as their treatment. Non-lignocellulosic biomass wastes (Dhungana et al., 2012a), such as chicken litter, digested and undigested sludge, food wastes (Poudel et al., 2015) and municipal solid wastes (Yuan et al., 2015), have also received some attention.

Further fundamental and applied R&D efforts are still required to provide sufficient design data with respect to operating conditions (i.e., temperature, residence time and feed particle size) and their relation to relevant product properties (i.e., that are desirable for its end use), decisive process performance parameters (such as process energy efficiency) and the composition of the gases liberated during torrefaction in order to evaluate the viability of an efficient use of alternative non-woody biomass wastes as a feedstock for torrefaction (Brachi et al., 2015b).

I.5.1.4.4 Rationale for a fluidized bed lab system

Although commercial torrefaction is expected to employ continuous process operation, most of the research on torrefaction is currently carried out in a batch mode, mainly due to the issues related to bulk solids handling (e.g., gas-tight introduction and removal of solids to and from the reactor), especially at small scale.

So far, a lot of the research on torrefaction has been performed at the micro-scale (powdered biomass) by analytical instruments such as TGA (Park et al., 2013; Mafu et al., 2016), in which only few milligrams of biomass (e.g., 5-20 mg) are typically processed. These experiments usually provide good insight on the kinetics of torrefaction (Brachi et al., 2015a), but they do not give evidence of possible heterogeneities in the torrefied materials, which typically occur at a larger processing scale (Cavagnol et al., 2015; Di Blasi et al., 2014), as induced by exothermic reactions and/or diffusional heat and mass limitations. Laboratory ovens and furnaces, which

41

can process a larger amount of raw biomass than TGA, have also be profusely used in torrefaction research (Wu et al., 2012; Peng et al., 2013), although they could not reveal much information useful for design and scale up of an actual torrefaction plant. Bench-scale apparatuses are certainly the most important early-stage tools for assessing and scaling new biofuels technologies, but only a few studies have been performed so far on torrefaction on this investigation scale, generally as a fixed-bed reactor (Peng et al., 2013; Grigiante and Antolini, 2015; Tran et al., 2016). As regards torrefaction in fluidized beds, only two works have been previously published. Specifically, Li et al.(2012) were able to properly fluidize (without slugging and channeling) and torrefy a bed made only of sawdust particles in the size range of 0-350 μm, with the aid of an inclined orifice distribution plate. Atienza-Martinez et al. (2013) torrefied dry sewage sludge (SWS) in the size range 250-500 μm in a bed consisting of torrefied SWS particles from previous experiments in order to reduce problems associated with the start-up phase. However, it is worth noting that, although the above fluidized bed configurations enjoy the benefit of avoiding the separation of the torrefied product from heat carrier solids, the well-known difficulty in fluidizing biomass particles alone (Cui and Grace, 2007) may restrict the use of such technology to a quite narrow range of biomass feedstocks.

Anyway, the torrefaction of agro-industrial residues on a scale larger than TGA has received rather little attention (Di Blasi et al., 2014; Toscano et al., 2015). Regarding such feedstocks, the main challenges is related to their specific chemical composition rich of extractives, hemicellulose and lignin, which degrade exothermically (Di Blasi et al., 2014; Chen et al., 2015) and can lead to overheated zones in the torrefaction reactor, with an increased risk for carbonization or even to a complete thermal runaway (Di Blasi et al., 2014; Cavagnol et al., 2015). These uncontrolled phenomena could significantly decrease the mass and the energy yields of the torrefaction process and generate strongly heterogeneous solid products. Biomass feedstock has a very low thermal conductivity and heat capacity. These properties coupled with the thermal effect involved in the torrefaction process may create some temperature gradients, mostly in a torrefaction reactor where the heat transfer is low, which may affect the torrefaction performance. The same challenges were highlighted by Grigiante and Antolini (2015) who in their paper have recently argued on the significance of the results they obtained from torrefaction tests carried out in a bench scale fixed bed torrefaction unit (i.e., 200 mm in length and 56 mm in diameter) employing both direct and indirect heat transfer mode to the biomass.

In this context, in order to overcome the above-mentioned limitations and obtain reliable results from torrefaction tests carried out on agro-industrial residues at a scale larger than TGA, a new sand-assisted torrefaction process based on fluidized bed (FB) technology was employed in this Ph.D. research

work. Even though uncommon in torrefaction, fluidized bed technology, by guaranteeing that biomass particles undergo torrefaction in a well-mixed state under uniform temperature, could provide an even product quality that is generally difficult to attain in many other reactors (Dhungana et al., 2012b). Moreover, the large thermal inertia and the high heat transfer rate within a dense bed of sand make this technology particularly suitable to deal with the exothermicity associated with the thermal degradation of non-woody biomass (i.e., agricultural and agro-industrial residues), which tends to ignite or carbonize easily during torrefaction (Kleinschmidt, 2011).

I.6 Fluidization and multiphase flow phenomena in fluidized beds

I.6.1 Fluidization phenomenon

Fluidization is commonly defined as the unit operation by which a bed of solid particles acquires fluid-like properties (Fig. I.12) through suspension in a gas or liquid (Kunii and Levenspiel, 1991).
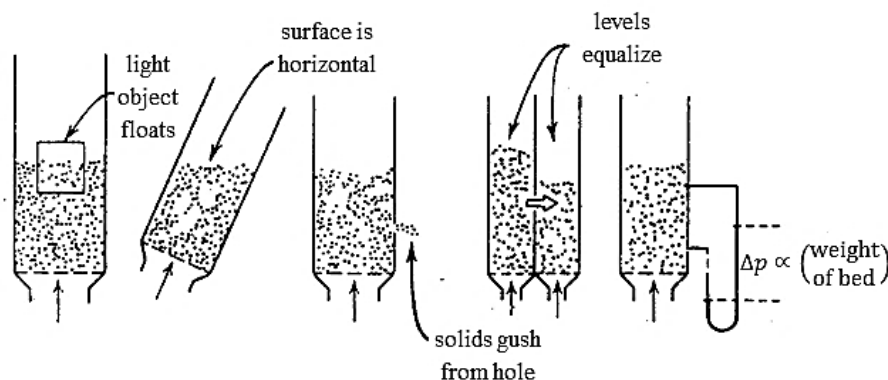
Figure I.12 *Liquid-like behavior of fluidized beds (source: Kunii and Levenspiel, 1991).*

Fluidization can be best pictured by considering a bed of solid particles supported on a fluid-distributing plate (i.e., a porous or perforated plate) in a vertical column. When there is no flow through the packed bed, the net gravitational force acts downward. When a fluid is blown upward and evenly through the bed of solid, friction forces act upward and counterbalance the net gravitational force. Specifically, at low flow rates, the aerodynamic drag on each particle is also low, and thus the fluid simply percolates through the particle interstitial space while the particles do not move. The bed behaves like a porous medium and the pressure drop, which occurs as a result of resistance to the fluid flow through the solid-particles, increases linearly with the volume flow rate of the fluid, while the bed height remains fixed

43

(Fig.I.13). This is called a fixed bed (Fig. I.14a). As the flow rate increases, a point is reached at which the frictional force acting on the particles equals the apparent weight of the bed (i.e., weight minus any upward buoyancy force), causing the particles to begin to separate from each other and float in the fluid and the bed to exhibit liquid-like behavior. At this critical value of the flow rate, the bed is considered just fluidized and is referred as an incipiently fluidized bed or a bed at a minimum fluidization (Fig. I.14.b). After this point is reached, the bed starts expanding in height while the pressure drop levels off and no longer increases as the fluid flow rate is increased (Fig.I.13). The superficial gas velocity at that point where fluidization starts is referred to as the minimum fluidization velocity, U_{mf}.
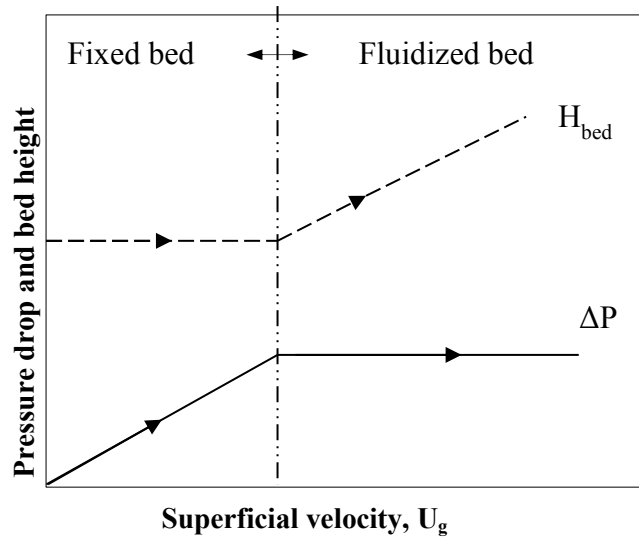
Figure I.13 *Transition from packed bed to fluidized bed.*

With reference to fluidization, it is worth noting that, in engineering practice, it has become customary, although physically not justified, to refer all velocities on the whole cross section (i.e., the gas flow rate per unit cross section of the bed) as if no solids were present (Oka, 2003).These velocities are lower than true gas velocities in the interspace between the particles.

Fluidized beds are coupled to many unit operations and used in a wide variety of industrial processes such as reaction, drying, mixing, granulation, coating, heating and cooling. As any other solid-fluid processing system, fluidized bed technology has advantages and disadvantages. Some of them are listed below (*Kunii and Levenspiel, 1991)*.

The advantages of fluidized beds are:

1. The smooth, liquid-like flow of particles allows continuous automatically controlled operation with easy handling;
2. The rapid mixing of solids leads to close isothermal conditions throughout the bed, hence the operation can be controlled simply and reliably;
3. In addition, the whole vessel of well-mixed solids represents a large flywheel that resists rapid temperature changes, responds slowly to abrupt changes in operating conditions and gives a large margin of safety in avoiding temperature runaways for highly exothermic reactions;
4. Heat and mass transfer rates between gas and particles are high when compared with other modes of contacting;
5. The rate of heat transfer between gas and an immersed object is high; hence heat exchangers within fluidized beds require relatively small surface areas.

The disadvantages of fluidized beds are:

1. Friable solids are pulverized and entrained by the gas and must be replaced;
2. Erosion of pipes and vessels from abrasion by particles can be serious;
3. For non-catalytic operations at high temperatures, the agglomeration and sintering of fine particles can require a lowering in temperature of operations, thereby reducing the processing rate considerably.
4. The rapid mixing of solids in the bed leads to non-uniform residence times of solids in the reactor. For continuous treatment of solids, this gives a non-uniform product and poorer performance, especially at high conversion level.

I.6.2 Fluidization regimes

Depending on the fluid flow rate as well as the fluid and the solid properties, different regimes of fluidization can occur, as shown in Figure I.14. In general, fluidization regimes can be classified into two broad categories: i. particulate (smooth) and ii. aggregative (bubbling) (Harrison et al., 1961). In particulate fluidization, the solid particles usually disperse relatively uniformly in the fluidizing medium with no readily identifiable bubbles (Yang, 2003). Thus, the particulate fluidization sometimes is also called homogeneous or smoothly fluidization (Figure I.14c). Most liquid fluidized beds under normal operation exhibit the particulate fluidization. In gas-solid systems, such a fluidized bed regime can be observed only under

special conditions of fine light particles with dense gas at high pressure (*Kunii and Levenspiel, 1991)*.
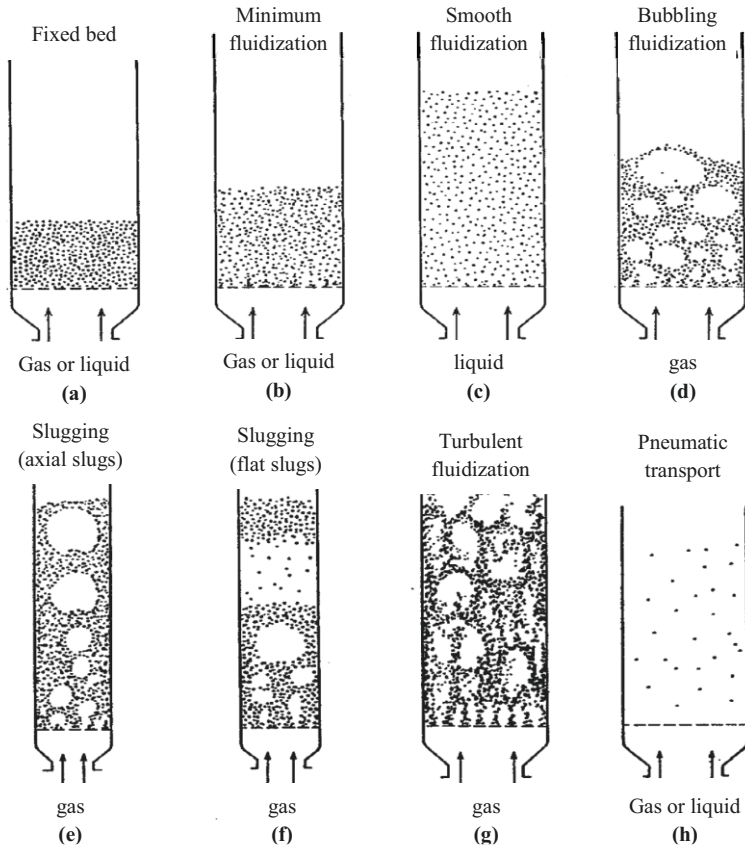
Figure I.14 *Schematic representation of fluidized beds in different regimes (source: Kunii and Levenspiel, 1991)*

In the heterogeneous or aggregative fluidization, voids containing no solids are usually observed. Those voids are called bubbles. Those voids can be well-defined, such as in a bubbling fluidized bed (Figure I.14d) and in a slugging bed (Figure I.14e-f), or they can appear as small voids where particle clusters dart to and from, such as in a turbulent bed or in a fast fluidized bed, as shown in Figure I.14g (Yang, 2003). Liquid-solid systems behave as bubbling beds only in a few rare cases, namely when very dense solids are fluidized by low density liquids (*Kunii and Levenspiel, 1991)*. In gas-solid systems, gas bubbles coalesce and grow as they rise through the bed, and in deep enough beds of small diameter they may eventually become large enough to spread across the vessel (Figure I.14e-f). This is called slugging regime.

Specifically, when the bubbles grow to approximately 2/3 of the bed diameter, the bed enters the slugging regime with periodic passing of large bubbles and regular large fluctuation of bed pressure drop corresponding to the bubble frequency (Yang, 2003). There are basically two types of slugging fluidized beds, namely: i. slugging beds consisting of axisymmetric round-nosed gas slugs where the particles flow past the gas slugs in an annular region close to the wall (Fig.I.14e), which usually occurs with bed materials that fluidize easily; ii. slugging beds having slugs that are essentially square-nosed (Fig.I.14f). The gas slugs occupy the complete bed cross section. The only way the solids can pass through the gas slug is by raining down through the slugs as solids streamers.

For cohesive and angularly shaped particles, this type of slugging bed is prevalent. Slugging regimes occur only in beds having a bed height to bed diameter ratio larger than about 2, as they provide enough time for bubbles to coalesce into bigger ones (Yang, 2003). The occurrence of slugging is usually accompanied by deterioration in quality of bed mixing and gas–solid contacting. Again, when particles are fluidized at a high enough gas flow rate, the terminal velocity (i.e., velocity of a falling particle for which gravitational, buoyancy and drag forces are in equilibrium) of the solids is exceeded, the upper surface of the bed disappears, entrainment becomes appreciable and, instead of bubbles, a turbulent motion of solid clusters is observed and voids of gas of different sizes and shapes appear. This is the turbulent fluidized bed, shown in Fig.I.14g.

With a further increase in gas velocity, solids are carried out of the bed with pneumatic transport of solids (Fig.I.14h). In both turbulent and lean-phase fluidization, a large amount of particles are entrained, precluding steady state operations (Kunii and Levenspiel, 1991).

Specifically, the present Ph.D. research was concerned with a fluidized bed where solids (i.e., biomass and/or sand particles) are suspended in a gas, therefore only this case will be considered in the following section.

I.6.3 Determination of the minimum fluidization velocity

The superficial gas velocity at which a bed of solid particles is just fluidized, is normally termed the minimum fluidization velocity, U_{mf}. The minimum velocity at which a bed of particles fluidizes is a crucial parameter needed for the design of any fluidization operation as it not only quantitatively indicates the amount of drag force needed to attain solid suspension in the fluid phase, but also constitutes a reference for the evaluation of the intensity of the fluidization regime at higher velocity levels (Zhang et al., 2009a). To find the value of the minimum fluidizing velocity, U_{mf}, different experimental (i.e., the pressure drop method, the voidage method and the heat transfer method) and theoretical approaches (i.e., the

dimensional analysis via direct correlation, the drag force method, the pressure drop method and the terminal velocity method) can be used, as described in more detail by Gupta and Sathiyamoorthy (1998). However, U_{mf} is preferably determined experimentally since many of the parameters used in theoretical calculations can only be estimated (Davidson and Harrison, 1963).

In particular, in the present investigation, the pressure drop method, which is the most popular method for determining U_{mf} experimentally, was employed and therefore only this approach will be described in more detail in the following section.

I.6.3.1 Pressure drop method

As has already been noted, when fluidization is established, the pressure drop remains constant if the superficial gas velocity continues to increase (Figure I.13). Therefore, the minimum fluidization velocity can be simply determined by using a diagram of the measured pressured drop as a function of superficial velocity of the fluidization medium. In particular, as a marked hysteresis effect exists when increasing and decreasing the gas flow rate in the bed, which is caused by the packing effect of the bed, in order to find U_{mf}, the pressure drop across the bed is typically measured as the gas flow rate is decreased from a high value (Tahmasebpoor et al., 2013), where the bed is fully fluidized, to no gas flow at all. This allows avoiding dependence of U_{mf} values on the initial bed loading pattern (Davidson and Harrison, 1963). Specifically, U_{mf} is identified with the superficial velocity at the intersection of the pressure drop line of the fixed bed mode with the constant pressure drop line corresponding to the state of fluidization, as shown in Figure I.15a.
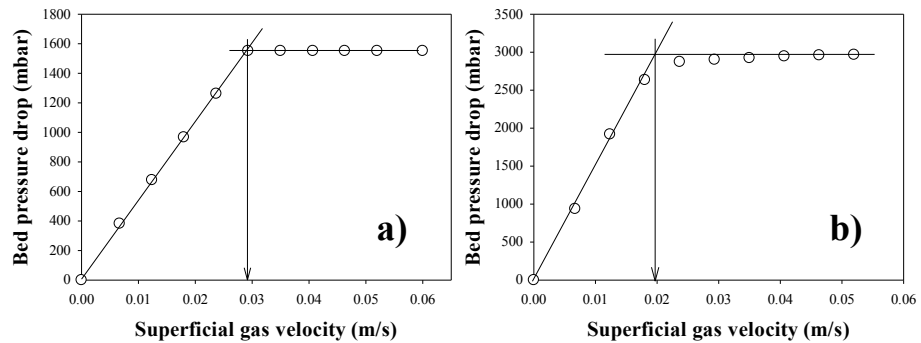
Figure I.15 *Frictional pressure drop as a function of gas superficial velocity for (a) monodisperse and (b) polydisperse particulate materials.*

However, it is worth noting that while for an ideal system of monodisperse particles the line presenting pressure drop across the fixed bed

breaks abruptly when the minimum fluidization velocity is achieved, as shown in Fig. I.15a, for a real system having a certain particle size distribution, the transition is more gradual as smaller particles usually begin to float at lower velocity than large particles. Therefore, the pressure drop curve is similar to that shown in Figure I.15b and the minimum fluidization velocity is generally determined at the crossing point of the extrapolated left and right branches of the pressure drop curves (Oka, 2003).

1.6.3.1.1 Minimum fluidization velocity of binary mixtures

The evaluation of the minimum fluidization velocity of binary mixtures has been a controversial subject in recent years (Zhang et al., 2009a). Although, the fluidization of binary beds was traditionally analyzed by defining a minimum fluidization velocity, U_{mf}, to be determined (as done with any "monosolid" systems) at the intersection between the (extrapolated) pressure drop line of fixed bed and the (extrapolated) horizontal line representing the suspended state, there is currently no a general agreement on its exact definition (Clarke et al., 2005; Zhang et al., 2009a). This is essentially a consequence of the fact that, as suggested by the actual phenomenology of the process, analyzed in detail elsewhere (Zhang et al., 2009a; Formisani et al., 2008), the onset of fluidization through a binary bed is a rather gradual process. It occurs within a quite wide velocity range where the transient and partial fluidization of the bed is commonly accompanied by a complex sequence of mixing and segregation phenomena whose specific pattern depend on the mixture properties (i.e., the system composition as well as difference in size, density and shape of the bed components) and the initial arrangement of the fixed bed (Formisani and Girimonte, 2003; Zhang et al. 2008). The peculiarities of this mechanism are fully reflected by the experimental pressure drop diagram of binary mixtures where two characteristic velocity thresholds can be typically recognized, just as shown in Figure I.16 for the specific case of a binary mixture obtained by the complete mixing of spheres differing only in diameter. These are the "*initial fluidization velocity*", U_{if}, at which ΔP first deviates from the fixed bed curve, and the "*complete fluidization velocity*", U_{cf}, at which the ultimate value of ΔP is first attained. Thus, these two limits identify the velocity range within which the entire particle collective undergoes suspension in the gaseous stream. Although it refers to a particular type of mixture, the diagram in Figure I.16 shows a common feature of any binary mixture,. i.e., that their transition to the fluidized state is never instantaneous with increasing U_g. Accordingly, some authors (Marzocchella et al., 2000; Zhang et al., 2009a) have recently proposed the replacement of the conventional concept of minimum fluidization velocity, U_{mf}, as discussed above, with the new concept of complete fluidization state, whose corresponding velocity,

U_{cf}, was defined as the superficial gas velocity where the bed pressure drop begins to decrease from the constant bed pressure line during defluidization.
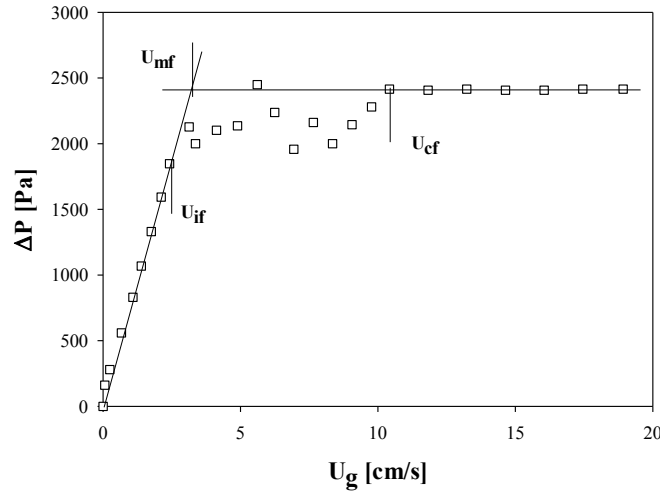
Figure I.16 *Pressure drop diagram of a two component mixture obtained by the complete mixing of spheres differing only in diameter (adapted from Formisani and Girimonte, 2003).*

I.6.4 Fluidization of binary mixtures involving biomass

Biomass particles have unusual properties (e.g., irregular in shapes, large in sizes and low in densities), which make them very difficult to fluidize. To improve fluidization and processing, typically a denser and more regular inert material, such as silica sand, alumina, calcite, etc., is added to the biomass to assist its fluidization (Zhang et al., 2009a). However, this approach is not a guarantee of good fluidization performance. In fact, it is well known that, depending on the mixture properties (i.e., differences in size, shape and densities between biomass inert particles and in inert/biomass mass ratio) as well as on the whole set of operating conditions, steady fluidization of a binary mixture may result in a stable state of mixing of the solid components that can range from almost total segregation into distinct layers to practically complete mixing (Formisani and Girimonte, 2003), as shown in Figure I.17. In many practical situations, however, an intermediate component distribution is found, so that every solid component exhibits a particular concentration along the bed height. During biomass processing, a good mixing of the bed components is essential to ensure a simple and reliable thermal control of the process, to avoid hot spots due to the heat released by highly exothermic reactions as well as to ensure a uniform quality of the product, which result in an improved process efficiency (Zhang et al., 2009b). Therefore, the mixture properties should be

thoroughly evaluated to avoid impediments to the proper fluidization, specifically intense segregation upon fluidization.

In spite of all the research reported in the literature, there is currently a little understanding of the biomass fluidization hydrodynamics as well as of the fluidization dynamics of multicomponent particle beds (Cui and Grace, 2007). Therefore, there are no general criteria for the specification of the optimum inert particles when these are needed to fluidized biomass; similarly, there are no general rules or well-established principles in resolving multiphase flow issues (Cui and Grace, 2007). Accordingly, design and operation of a fluidized bed involving biomass are currently based on conventional fluidization knowledge and methodologies, finally leading to trial and error *ad hoc* solutions (Zhang et al., 2008; Cui and Grace, 2007).
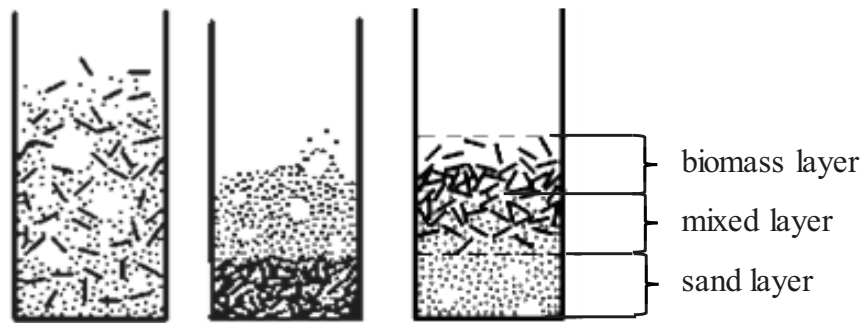
Figure I.17 *Possible fluidization pattern for sand and biomass binary mixtures: a) complete mixing; b) total segregation into distinct layers and c) partial mixing and segregation (adapted from: Zhang et al. 2008).*

This is precisely the approach that has been pursued in the present Ph.D. thesis to investigate the fluidization of the binary mixtures resulting from the addition of the selected biomass particles (i.e., dry tomato peels) to a bed of inert solid (i.e., sand).

Materials and Methods

II.1 Biomass and inert bed materials sampling, processing and characterization

II.1.1 Raw biomass and inert bed materials

Tomato peels (TPs) from a tomato processing industry located in Salerno (40°47'24.5"N, 14°46'15.8"E) and virgin olive husk (OH) from an oil mill located in Benevento (41°9′22″N, 14°31′48″E) were used as biomass feedstocks in this Ph.D. research work. The pictures of both the agro-industrial residues are shown in Figure II.1.

Figure II.1 *Picture of raw virgin olive husk (left) and raw tomato peels (right) agro-industrial residues.*

Since damp materials are more easily subjected to fungal attack and biodegradation than the dry ones, the wet samples, collected between September (i.e. TPs) and November 2013 (i.e., OH), were stored in an air-tightened plastic bag and frozen at -20 °C in order to preserve them before any further analysis. Prior to use, materials were removed from the bag and placed in a ventilated fume hood for approximately 24 hours of exposure to fresh air. After air-drying and before any tests or analyses, the moisture

content of samples was checked by means of a Kern DBS Halogen Moisture analyzer that heated the sample up to 120 °C. When required, biomass samples were also first ground in a batch knife mill (Grindomix GM 300 by Retsch) at 3200 rpm for 20 s, one or more times depending on the desired particle sizes, and then sieved manually in order to match feedstock specifications for the specific use.

Geldart group B silica sands in size range of 100-400 μm (Fine SS: Particle density = 2813 kg/m^3; Bulk density = 1475 kg/m^3; Saunter mean diameter, D[3, 2] = 140 μm) and in the size range 100-700 μm (Coarse SS: particle density = 2970 kg/m^3, Saunter mean diameter, D[3, 2] = 245 μm) were tested in cold flow experiments and then used as inert bed material to assist biomass fluidization and to maintain the desired hydrodynamics of the bed during torrefaction experiments. Both silica sands were kindly supplied by IRC-CNR of Naples and were used as received without further sieving.

II.1.2 Characterization tests of raw and torrefied materials

In order to investigate the effects of torrefaction process parameters on biomass feedstock upgrading, the main chemical and physical properties of raw and torrefied biomass samples were determined through the following analysis techniques:

Proximate analysis. The determination of the moisture, ash, volatile matter and fixed carbon contents of raw and torrefied biomass feedstocks was carried out by using a TGA 701 LECO thermogravimetric analyzer, which was kindly made available by IRC-CNR in Naples (Italy). Analyses were performed in triplicate at least and the mean values used. Results from analyses performed on tomato peels and olive husk samples are shown in Table II.1.

Elemental analysis. The determination of the carbon (C), hydrogen (H) and nitrogen (N) content of raw and torrefied biomass feedstocks was carried out by using a CHN 2000 LECO analyzer, which was kindly made available by IRC-CNR in Naples (Italy). The oxygen content was calculated by subtraction of the ash and CHN content from the total. Analyses were performed in triplicate at least and the mean values used. Prior to ultimate analysis, samples were dried in an oven at 105 °C for 24 h. Oven-dried samples were then stored in desiccators while cooling, in order to minimize the uptake of moisture. Results from analyses performed on tomato peels and olive husk samples are shown in Table II.1.

Heating values. A Parr 6200 Calorimeter, kindly made available by IRC-CNR in Naples (Italy), was used to determine the higher heating value

(HHV, MJ/kg) of raw and torrefied biomasses. Samples (about 1.0 g each) were placed in a crucible and fired inside the bomb calorimeter using an ignition wire in the presence of oxygen. Before analysis, samples were dried in an oven at 105 °C for 24 h. Oven-dried samples were then stored in desiccators while cooling, in order to minimize the uptake of moisture. Measurements were repeated at least 2 times, and the mean value was used to calculate the lower calorific value (LHV) in MJ/kg by means of the following eq. (II.1). Results from analyses performed on tomato peel and olive husk samples are shown in Table II.1, both as HHV and LHV, on dry basis.

$$LHV_{dry} = HHV_{dry} - 2.442(8.936 \cdot H/100) \qquad (II.1)$$

Hygroscopicity tests. The hygroscopic behavior of raw and torrefied biomass was examined based upon the determination of the equilibrium moisture content (ECM) of samples exposed at the same predetermined conditions of temperature and relative humidity (HR). The conventional static desiccator technique (Bellur et al, 2009; Vasquez and Coronella, 2009; Lu and Chen, 2014) was employed for the determination of the EMC. It employs a glass desiccator containing a supersaturated salt solution as humidity control chamber. Specifically, in this Ph.D. research work, a supersaturated solution of KBr (Winston and Bates, 1960) was used to expose samples to 80 ± 2 % HR at room temperature (i.e., 25 ± 2 °C). In order to minimize temperature changes the desiccator was partially submerged in a water bath. Approximately 100-200 mg of oven-dried samples in the size range 1-2 mm were put into an open weighing bottle and then placed into the desiccator for testing. The humidity and temperature in the glass desiccator were checked by using a digital thermo-hygrometer (30.5005 TFA Dostmann). Equilibrium moisture content (ECM) of each sample was measured by using a Kern DBS Halogen Moisture analyzer up to an exposure time of 120 days.

Bulk density. The bulk density of a granular material is often very difficult to measure with good reproducibility and, in reporting the results, it is essential to specify how the determination was made. In the present investigation both the following bulk and tapped methods were used:

Bulk method: The bulk density is obtained by adding a known mass of powder to a graduated cylinder. The density is calculated as mass/volume.

Tapped method: The tapped density is obtained by mechanically tapping a graduated cylinder containing the sample until little further volume change is observed. The tapping can be performed using different techniques. The

tapped density is calculated as mass divided by the final volume of the powder.

Table II.1 *Tomato peels and virgin olive husk properties*

	Tomato peels	**Virgin olive husk**
Moisture (wt.%, as received)	80.50	62.71
Proximate analysis (wt.%, dry basis)		
Volatile Matter	86.52	82.06
Fixed Carbon	11.67	15.76
Ash	1.81	2.18
Ultimate analysis (wt.%, dry basis)		
C	58.38	52.58
H	7.72	7.23
N	1.49	0.78
O (by diff.)	30.60	37.23
Calorific value (MJ/kg, dry basis)		
HHV	25.82	21.88
LHV	24.14	20.49
True density (kg/m^3)	1049.9	1219.4

II.2 TGA coupled with evolved gas analysis by mass spectrometry

Thermogravimetric analyses were carried out both on air-dried tomato peels (TPs) and on oven-dried olive husk (OH) samples by using a thermal analyzer TA Instruments SDT Q600. Nitrogen was used as purge gas at a flow rate of 100 ml/min to ensure an inert atmosphere and to prevent secondary reactions of volatiles produced during the solid thermal decomposition. Low sample weights (approximately 10-15 mg) and small particle sizes (size range: 0-400 μm for TPs and 0.5-1 mm for OH) were selected in order to reduce the effect of intra-particle mass and heat transport limitations and thus to avoid problems associated to the "thermal lag" between the sample and the controlling (external) thermocouple during the tests.

Both isothermal and dynamic measurements were performed, according to the temperature programs and the linear heating ramps described below. In particular, three isothermal thermogravimetric runs in the temperature range of interest for torrefaction (i.e., 200, 250 and 300 °C) were performed. During each run, the air-dried dried sample was first heated up to a

temperature of 105 °C, which was held for 10 min. Then the temperature was increased to the desired test value at a heating rate of 5 °C/min and kept constant for 7 h. Note that the aforesaid isothermal time excludes the warm-up phase, which globally lasted for about 1 h. These tests allowed determining the onset-decomposition temperature of both investigated biomass feedstocks as well as to obtain useful information on the qualitative composition of the torgas evolved during torrefaction tests. The onset-decomposition temperature was needed to define the torrefaction time, which is the total time that the biomass spends in the temperature window where the torrefaction decomposition reactions occur, namely above the onset decomposition temperature (see "*Section 2.4.4.3.1*").

The gases evolved during the isothermal runs carried at the heating rate of 5 °C/min were analyzed in situ by using a mass spectrometer (ThermoStar TM GSD 301 T300 from Pfeiffer Vacuum) connected to TGA. MS data were acquired in the m/z range 0-200 and saved at a rate of 0.08 Hz. After the analysis, the measured peak intensities were analyzed as function of the sample temperature. If the difference between the background level and the highest intensity value resulted close to the noise level, the mass spectrometric ion was rejected. In keeping with Varehegyi et al. (1989), the mathematical criterion for rejecting was a signal/noise ratio lower than 10. Since it is difficult to assign a given fragment to a single compound without confirmation by complementary methods, the main detected m/z values were associated with the chemical species that are commonly present in gases evolved during biomass torrefaction or early stage of pyrolysis.

Dynamic runs were also performed over the temperature range from room temperature to 1000 °C at six different linear heating rates, i.e., 2, 5, 10, 20, 40, 60 °C/min. Both thermogravimetric and differential temperature measurements were recorded simultaneously during each test.

II.3 Non-isothermal kinetics based on isoconversional methods

Kinetic analysis of the thermal decomposition of olive husk and tomato peel residues was performed by using data from dynamic thermogravimetric measurements carried out at the heating rate of 2, 5, 10, 30 and 40 °C/min. Different integral and differential model-free isoconversional methods, were employed, in this Ph.D. research work, in order to determine, the dependence of the activation energy on the conversion degree and no further computations aimed at evaluating the pre-exponential factor and the reaction model were performed. The reason is that the sole goal of the kinetic analysis performed in this Ph.D. project was to get a tool to predict the characteristic time needed to achieve a prefixed conversion degree under typical torrefaction conditions or in a more general setting under pyrolysis

conditions, being torrefaction basically a "mild pyrolysis" treatment. In this regard, it is worth noting that, when it is coupled with eqs. (12) and (18) by Vyazovkin (1996), the knowledge of the E_α vs. α dependence is by itself sufficient to do the above predictions, as described in more details below.

II.3.1 Model-free isoconversional methods: theoretical background

Isoconversional methods take their origin in the following single-step kinetic eq. (II.2)

$$\frac{d\alpha}{dt} = A \, exp\left(-\frac{E}{RT}\right) \cdot f(\alpha) \qquad (II.2)$$

where A and E are the kinetic parameters, namely the pre-exponential factor and the apparent activation energy respectively, R is the gas constant, T the absolute temperature, $f(\alpha)$ the reaction model and α the reacted fraction of the sample (or conversion degree), which is defined by the following eq. (II.3):

$$\alpha = \frac{W_0 - W_t}{W_0 - W_f} \qquad (II.3)$$

where W_t is the normalized mass of the sample at the time t and W_0 and W_f refer to the values at the beginning and at the end of the mass event of interest, respectively.

All isoconversional methods make use of the so-called "isoconversional principle", which states that the reaction rate at constant extent of conversion is only a function of the temperature. This can be easily demonstrated by taking the derivative of the reaction rate, eq. (II.2), at α = cost, which returns:

$$\left[\frac{\partial ln(d\alpha/dt)}{\partial T^{-1}}\right]_\alpha = -\frac{E_\alpha}{R} \qquad (II.4)$$

It follows from eq. (II.4) that the temperature dependence of the isoconversional rate can be used to evaluate isoconversional value of the activation energy, E_α, regardless of any previous knowledge of the kinetic model. This is the reason why isoconversional methods are frequently called "model-free" methods. To experimentally obtain the temperature dependence of isoconversional rate, a series of 3-5 runs at different heating rates or a series of runs at different constant temperature are typically performed (Vyazovkin et al., 2011). Although the isoconversional activation energies can be used in application without interpretation, however some useful clues can be inferred from E_α vs α dependencies. For example, if E_α is roughly constant over the entire conversion range it is likely that the process

is dominated by a single step and can be adequately described by a single-step model. Conversely, a significant variation of E_α with α indicates that the process is kinetically complex, i.e., one cannot apply the single-step eq. (II.2) to describe the kinetics of such a process throughout the whole range of experimental conversion and temperature investigated (Vyazovkin and Wight, 1998). In such a case, however, an analytical approach involving the deconvolution of the individual processes from the overall differential kinetic curves, followed by the application of model free-isoconversional methods to the separated decomposition steps, could be a solution (Perejon at al., 2011). Under this scenario, by assuming a multicomponent process where the decomposition of each component occurs as a single step, the eq. (II.2) changes into the following eq. (II.5).

$$\frac{d\alpha}{dt} = \sum \gamma_j \, A_j \, exp\left(-\frac{E_j}{RT}\right) f\left(\alpha_j\right) \tag{II.5}$$

where γ_i is the contribution of jth pseudo-component to the total mass loss which must accomplish the following relationships:

$$\sum \gamma_j = 1 \tag{II.6}$$

$$\sum \gamma_j.\alpha_j = \alpha \tag{II.7}$$

Isoconversional methods can be split in two main categories: differential and integral.

II.3.1.1 Integral isoconversional methods

Different integral isoconversional methods originate from the various ways of integrating the above single step kinetic eq. (II.2). In particular, for a constant heating rate program, where the temperature is raised at a constant rate $\beta = dT/dt$, the integration of eq.(II.2), yields:

$$g(\alpha) \stackrel{\text{def}}{=} \int_0^\alpha \frac{d\alpha}{f(\alpha)} = \frac{A}{\beta} \int_0^T exp\left(-\frac{E}{RT}\right) dT = \frac{A}{\beta} I(E,T) \tag{II.8}$$

where $g(\alpha)$ is the integrated form of the reaction model $f(\alpha)$ and $I(E, T)$ the temperature integral. Since the temperature integral in eq. (II.8) has no analytical solution, it is typically solved by using approximations or numerical integration, each of which is at the base of a different integral isoconversional method. It is worth noting that, although the use of approximation of the temperature integral instead of an accurate numerical method, induces an error in the value of the activation energy, such approximations are typically preferred since lead to the simplest final plots

(i.e., linear), yielding the activation energy very quickly (Vyazovkin and Dollimore, 1996). For example, the application of the very crude Doyle's approximation (Ozawa, 1965) leads to the following linear eq. (II.9) that is at the base of the popular linear Ozawa-Flynn-Wall method:

$$ln\beta_i = ln\left(\frac{A \cdot E_\alpha}{g(\alpha) \cdot R}\right) - 5.3305 - 1.052\frac{E_\alpha}{RT_{\alpha,i}} \qquad (II.9)$$

where $T_{\alpha,i}$ is the temperature at which the conversion α is experimentally achieved at the heating rate β_i and the subscript i is an integer number representing experiments performed at the heating rate, β_i. Through the eq. (II.9), this method allows to obtain the value of the apparent activation energy E_α at a fixed conversion value α, from the slope of the straight line generated in the plot of log (β_i) versus $1/T_{\alpha,i}$, for a number n of thermogravimetric experiments carried out at different heating rates (β_i). Instead, according to the more accurate nonlinear Vyazovkin method, for each given value of α, the apparent activation energy value, E_α, can be determined by minimizing the following function $\Phi(E_\alpha)$,

$$\Phi(E_\alpha) = \sum_{i=1}^{n} \sum_{h \neq i}^{n} \frac{I(E_\alpha, T_{\alpha,i}) \cdot \beta_h}{I(E_\alpha, T_{\alpha,h}) \cdot \beta_i} \qquad (II.10)$$

where the temperature integrals are solved numerically, with a very time consuming procedure.

II.3.1.2 Differential isoconversional methods

The most common differential isoconversional methods is that of Friedman, which is based on the following eq. (II.11):

$$ln\left(\frac{d\alpha}{dt}\right)_\alpha = ln\left[\beta_i\left(\frac{d\alpha}{dT}\right)_\alpha\right] = ln[A_\alpha f(\alpha)] - \frac{E_\alpha}{RT_{\alpha,i}} \qquad (II.11)$$

which can be easily derived by computing the natural logarithm of the eq. (II.2). Through the eq. (II.11), this method allows to obtain the value of the apparent activation energy E_α at a fixed value of the conversion degree, α, from the slope of the straight line generated in the plot of log(dα/dt)α versus $1/RT_{\alpha,i}$, for a number n of thermogravimetric experiments carried out at different heating rates (β_i). Since the differential isoconversional methods do not make use of any approximations, they are potentially more accurate than the integral methods considered in the previous section.

II.3.2 Isoconversional decomposition kinetics of virgin olive husk

Kinetic analysis of the virgin olive husk degradation in the temperature range of interest for torrefaction was performed by using data from dynamic thermogravimetric measurements carried out at the heating rate of 2, 5, 10, 30 and 40 °C/min (Brachi et al., 2015a). Two selected integral isoconversional methods, i.e., the nonlinear Vyazovkin incremental approach (eq. (II.10)), which is more accurate but time-consuming, and the linear Ozawa-Flynn-Wall (OFW) method (eq. (II.9)), which is less accurate but computationally simpler, were used, in this Ph.D. research work, in order to determine, the dependence of the activation energy on the conversion degree. All the integral curves derived from the dynamic thermogravimetric experiments (TGA) were used in the kinetic analysis, after being converted to the plot of conversion (α) versus temperatures by eq.(II.3), where 150 °C and 450 °C were taken, respectively, as the beginning and the end of the mass event of interest (i.e., torrefaction). The motivation for this choice lies in the fact that degradation of cellulose and hemicellulose from virgin olive husk mainly occurs in this temperature range (see detailed discussion in "*Section III.1.1*") and although the major objective of torrefaction is substantially the complete degradation of its hemicellulose content, it is unavoidable that such decomposition takes place without a simultaneous and partial degradation of the others biomass components, in particular the cellulose fraction (Tumuluru at al., 2011).

The standard Solver function, contained in the Microsoft Excel spreadsheet package, was used to obtain the value of E_α minimizing the function $\Phi(E_\alpha)$, in eq. (II.10). This solver applies the Generalized Reduced Gradient (GRG) nonlinear solving algorithm that is one of the most robust nonlinear programming methods (Lwin, 2000). For each run, in particular, after substituting experimental values of T_α and β into the nonlinear eq. (II.10), the value of each temperature integral was found by applying the trapezoidal integration rule with a temperature step of 10^{-2} K and assuming the constancy of E_α only for a small integral conversion $\Delta\alpha$ (= 0.05) according to the following eq. (II.12) by Vyazovkin and Sbirrazzuoli (2006):

$$I^*(E_\alpha, T_\alpha) = \int_{T_{\alpha-\Delta\alpha}}^{T_\alpha} exp\left(-\frac{E_\alpha}{RT}\right) dT \qquad (II.12)$$

Note that the original method (Vyazovkin, 1997) uses the regular integration from 0 to T_α in the temperature integrals in eq. (II.10), according to the definition shown in eq. (II.8). However, since as a result of this formulation, each value of E_α became averaged over the region 0-α and the whole E_α dependence underwent an undesirable flattening, the method was subsequently modified to adequately account for a variation of E_α with α (Vyazovkin, 2000). In order to do this, the regular integration from 0 to T_α

61

was replaced by the integration over small temperature segments as in eq. (II.12). Specifically, in this Ph.D. research, the dependence of E_α on α was obtained by determining the value of E_α in the range of $\alpha = 0.05 - 0.95$ with a step of 0.05, by means of both the abovementioned integral methods.

Following the pragmatic guidance from the ICTAC Kinetics Committee (Vyazovkin et al., 2011), the reliability of the global activation energy obtained from the kinetic analysis, was checked by simulating isothermal conversion profiles, which was obtained from thermogravimetric measurements not used in the previous kinetic analysis, by means of the following eq. (II.13) by Vyazovkin (1996):

$$t_\alpha^* = \frac{\frac{1}{\beta^*}\int_0^{T_\alpha^*} exp\left(-\frac{E_\alpha}{RT}\right)dT}{exp\left(-\frac{E_\alpha}{RT_o}\right)} \qquad (II.13)$$

where t_α^* is the time to reach the conversion degree α at an arbitrary temperature T_o under isothermal conditions, T the absolute temperature, T_α^* the temperature at which the conversion α is experimentally achieved at the heating rate β^*, R the gas constant and E_α the activation energy related to the extent of conversion, α. To provide a standard reference for all the experimental variables dependent on the conversion degree by both isothermal and non-isothermal TG, during this validation step, the aforesaid independent variable α, (eq.(II.3)), was re-defined as follows:

$$\alpha = \frac{W_0 - W_t}{W_0} \qquad (II.14)$$

Specifically, in this Ph.D. study, eq. (II.13) was used to compute the time at which different conversion degrees were reached at 250 °C and 300 °C, respectively, under isothermal conditions. The integral in eq. (II.13) was solved on the basis of the values of E_α obtained by the application of the OFW method and the experimental values of T_α^* obtained by dynamic thermogravimetric runs performed at the same heating rate of the simulated isothermal ones (i.e., 5 °C/min).

II.3.3 Isoconversional decomposition kinetics of tomato peels

The kinetics of the thermal decomposition of tomato peel residues under an inert atmosphere was investigated by non-isothermal thermogravimetric analysis in the heating rate range 2-40 °C/min. Due to the complexity of the investigated process, which implies simultaneous multi-component degradation reactions, an analytical approach involving the deconvolution of the overlapping degradation steps from the overall differential thermogravimetric curves (DTG curve) and the subsequent application of model-free kinetic methods to the separated peaks was employed in this Ph.D. work.

II.3.3.1 Separation of independent overlapping pseudo-component

degradation reactions

The separation of the independent and overlapping pseudo-component decomposition steps from the set of experimental DTG curves, recorded at the different heating rates (i.e., 2, 5, 10, 20, 40 °C/min) to be considered in the kinetic analysis, was performed by means of two different open-source Matlab functions, namely ipf.m and peakfit.m (Copyright (c) 2014, 2015 Thomas C. O'Haver[1]). These latter use a non-linear optimization algorithm to decompose a complex pattern of overlapping peaks into its component parts and are available free of charge on the Mathworks File Exchange website. Different statistical distribution equations (i.e., Gaussian, Voigt, Pearson, Lorenzian, equal width Gaussian and equal width Lorenzian), which are included as standard functions in the abovementioned Matlab m-functions, were tested for the deconvolution. The best fits were obtained by using a suitable combinations of Gaussian and Lorentzian peak-shape functions, which are described by the following eqs. (II.15) and (II.16), respectively:

$$y = y_0 + \frac{S}{w\sqrt{\frac{\pi}{2}}} \exp\left[-\frac{2(x-x_o)}{w^2}\right] \qquad (\text{II.15})$$

$$y = y_0 + \frac{2S}{\pi} \cdot \frac{w}{4(x-x_0)^2 + w^2} \qquad (\text{II.16})$$

where y_0 is the baseline offset, S the total area under the curve from the baseline, x_0 the center of the peak, w the width of the peak at half height. Specifically, for the separation of the different decompositions stages, the experimental DTG data were first loaded into the ipf.m function, which provided the best-fit description of the experimental curve by varying the number, the position, the shape and the width of discrete peaks at each heating rate. Then, the determination of fitting parameters (i.e., y_0, S, w, x_0) and the model error was performed by using the peakfit.m function.

II.3.3.2 Pseudo-component kinetic analysis

Friedman's differential isoconversional method, which is based on eq. (II.11), was employed in order to determine the E_α vs. α dependence for each tomato peel pseudo-component resulting from the peak deconvolution

---

[1] Permission is hereby granted, free of charge, to any person obtaining a copy of this software and associated documentation files (the "Software"), to deal in the Software without restriction, including without limitation the rights to use, copy, modify, merge, publish, distribute, sub-license, and/or sell copies of the Software, and to permit persons to whom the Software is furnished to do so.

procedure. To this end, deconvoluted DTG data were first converted in conversion degree, α_j, by using the following eq. (II.17)

$$\alpha_j = \frac{W_{j0} - W_{jt}}{W_{j0} - W_{jf}} \qquad (II.17)$$

where W_{jt} is the mass of the jth pseudo-component at the time t and W_{j0} and W_{jf} refer to the values at the beginning and at the end of the mass event investigated. Then, for each of the 19 conversion levels (α_{ij}) evaluated in the range 0.05-0.95 with a step of 0.05, the experimental values of the conversion rate, $(d\alpha_j/dt)_{\alpha i,j}$, and the associated temperatures, $T_{\alpha j,i}$, were determined, at the different heating rates. In more detail, $T_{\alpha j,i}$ is the temperature at which the extent of conversion of the jth pseudo-component $\alpha_{j,i}$ is experimentally reached under the ith heating rate, β_i. The following eq. (II.18) was employed for the determination of the conversion rate values, $(d\alpha_j/dt)_{\alpha i,j}$:

$$\left(\frac{d\alpha_j}{dt}\right)_{\alpha_{j,i}} = -\left(\frac{dW_{jt}}{dt}\right)_i \frac{1}{(W_{j0} - W_{jf})_i} \qquad (II.18)$$

The subscripts i and j were introduced to denote the different heating rates and the different pseudo-components, respectively. Afterwards, for each heating rate investigated, the logarithm of the conversion rate, $\ln(d\alpha_j/dt)_{\alpha j,i,}$ was plotted as a function of the reciprocal absolute temperature $1/T_{\alpha j,i.}$. This allowed determining the activation energy as the slope of the straight line drown through the points with the same conversion value. Thus the dependence of $E_{\alpha j}$ on α_j was obtained.

Following the pragmatic guidance from the ICTAC Kinetics Committee Vyazovkin (1996), the reliability of the computed kinetic parameters was checked by pursuing the approach of simulating non-isothermal conversion profiles obtained at heating rates which had not been used in kinetic analysis. According to the ICTAC Kinetics Committee, the validation of the computed kinetic parameters performed by demonstrating that they can be used to satisfactory predict experimental curves not included in the computation rather than experimental curves used to derive the same kinetic parameters, is the most rigorous approach (Vyazovkin et al., 2011). Specifically, in this Ph.D. research work, the simulation of an experimental conversion curve obtained under dynamic conditions at the constant heating rate of 60 °C/min was carried out by using the following eq. (II.19) by Vyazovkin (1996):

$$\frac{1}{\beta}\int_0^{T_\alpha} exp\left(-\frac{E_\alpha}{RT}\right)dT = \frac{1}{\beta^*}\int_0^{T_\alpha^*} exp\left(-\frac{E_\alpha}{RT}\right)dT \qquad (II.19)$$

where E_α is the value of activation energy related to the extent of conversion α (as obtained from kinetic analysis), T_α^* is the temperature at which the conversion degree α is experimentally achieved at the heating rate β^* and finally, T_α, to be found as a solution of eq.(II.19), is the temperature at which the selected conversion α will be reached at an arbitrary heating rate, β. By solving eq. (II.19) for different conversion degrees, it is possible to predict a dependence of α on T at an arbitrary heating rate.

In more detail, eq. (II.19) was employed to simulate the conversion curve of each pseudo-component (i.e., dependence of α_j on T) at the heating rate of 60 °C/min, on the basis of the values of $E_{\alpha j}$ which were obtained from the isoconversional kinetic analysis. The integral on the right hand side of eq. (II.19) was solved numerically by using the trapezoidal rule in Microsoft Excel spreadsheet package and by using the experimental values of T_α^* obtained from the dynamic TG curve recorded at 40 °C/min. Finally, the global decomposition curve of tomato peels (i.e., dependence of α on T) at the heating rate of 60 °C/min was determined as the weighted sum of the simulated curves related to each pseudo-component, according to eq. (II.5). In eq.(II.5), the contribution γ_j of jth pseudo-component to the total mass loss was assumed equal to the average of the values obtained at the different five heating rates investigated (i.e. β_i = 2, 5, 10, 20, 40 °C/min) according to the following eq. (II.20):

$$\gamma_j = \frac{1}{5} \cdot \Sigma_i \gamma_{ji} = \frac{1}{5} \cdot \Sigma_i \left(\frac{S_{ji}}{\Sigma_j S_{ji}} \right) \tag{II.20}$$

where γ_{ji} is the contribution of jth pseudo-component to the total mass loss at the ith heating rate and S_{ji} is the total area under the DTG curve of the jth pseudo-component at the ith heating rate, just as obtained by the peak deconvolution procedure and reported in Table III.5. The quality of the fit between simulated and experimental data was evaluated through the average deviation percentage (AVP) proposed by Orfao et al. (1999):

$$AVP = 100 \cdot \sqrt{\frac{\Sigma_{k=1}^{N} \left[(\alpha)_{k,exp} - (\alpha)_{k,calc} \right]^2}{N}} \tag{II.21}$$

where N is the number of experimental points employed.

II.4 Experimental apparatuses and design of experiments

II.4.1 Laboratory-scale fluidized bed set-up

A new laboratory-scale experimental apparatus was designed and built to carry torrefaction tests. A schematic representation and a picture of the torrefaction setup is shown in Figure II.2. Basically, it consists of a gas

supply unit, a gas heating system, a torrefaction unit and a data acquisition system. The centerpiece of the system is represented by the batch fluidized bed reactor (Figure II.3) consisting of tubular glass column of 100 mm in ID and 750 mm (i.e., total volume ~ 5.9 L) in height surrounded by a glass jacket which was purpose-designed to operate under high vacuum conditions.
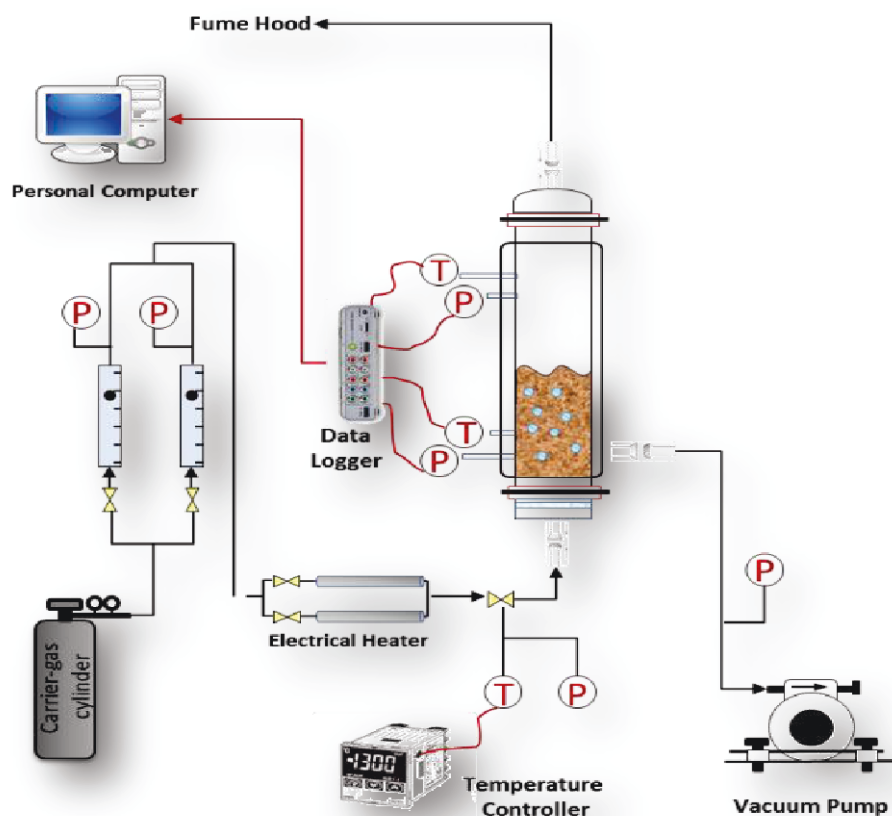
Figure II.2 *Schematic representation (not to scale) of the fluidized bed experimental setup*

Specifically, a high vacuum in the order of 10^{-3} mbar was typically created by a two stage vacuum pump (Rotary-Vane by 3B Scientific) in order to ensure the thermal isolation of the reactor without losing the advantage of its transparency. A vacuum jacket, in fact, virtually eliminates all heat exchange between the jacket outer surface and the atmosphere, thus no heat insulating materials are needed even at high operating temperatures (Fuchs et al., 2012). This arrangement allowed visual monitoring the fluidization pattern and movement of particles in the bed at any time and temperature (i.e., up to 500 °C, the maximum working temperature of

borosilicate glass) and what is particularly interesting also when biomass particles experience different degrees of devolatilization depending on the severity of the heat treatment. A distributor plate consisting of a 6 mm-tick high pressure drop quartz fritted disk with porosity 3 (i.e., with a nominal pore size 16-40 μm) and diameter 9.5 mm, was selected to support the bed material inside the reactor in order to prevent particles passing through and to ensure uniform fluidizing gas distribution across the bed. For the torrefaction experiments, nitrogen was selected as the fluidizing medium to ensure an inert environment in process vessel. Addition of air to the system was also possible.

Figure II.3. *Picture of the lab-scale batch fluidized bed torrefier.*

In particular, the nitrogen supply unit, which is the tapping point of a centralized gas supply system consists of: i.) a ball valve DN 10; ii.) a pressure regulator (Model R138 bar by Insert Deal srl for inlet pressure up to 50) which is able to provide a stable outlet pressure adjustable within the

range 0-2.5 bar and iii.) two nitrogen flowmeters (Asameter Model E by ASA) with needle valve, the first for low flow applications (flow range 100-1000 Nl/h) and the second for high flow applications (flow range 1000-6000 Nl/h). The gas heating system consists of two electrical gas heaters (AH75-6 750W 240V by RS), each one able to provide hot gas up to 550 °C in the range of flow rates of interest. The temperature of the fluidizing gas is regulated by means of a proportional integral derivative (Gefran 600 PID) temperature controller that reads the temperature of the gas by a K-type thermocouple while the power of the gas-heater is controlled by a solid state relay (SSR) power controller. The pressure drop across the fluidized bed is measured by two piezoresistive pressure sensors (GE Druck PTX 7200 Series Pressure Transmitter) with a working pressure range from 0 to 250 mbar. K-type thermocouples are used to measure the bed temperature and the outlet temperature of the gas and/or volatiles released during hot fluidization tests.

II.4.2 Bench-scale fixed bed set-up

A schematic representation and a picture of the bench-scale fixed bed apparatus are shown in Figure II.4. It includes a stainless steel tube of 55 mm ID and 120 mm length (i.e., total volume ~ 0.34 L), which is twined with heating tapes (FGR-060/240V-ROPE HEATER 250W) and placed inside an insulating cylinder (closed superiorly and inferiorly) made of mineral wool.
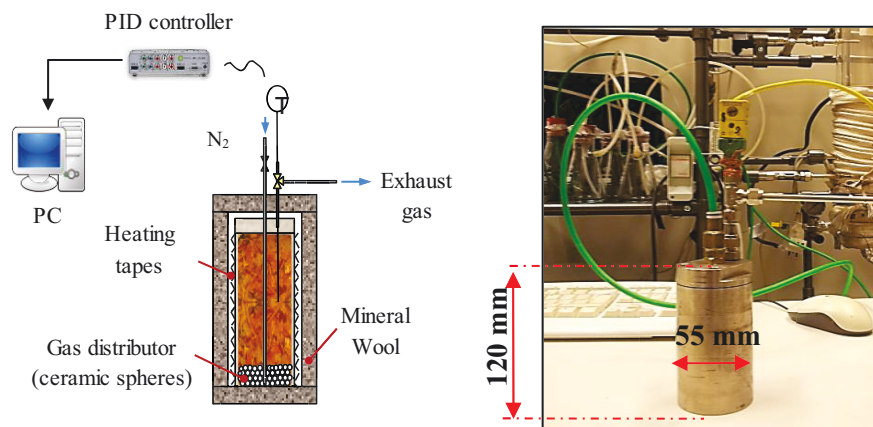
Figure II.4 *a) Schematic representation (not to scale) and b) picture of the bench-scale fixed bed set-up.*

The temperature of the reactor is regulated by means of a proportional integral derivative temperature controller (Gefran 600 PID), which reads the bed temperature by means of a K-type thermocouple inserted in the center of

reactor. The nitrogen supply unit consist of a needle valve and a nitrogen flowmeter (Asameter Model E by ASA) with a 100-1000 Nl/h flow range. Specifically, the carrier gas enters the top of the reactor, but percolates the biomass bed upward leaving from the bottom.

II.4.3 Raw feedstock pre-treatments prior to torrefaction tests

In this research, some pre-treatments steps were adopted before the experimental phase. These pre-treatments were not only needed to meet the specific requirements of the selected torrefaction technology (i.e., size restrictions required to maintain correct fluidization properties and mixing), but also mandatory for preparing the samples for the torrefaction pre-treatment. It is worth noting that pre-treatments prior to torrefaction are necessary and critical to control the feedstock properties to obtain a homogeneous product quality (see "*Section I.5.1.4*"). Typically, pre-drying the biomass to a moisture content of 15 % or lower is needed since a higher moisture content not only increases the required residence time for torrefaction, but also could result in inefficient combustion of the "wet" torgas (Kleinschmidt, 2011). Moreover, regardless of the particular reactor technology, feedstock particles with small size distribution are recommended to achieve an optimized torrefaction efficiency and product quality (Lam et al., 2013).

II.4.3.1 Virgin olive husk

Virgin olive husk is a heterogeneous and semi-solid residue that consists of olive pulp, skins and stone fragments (Figure II.1) and it is characterized by a high moisture content (approximately 60 % wt., cf. Table II.1).

dry olive pulp
agglomerates
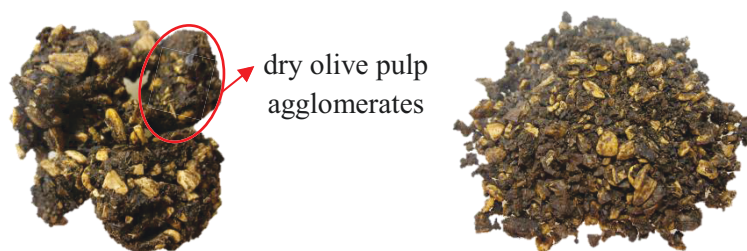
Figure II.5 *Picture of (left) air-dried virgin olive husk and (right) air-dried olive husk further processed by using a knife mill.*

Therefore, before torrefaction tests, it was subjected to a pre-treatment stage. Firstly, it was conditioned to approximately 10 %wt. moisture content, which is the equilibrium moisture content (EMC) that such feedstock reached if left in a laboratory fume hood for two days at room temperature.

Then, it was processed by using a knife mill (Grindomix GM 300 by Retsch) at different grinding times and mill speed conditions, to reduce its size.

Pretreatment runs highlighted a practical limitation in reducing the intrinsic size polydispersity of this residue, due to the difficulty in making olive stone fragments smaller in size by means of the knife mill (Figure II.5). This led to discard such residue as a potential feedstock for subsequent fluidized bed torrefaction tests. Inconsistent particle size distribution may not only lead to more complicate and less reliable experiments in fluidized bed reactor (i.e., segregation, elutriation of fines, etc.) but could also result in a poor torrefaction process controllability and product quality (Koppejan et al.,2012). As a further disadvantage, air-dried virgin olive husk also showed a strong tendency to create airborne dust during milling as a consequence of the breakdown of dry olive pulp agglomerates resulting from the drying step (Figure II.5).

II.4.3.2 Tomato peels

Tomato peels (TPs) clearly appear as non-standard particles (see Figure II.1) - large in size, extreme in shape (i.e., flat-like particles) and pliable – compared to particulate matter typically handled in fluidized beds or considered for the torrefaction treatment. Therefore, before fluidized bed torrefaction experiments, some pre-treatments steps were adopted. Specifically, tomato peels were first conditioned to approximately 6 % moisture content, which is the equilibrium moisture content (EMC) that such kind of feedstock reached if left in a laboratory fume hood for two days at room temperature. After air-drying and before further processing, the moisture content of samples was checked by means of a Kern DBS Halogen Moisture analyzer that heated the sample up to 120 °C. Air-dried tomato peels were then subjected to grinding in a batch knife mill (Grindomix GM 300 by Retsch) for 20 s at a speed as high as 3200 rpm. The milled TP was finally sieved and the 1000-2000 μm size fraction selected for the torrefaction tests.

The choice of this particle size range comes from preliminary cold fluidization tests (Brachi et al., 2015b) in which the mixing and segregation behavior of different tomato peels and sand binary mixtures was investigated by means of visual observation. Briefly, the fluidization tests showed that: i. binary mixtures obtained by mixing fine silica sand (Fine SS: Particle density = 2813 kg/m^3; bulk density = 1475 kg/m^3; Saunter mean diameter, D[3, 2] = 140 μm) with tomato peels either in their original size or in sieve fractions larger than 2 mm, segregated upon fluidization regardless of the initial mixing conditions (i.e., well mixed or full segregated sand/TPs bed);

ii. binary mixtures obtained by mixing the fine silica sand (Fine SS) with tomato peel particles in the size range 1-2 mm gave rise to a stable state of mixing of the bed components upon fluidization, showing only a local segregation during the so called transient fluidization regime (see "*Section I.6.3.1.1*").

II.4.4 Laboratory-scale experimental procedures

II.4.4.1 Cold fluidization tests

A systematic experimental investigation on the effect of the biomass weight fraction on the characteristic velocities (i.e., minimum fluidization velocity, complete fluidization velocity and minimum slugging velocity) of different binary mixtures (see "*Section I.6*") was carried out in order to select the maximum biomass batch loading (i.e., the critical weight fraction of biomass in the mixtures beyond which the fluidization properties deteriorate) to be used during the subsequent fluidized bed torrefaction tests. Two different kinds of binary mixtures were investigated, namely: i. binary mixtures obtained by mixing air-dried tomato peels particles in the size range 1-2 mm with the silica sand particles in the size range of 100-400 μm (TP/FSS mixtures) and ii. binary mixtures obtained by mixing air-dried tomato peels particles in the size range 1-2 mm with the silica sand particles in the size range of 400-700 μm (TP/CSS mixtures). Specifically, fluidization tests were performed on sand-TP binary mixtures with a biomass weight fraction up to 9 % as shown in Table II.2 and Table II.3 for TP/FSS and TP/CSS mixtures, respectively. During tests the bed aspect ratio, which is defined as the ratio of bed height (H) to bed diameter (D), was maintained nearly constant and equal to 1.6 ± 0.2.

Table II.2 *Bed compositions in fluidization tests with TP/FSS mixtures*

TP, % wt.	TP, % vol.[*]	H[**]/D (-)	
0	100	1.7	
0.9	≈ 10	≈ 1.7	
2.1	≈ 20	≈ 1.6	
3.5	≈ 35	≈ 1.5	
5.2	≈ 44	≈ 1.6	
9	≈ 49 (see attached photo)	≈ 1.8	

* Calculated on the basis of its bulk volume.
** Static bed height, H, was measured visually by using a scale attached along the height of column.

The mixing ratio of biomass to sand was selected on a weight rather than on a volume basis because of the inaccuracy in determining the bulk volume of irregular biomass particles. It is worth noting that due to the low bulk density of the air-dried tomato peels particles in the size range 1-2 mm (~ 125 kg/m^3 *via* tapped method) compared to that of both FSS (bulk density = 1475 kg/m^3

via tapped methods) and CSS (bulk density = 1497 kg/m^3 *via* tapped methods), a small increase in the biomass weight fraction resulted in a large increase in its volume fraction as shown in Table II.2. and Table II.3.

Table II.3 *Bed compositions in fluidization tests with TP/CSS mixtures*

TP, % wt.	TP, % vol.*	H**/D (-)	
0	100	1.6	
0.9	≈ 12	≈ 1.6	
2.1	≈ 26	≈ 1.7	
3.5	≈ 37	≈ 1.7	
5.2	≈ 44 (see attached photo)	≈ 1.7	

* Calculated on the basis of its bulk volume.
** Static bed height, H, was measured visually by using a scale attached along the height of column.

For each fluidization test of binary mixtures, the sand and the biomass samples were initially thoroughly mixed and then put inside the fluidizing chamber. Almost all tests were performed using the procedure of increasing and decreasing step by step the nitrogen flow rate. The bed height and the pressure drop across the bed were continuously recorded during each experiment in order to define the onset of both the conditions of incipient (U_{mf}) and complete fluidization (U_{cf}) by means of the conventional graphical methods described in more details in the "*Section I.6.3.1.1*". In order to avoid dependence on the initial bed loading pattern the characteristic velocities of the binary mixtures investigate were determined based on the de-fluidization curve (see "*Section I.6.3.1*"). Specifically, U_{mf} was identified with the superficial gas velocity at the intersection of the pressure drop line corresponding to the state of fixed bed with the content pressure drop line corresponding to the fluidization state (see "*Section 1.6.3.1.1*"). U_{cf} was instead identified with the minimum value of the superficial gas velocity where a pressure drop equal to the weight of the bed per unit cross-sectional area is detected in the descending curve (see "*Section 1.6.3.1.1*"). Finally, visual observation was used to identify the onset of the undesired slugging regime (see "*Section I.6.2*"), and thus to determine the corresponding minimum slagging velocity, U_{ms} (Broadhurst and Becker, 1975).

II.4.4.2 Torrefaction tests

II.4.4.2.1 Fluidized bed configuration

On the basis of the results obtained from cold flow fluidization tests (see "*Section III.4*"), batch torrefaction tests were performed on fluidized beds consisting of fine silica sand (Fine SS: Particle density = 2800 kg/m^3; bulk density = 1475 kg/m^3; D[3,2] = 140 μm) and tomato peel (1-2 mm particle size and 6 %wt. moisture content) binary mixtures, with a biomass batch loading equal to 2 % wt. (cf. Table II.2).

At start up, the sand bed was heated to the selected torrefaction temperature by means of heating tapes wrapped around the fluidization column and by using hot fluidizing air at the minimum fluidization velocity in order to reduce heat losses. When the fluidized bed reached its prefixed steady state temperature, the glass jacket was evacuated by the vacuum pump up to the final pressure of about $3 \cdot 10^{-3}$ mbar and the fluidizing gas was switched to nitrogen. Then, a preset batch of tomato peels was dropped into the reactor from the top. During each test, the bed was fluidized by hot nitrogen and kept under fluidization for a desired torrefaction time. In particular, the nitrogen flow rate was chosen such as to ensure a superficial gas velocity, at the torrefaction temperature, equal to the value of the minimum fluidization velocity (i.e., 0.04 m/s, cf. Table III.8) obtained from the cold fluidization test for the selected biomass weight fraction. This allowed to obtain experimentally a good mixing of solids while preventing the elutriation of low density tomato peel particles. Accordingly, the gas-solid contact time in the fluidized bed (FB) reactor, which was calculated as the ratio of the fluidized bed height to the superficial gas velocity, resulted approximately 5 s. After the prefixed holding time for the TP batch was passed, the pump venting valve was opened so that the outer jacket started taking atmospheric air in. Then, the bed was quickly cooled down by using a cold nitrogen flow as fluidizing gas and by sending a continuous flow of cold air through glass jacket. In the end, the bed material was collected and weighted. The amount of torrefied biomass was calculated by subtracting the initial sand bed mass from the total bed mass. The torrefied biomass was then separated from the inert bed component by sieving. In the present Ph.D. Thesis, the volatiles produced during torrefaction process were not analyzed.

Table II.4 *Overview of torrefaction tests performed on air-dried tomato peels in the size range 1-2 mm*

TEST No.	Torrefaction temperature (°C)	Torrefaction time (min)	Fluidized bed	Fixed bed
1	200	5	✓	
2	200	15	✓	
3	200	30	✓	✓
4	240	5	✓	
5	240	15	✓	✓
6	240	30	✓	
7	285	5	✓	
8	285	15	✓	
9	285	30	✓	

The torrefaction tests were carried out on tomato peel residues at three different temperatures (i.e., 200, 240, and 285 °C) and torrefaction times

(i.e., 5, 15, and 30 min), as shown in Table II.4. Each test was repeated twice. Errors on mass yield were in the range 1-3 %wt.

II.4.4.2.2 Fixed bed configuration

Fixed bed torrefaction tests on air-dried tomato peels were carried out by assuming the same particle size range (i.e., 1-2 mm) and the same gas–solid contact time (i.e., approximately 5 s) used for fluidized bed torrefaction tests in order to compare the performance of the two reactor concepts under identical operating conditions. However, due to the performance drawbacks emerged when operating such a reactor (they are described in detail in the "*Sections III.5.3 and III.5.4*"), in spite of what was originally scheduled, only two of the nine tests previously conducted in the fluidized bed reactor were reproduced in a fixed bed condition. Specifically, only tests No. 3 (200 °C and 30 min) and test No. 5 (240 °C and 15 min) previously conducted in the fluid bed reactor were also carried out in a fixed bed condition, as shown in Table II.4.

The experimental protocol of fixed bed torrefaction tests included: i. to set the bed temperature at 20-30 °C below the target torrefaction temperature in order to prevent temperature overshoot; ii. to slowly increase the bed temperature up to target temperature; iii. to monitor the bed temperature against the target value through the preset holding time; iv. after the prefixed holding time was passed, to cool down the bed temperature as fast as possible below the onset-decomposition temperature of the feedstock by tuning the electrical heater off, removing the reactor from the insulating cylinder and blowing cool compressed air on the surface of the reactor.

II.4.4.3 Torrefaction process parameters

II.4.4.3.1 Definition of torrefaction time and torrefaction temperature

Since any misunderstanding about the torrefaction time definition automatically leads to inaccuracies in relating product quality to torrefaction operating conditions as well as in comparing the results from different investigations, in keeping with Bergman et al. (2005b) the use of reactor residence time, which only expresses the hold-up time of biomass in a torrefaction reactor, was abandoned and the use of reaction time was instead adopted in this Ph.D. work, as described below.

In this regard, it is worth noting that, depending on the different time-temperature pathway which the biomass is subjected to during a batch torrefaction test, different stages can contribute to determine the batch torrefaction time. They are the *heating time* (i.e., time during which the biomass is heated from the onset decomposition temperature to the torrefaction temperature), the *holding time* (i.e., time during which the

biomass is kept at the preset torrefaction temperature) and the *cooling time* (i.e., time during which the temperature decreases to the onset decomposition value again), as schematically shown in Figure II.6.
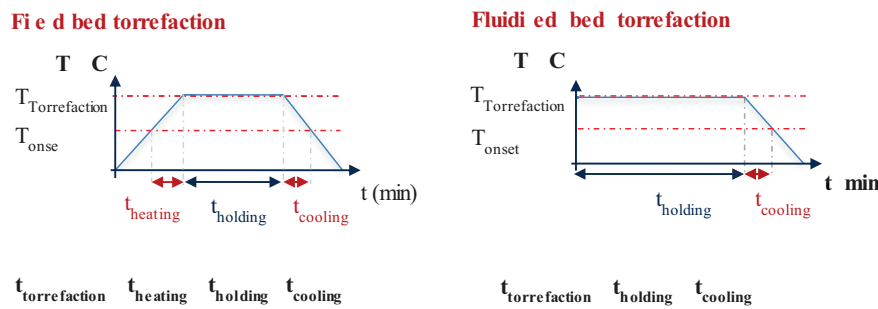
Figure II.6 *Temperature-time profile and torrefaction time definition for fixed and fluidized bed batch torrefaction experiments.*

Specifically, in the current Ph.D. research work, the reaction time was defined as the sum of the heating time and the holding time for fixed bed torrefaction test, whereas it was assumed equal to the holding time for fluidized bed torrefaction tests. In accordance with Bergman et al. (2005b), the cooling time was considered of negligible effect, as it is supposed that the most thermally labile or reactive parts of the biomass feedstock have already reacted and so it is expected that the decomposition reactions stop as soon as the temperature is decreased.
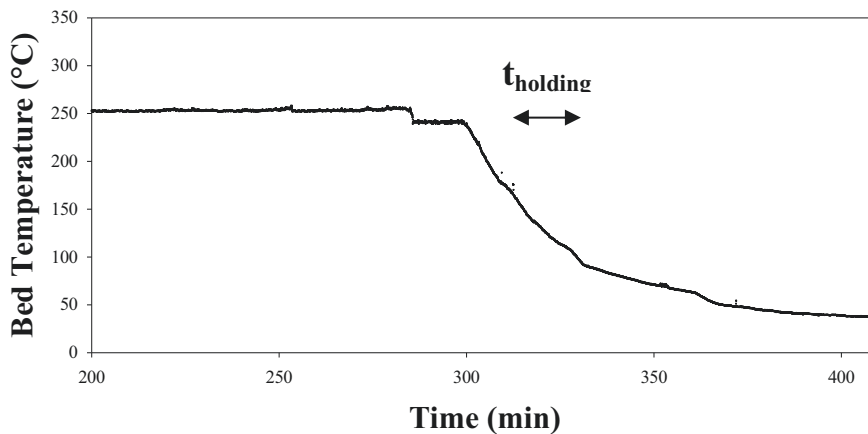
Figure II.7 *A typical bed temperature profile during a batch fluidized bed torrefaction test with an holding time of 15 min (test temperature set at 240 °C).*

In addition, only for fluidized bed torrefaction tests, it was assumed that the torrefaction temperature was the constant value that the bed reached after

a sudden, but slight (typically by 7-8 °C) cooling it underwent upon loading tomato peels into the hot sand bed, as shown in Figure II.7 for a specific torrefaction test (i.e., 240 °C and 15 min).

II.4.4.3.2 Performance parameters

The mass yield (M_Y), the energy yield (E_Y) and the energy densification index (I_{ED}) are the main parameters in the evaluation of the torrefaction process. Specifically, the following definitions have been applied in the present Ph.D. work:

$$M_Y(\%, daf) = \left. \frac{m_{torrefied\ tomato\ peels}}{m_{tomato\ peels}} \right|_{daf} \tag{II.22}$$

$$I_{ED}(-)|_{daf} = \left. \frac{LHV_{torrefiedtomatopeels}}{LHV_{tomatopeels}} \right|_{daf} \tag{II.23}$$

$$E_Y(\%, daf) = M_Y(\%, daf) * I_{ED} \tag{II.24}$$

In keeping with Duhungana et al. (2013), these parameters were adopted also to assess the effect of reactor type on the torrefaction performance.

II.4.4.3.3 Data analysis

A final data analysis was performed on the experimental results from torrefaction tests with the following aims: i. comparing the main physical and chemical properties (i.e., elemental composition, calorific value, hydrophobicity, skeletal or true density) of raw and torrefied tomato peels; ii. developing simple descriptive mathematical models (i.e., multiple regression model) able to predict the dependence of the main physic-chemical properties of tomato peels and the process yields on both torrefaction temperature and time between.

In more detail, a multiple linear regression approach was performed by assuming the following general eq. II.25:

$$f(T, t) = z_o + a*T + b*t \tag{II.25}$$

where $f(T,t)$ is the value of the dependent variable (i.e., carbon content, heating value, mass and energy yields, etc.) to be predicted, T and t are the torrefaction temperature and time and, finally, z_o, a and b are the estimated regression coefficients. In this Ph.D. research work, the regression analysis was performed by using SigmaPlot© software.

Results and Discussion

III.1 Non-isothermal TG/DTG curves

III.1.1 Non-isothermal decomposition behavior of virgin olive husk

Mass loss (TG) and derivative mass loss (DTG) curves for the thermal decomposition of virgin olive husk (OH) at different heating rates (i.e., 2, 5, 10, 20, 40 °C/min) are shown in Figure III.1. As expected, due to the presence of residual oil that, inevitably and in a variable amount, remains trapped within the matrix of this residue after the extraction process (Brachi et al., 2015a), OH does not show the typical thermogravimetric behavior of a standard lignocellulosic biomass typically characterized by three decomposition phases, in addition to a first one associated with the removal of water and water soluble components. In fact, as shown by the thermogram recorded at the heating rate of 2 °C/min (Figure III.1) and zoomed for better readability in Figure III.2, five distinct weight loss phases could be identified on TG curve of OH. They are related to the four peaks observed on the DTG curve (the last three being partially overlapping) and to the final gently sloping baseline. The first phase, corresponding to the reduction in mass (≈ 4.5 wt.% of the total mass loss) at temperature lower than 150 °C, can be attributed to the removal of water and light volatiles. The second phase, between 150 and 275 °C, which accounts for approximately 23.4 wt.% of the total mass loss, can be attributed mainly to the thermal degradation of the hemicellulose fraction, which is the most reactive part of a biomass and typically decomposes in the range 220-280 °C (see "*Section I.3.1*"), and partly to the beginning of cellulose decomposition. The third phase (275-395 °C), which accounts for approximately 40 wt.% of the total mass loss, in turn can be attributed mainly to the thermal degradation of cellulose, typically occurring in a higher temperature range, i.e., of 240-350 °C (Tumuluru et al., 2011), and partly to the end of hemicellulose decomposition.
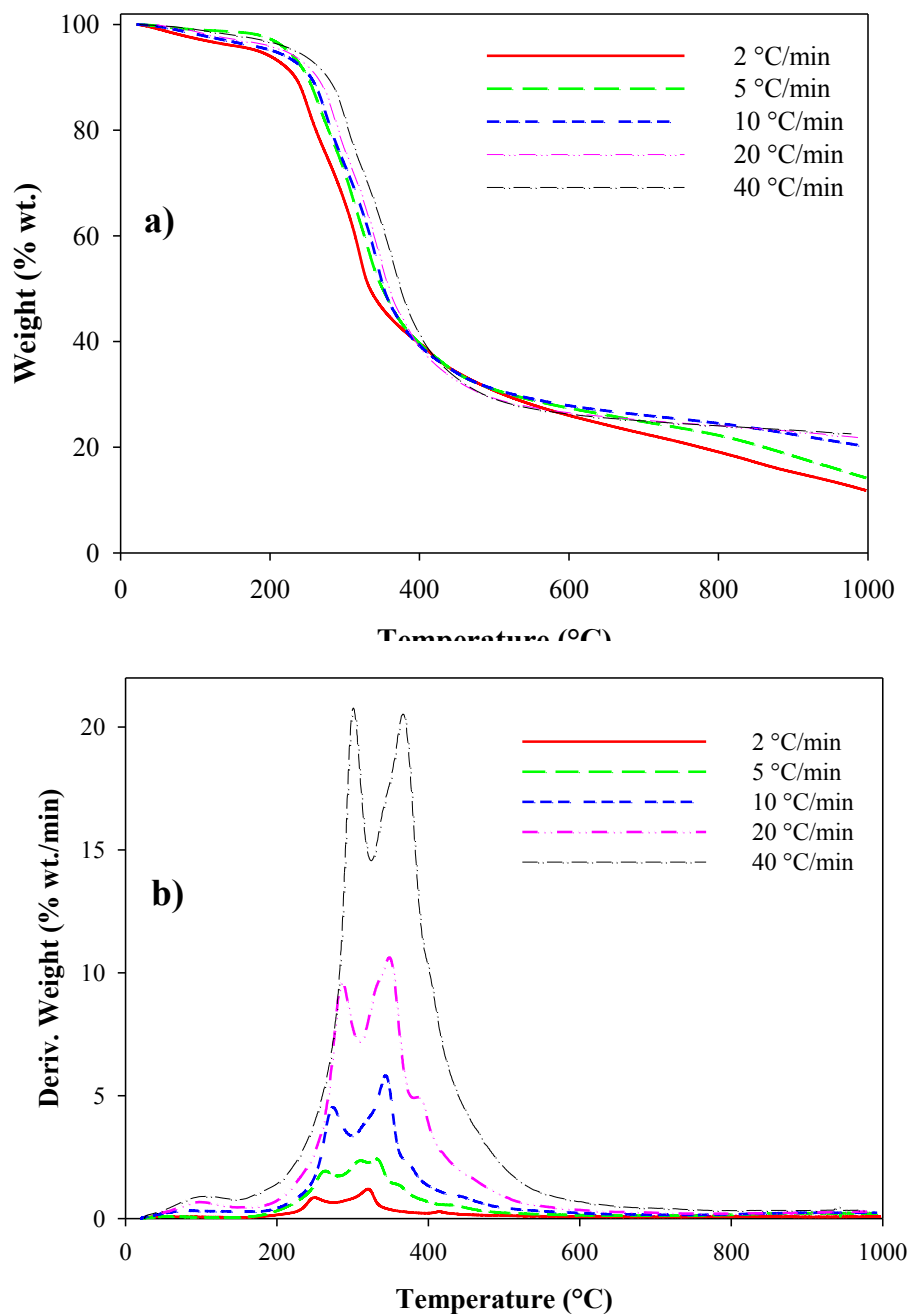
Figure III.1 *Virgin olive husk (a) TG and (b) DTG curves at different heating rates (i.e., 2, 5, 10, 20, 40 °C/min) recorded under nitrogen atmosphere with a purge rate of 100 ml/min from ambient temperature to 1000 °C.*

In the fourth phase, over the temperature range from 395 to 450 °C, there was a negligible weight loss ($\approx$ 6.9 wt.% of the total mass loss) that can be attributed to the thermal decomposition of the OH oily fraction. Finally, the fifth phase located between 450 and 1000°C corresponds to the slow (i.e., without a characteristic peak) weight loss of lignin whose degradation typically occurs over a wider temperature range (see "*Section I.3.1*") as a consequence of the different thermal stability of the various oxygen functional groups from its structure (Brebu and Vasile, 2010). This stage
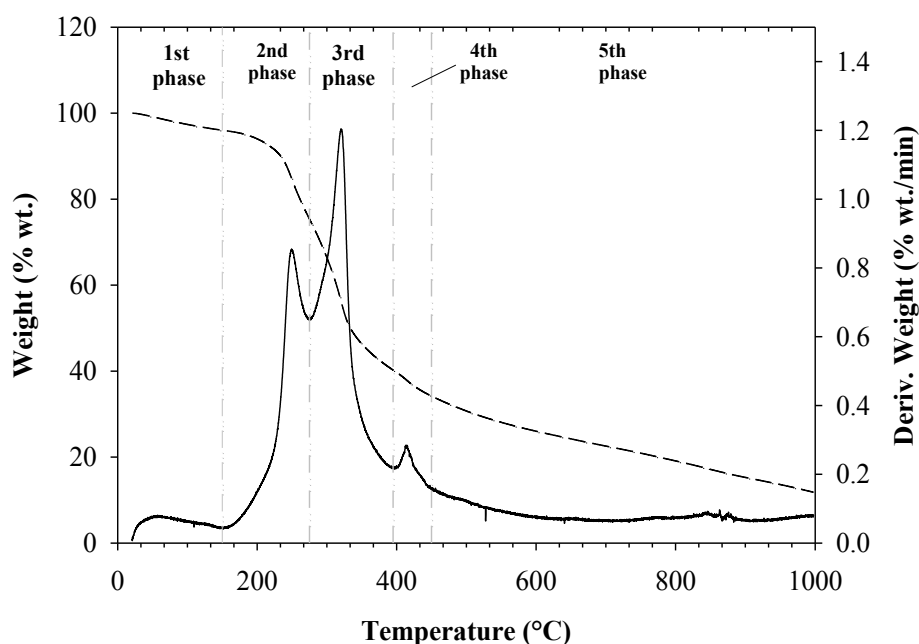
Figure III.2 *Virgin olive husk TGA (--) and DTG (−) curves at β=2 °C/min recorded in nitrogen atmosphere with a purge rate of 100 ml/min. Vertical dashed-dotted lines delimit the five distinct weight loss phases.*

The characteristics related to all decomposition phases such as the starting temperature (T_i), the ending temperature (T_f), the weight loss, the maximum weight loss rate (W_{max}) and the temperature (T_{max}) where this rate occurred, were exactly determined for all the investigated heating rates (i.e., 2, 10, 20, 40 °C/min) and their values are given in Table III.1. It is well known that the heating rate affects TG and DTG curves considerably (Yeng, 2008). More specifically, it can change the curve shape and characteristic temperatures indicated in a curve. In Figure III.1 the effects of the heating rate on the TG (Figure III.1a) and DTG (Figure III.1b) curves of OH are shown. It appears that higher heating rates gave globally a lower weight loss (or conversion). In addition, when the heating rate increases, TGA-curves are shifted toward the right and the peaks of DTG curves are slightly shifted towards higher

temperatures. Accordingly, all the characteristic temperatures in Table III.1 were shifted to higher values with increasing heating rate. The findings observed in this Ph.D. study are in agreement with those from previous investigations that have examined the same effects (Miranda et al., 2009).

III.1.2 Non-isothermal decomposition behavior of tomato peels

The TG and DTG curves of the of tomato peel residues under nitrogen atmosphere, recorded at five different heating rates (i.e., 2, 5, 10, 20, 40, 60 °C/min), are shown in Figure III.3a and Figure III.3b, respectively. The TG curves show the mass loss of tomato peels over the temperature range from room temperature up to about 1000 °C. It can be observed that the actual temperature range from the start to the finish of the tomato peel decomposition is narrower at a lower heating rate with respect to a higher heating rate (Figure III.3a). It also results that higher heating rates are accompanied by higher reaction rates and higher reaction temperatures (i.e., the DTG peak temperature shifts to a higher value with increasing heating rates), as shown in Figure III.3b. Moreover, the separation of the DTG peaks is more evident at low heating rates, even though it not clearly revealed in Figure III.3b due to the difference in scale between the different curves.

These findings agree with those found in literature for other kinds of biomass (Vasile et al., 2011). Basically, there are two reasons for the observed effects of the heating rate on the TG and DTG curve shape and characteristic temperatures. First, a high heating rate is more likely to generate a temperature difference between the sample and the TGA thermocouple built-in sensor. The real sample temperature may lag behind that of the thermocouple. Second, in a decomposition with volatile products, it takes time for those products to diffuse out of the sample and to be carried away by flowing gas (Leng., 2008). A low heating rate is more likely to generate thermal equilibrium and give a reproducible result for the analysis. Thermogravimetric measurements suggest that the thermal decomposition of the tomato peels is a rather complex process that occurs in several stages as it is clearly reflected by the presence of several DTG peaks (Figure III.3b). They are also reflected in less noticeable changes in the slope of the TG curves. The complicated thermal behavior exhibited by tomato peels is a likely consequence of its very complex chemical composition, which is characterized by the presence of several macro-components, i.e., cellulose, hemicelluloses and lignin and minor constituents (e.g., lipid, waxes, protein, oil, etc.) in different amounts (Lazos and Kalathenos, 1988; Knoblich et al., 2005).

Table III.1 *Virgin olive husk thermal decomposition at different heating rates (source: Brachi et al., 2015a)*

Decomposition phase	Parameter	$\beta = 2$	$\beta = 10$	$\beta = 20$
First decomposition phase	T_i	21.5	21.1	48.9
	T_f	152.2	175.4	282.2
	T_{max}	51	80.9	96.1
	W_{max}	0.1	0.3	0.7
	Weight loss	3.6	3.7	3.5
Second decomposition phase	T_i	152.2	175.4	182.2
	T_f	274.9	298.5	309.5
	T_{max}	249.5	272.7	286.6
	W_{max}	0.8	4.5	9.6
	Weight loss	20.9	24.0	23.7
Third decomposition phase	T_i	249.5	298.5	309.5
	T_f	395.7	436.7	378.5
	T_{max}	320.5	343.1	347.8
	W_{max}	1.2	5.8	10.6
	Weight loss	35.32	36.8	28.73
Fourth decomposition phase	T_i	395.7	436.7	378.5
	T_f	445.4	467.2	415.8
	T_{max}	413.5	442.5	388.9
	W_{max}	0.3	0.9	4.9
	Weight loss	6.0	2.3	7.56
Fifth decomposition phase	T_i	445.4	467.2	415.8
	T_f	1000	1000	1000
	T_{max}	-	-	-
	W_{max}	-	-	-
	Weight loss	21.86	12.34	14.52

Figure III.3 *Tomato peels (a) TG and (b) DTG curves at different heating rates (i.e., 2, 5, 10, 20, 40, 60 °C/min) recorded under nitrogen atmosphere with a purge rate of 100 ml/min from ambient temperature to about 1000 °C.*

The negligible weight loss (i.e., approximately 7 % wt.) observed at temperature lower than 200 °C can be attributed to the removal of moisture and to the start of polysaccharides hydrolysis (Aboyade et al., 2011), whereas the second and third decomposition stage can be most likely ascribed to the thermal degradation of hemicelluloses and cellulose (see "*Section I.3.1*"). Hemicelluloses typically decompose in the range of 160-360 °C, while cellulose degrades at the higher temperature range of 240-390 °C (Aboyade et al., 2011). However, a clear attribution of all the decomposition events or peaks to a specific chemical species appeared to be hardly achieved when analyzing the DTG profiles only, because mass losses of several minor chemical components probably occurred during each step at the same time.

III.2 TGA coupled with evolved gas analysis by MS

III.2.1 Isothermal TG/DTG curves and MS signal for olive husk

Figure III.4 shows the weight loss (TG) curves and derivative of the mass loss curves (DTG) obtained from three isothermal runs performed at 200 °C (a), 250 °C (b) and 300 °C (c), under inert atmosphere. They also include the temperature versus time plots describing the temperature program adopted. It results that the onset decomposition temperature of virgin olive husk, which is dictated by the thermal stability of its hemicellulose content (see Table I.13), is around 220 °C. This latter is the temperature corresponding to the onset of the second peak in the DTG curve at 250 °C (Figure III.4b) and 300 °C (Figure III.4c). The second peak in the DTG curve at 200 °C (Figure III.4a), which is characterized by an onset temperature of 145 °C, was instead attributed to the removal of extractives, which are believed to be not involved in the torrefaction decomposition reactions, but rather driven off the biomass by evaporation (Bergman and Kiel, 2005), just as for moisture. Data also show that the cellulose only starts decomposing at temperature higher than 250 °C, as suggested by the appearance of a third peak in the DTG curve at 300 °C (Figure III.4.c). The first decomposition stage was trivially attributed to the removal of moisture and light volatiles. In more detail it results that virgin olive husk heated to 200, 250 and 300 °C over a test time of 466, 475 and 485 min retained about 86.7 %wt., 65.0 %wt. and 43.7 %wt. of its initial dry mass, respectively. For each temperature, however, the most evident and considerable weight loss (approximately 40 - 60 %wt. of the total anhydrous mass loss) occurred in a narrow time range (i.e., approximately 50 – 80 min) beyond which an almost steady weight loss value was approached. This confirms that the temperature exerts a larger influence than time on the yield of the solid product under torrefaction conditions, in agreement with that observed by Carrasco et al. (2013).

Figure III.4 *TGA (---) and DTG (—) curves of virgin olive husk recorded under an inert atmosphere, following a quasi-isothermal, preset temperature program (—) up to: a) 200 °C, b) 250 °C and c) 300 °C.*

III.2.1.1 Evolved gas analysis

MS data in the mass to charge ration (m/z) range 0-200 were scanned during the thermal treatment of oven-dried virgin olive husk samples at three different torrefaction temperatures (i.e., 200, 250 and 300 °C), but many of these only showed noise during the experiments. This is expected to be mainly due to the little formation of these compound and/or condensation in the transfer line. MS signals that showed more than just noise are summarized in Table III.2.

For the assignment of the m/z signals, different MS libraries were consulted. However, since it is difficult to assign a given fragment to a single compound without confirmation of complimentary methods, the main MS signals detected in the present investigation were associated with the chemical species that are commonly present in the gas product of biomass torrefaction or early stage of pyrolysis. Taking into account this, the assignment of m/z signals to the fragment ions is presented in Table III.2. Basically, the main gases evolved during the thermal treatment of OH and their main signals include: i. the CH_3- fragment (m/z = 15), coming from methane and methyl group; ii. OH- (m/z = 17) coming from hydroxyl group; iii. water (m/z = 18); iv. various aldehydes (m/z = 29); v. CH_3O- coming from methyl alcohol (m/z = 31); vi. several alkyl carbocations coming from different hydrocarbons (m/z = 12, 13, 14, 26, 27, 29, 42); vii. acetic acid (m/z = 43, 45, 60) and vii. carbon dioxide (m/z = 44). Carbon monoxide, which together with the light hydrocarbons is one of the main gas typically evolved during biomass torrefaction, was not monitored in this investigation, due to the interference of the purge gas (i.e., N_2) in its main signal (i.e., m/z = 28).

Table III.2 *Assignment of Mass Spectrometric signals (Virgin Olive Husk)*

m/z	Assignation	200 °C	250 °C	300 °C
12	C^+, hydrocarbons		✓	✓
13	CH^+, hydrocarbons	✓	✓	✓
14	$CH_2{}^+$, hydrocarbons			✓
15	$CH_3{}^+$, coming from methyl group		✓	✓
17	OH-		✓	✓
18	H_2O	✓	✓	✓
26	$C_2H_2{}^+$, hydrocarbons	✓	✓	✓
27	$C_2H_2{}^+$, hydrocarbons	✓	✓	✓
29	CHO^+, Aldehydes, Hydrocarbons, Formic acid			✓
31	CH_3O^+, methyl alcohols			✓
42	$C_3H_6{}^+$, hydrocarbons		✓	✓
43, 45, 60	Acetic acid (CH_3COOH)		✓	✓
44	Carbon dioxide (CO_2)	✓	✓	✓

The possibility of interference at m/z=29 between light hydrocarbons, aldehydes and formic acid should also be considered. The acetic acid and methanol from acetoxy- (m/z = 43) and metoxy- (m/z 31) groups are typically the major constituents of volatiles released during the thermal degradation of hemicellulose together with light gases such as CO_2, CH_4, CO and traces of H_2 (Prins et al., 2006). The absence of signals at m/z = 31 and m/z = 43 in mass spectra recorded at 200 °C confirm the previous assumption (see "*Section III.2.1*") that the first chemical event of the virgin olive husk decomposition at 200 °C (i.e., the second peak in the DTG curve) is not related to the degradation of hemicellulose, but rather to the removal of extractives and light hydrocarbons. The removal of methoxy- group, CH_3O -, occurs also during the thermal decomposition of lignin (Yang et al., 2007). The evolution of gases corresponding to the m/z signals of 15, 18, 31, 42, 44, 60 from the MS spectra recorded at 300 °C is shown in Figure III.5. The spectra have been background corrected. It is worth noting that the MS
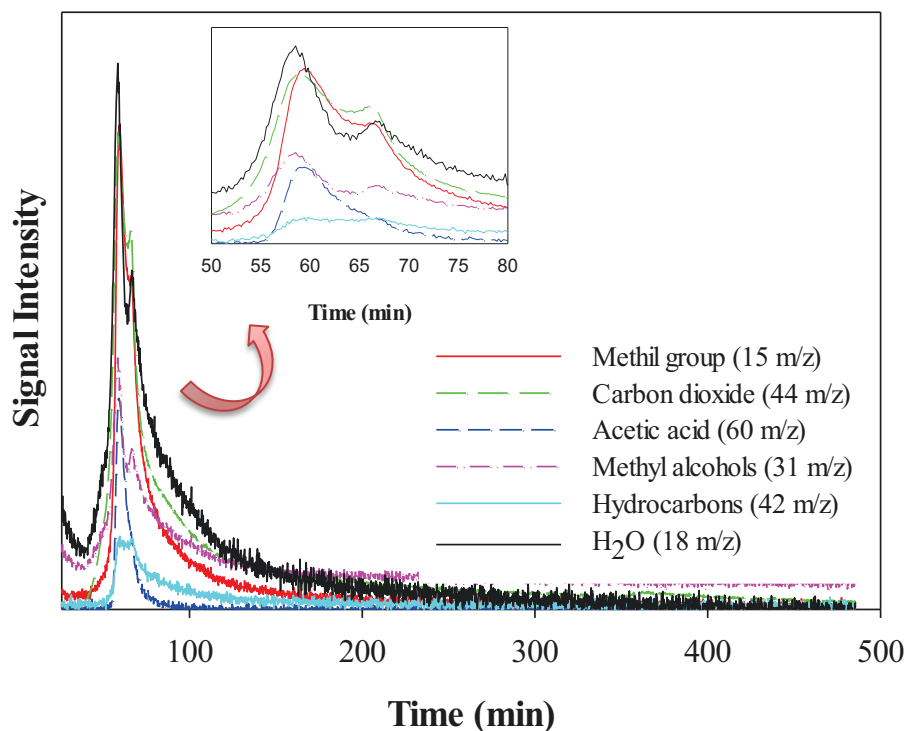
Figure III.5 *MS profiles of the main gases evolved during the isothermal decomposition of virgin olive husk at 300 °C.*

The zoomed spectra in Figure III.5 show that, with the sole exception of the acetic acid (m/z = 43), all the other species evolved exhibit two "rather

separated" maxima: the first one corresponding to their evolution from hemicellulose decomposition and the second one from cellulose decomposition. This is also confirmed by the fact that the mass spectrometric intensities belonging to the species plotted in Figure III.5 have a shape and time dependence similar to those of the DTG curve in Figure III.4c.

III.2.2 Isothermal TG/DTG curves and MS signal for tomato peels

Figure III.6 shows the weight loss (TG) and the derivative weight loss (DTG) curves from three isothermal runs performed at 200 (a), 250 (b) and (c) 300 °C, under inert atmosphere. It also includes the temperature versus time plot describing the adopted temperature program.

It results that the onset decomposition temperature of tomato peels (TPs), which is dictated by the thermal stability of its hemicellulose content (see "*Section I.3.1*"), is around 180 °C. This latter is the temperature corresponding to the onset of the second peak in the DTG curve at 200, 250 and 300 °C (Figure III.6). Data also show that the cellulose only starts decomposing at temperature higher than 250 °C, as suggested by the appearance of a third peak in the DTG curve at 300 °C (Figure III.6c). It is worth noting that, even though only a small amount of the cellulose typically degrades within the torrefaction temperature range (i.e., 200-300 °C), the water vapor and acids released from hemicellulose may also enhance its degradation (Nhuchhen et al., 2014). The first peak in the DTG curves shown in Figure III.6a-c, was trivially attributed to the removal of moisture and light volatiles.

In more details, TGA data show that tomato peels heated to 200, 250 and 300 °C over a test time of 467, 477 and 487 min retained, respectively, approximately 90.3 %wt., 69.1%wt. and 47.1 %wt. of their initial dry mass. For each temperature, however, the most evident and considerable weight loss (i.e., about half of the total anhydrous mass loss) occured in a narrow time range (i.e., approximately 45 -75 min) beyond which an almost steady weight loss value was approached. The above results confirm that the temperature exerts a greater influence than torrefaction time on the solid product yield, in agreement with that observed for virgin olive husk (see "*Section III.2.1*").
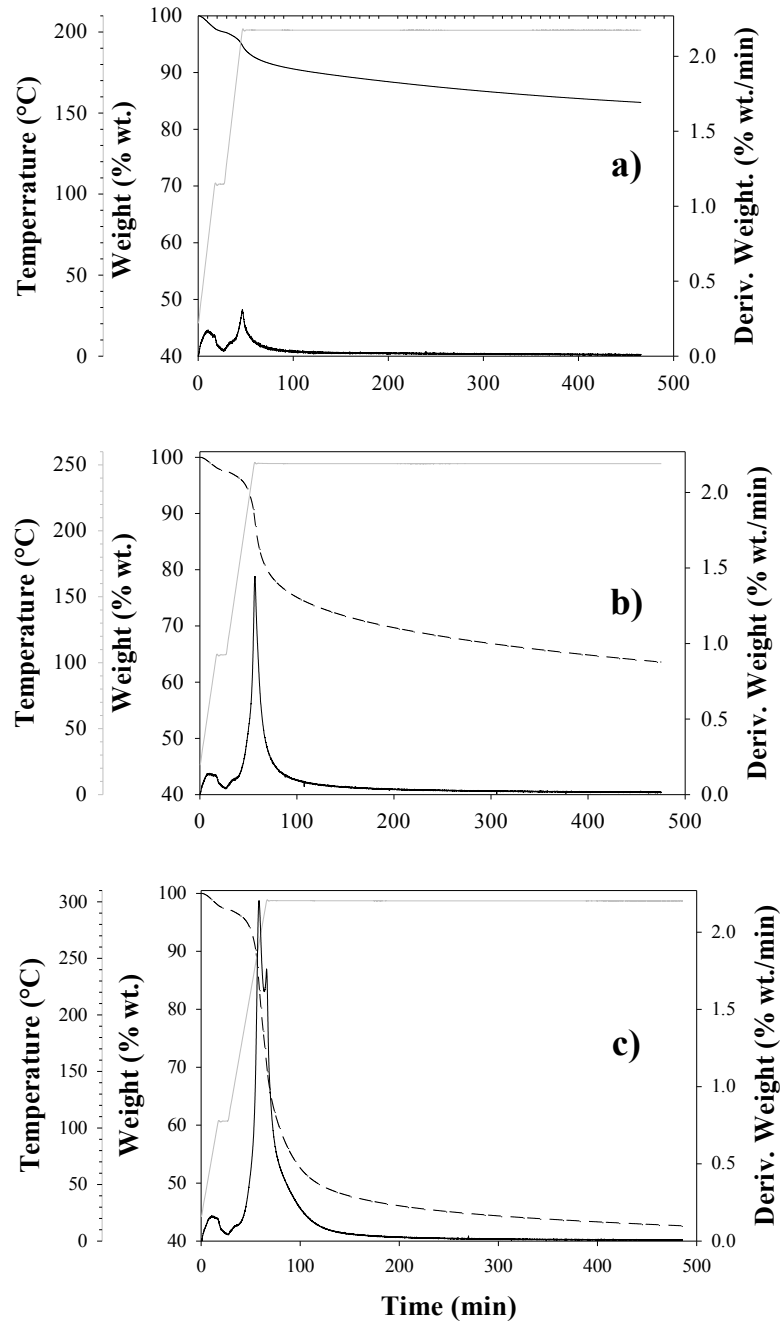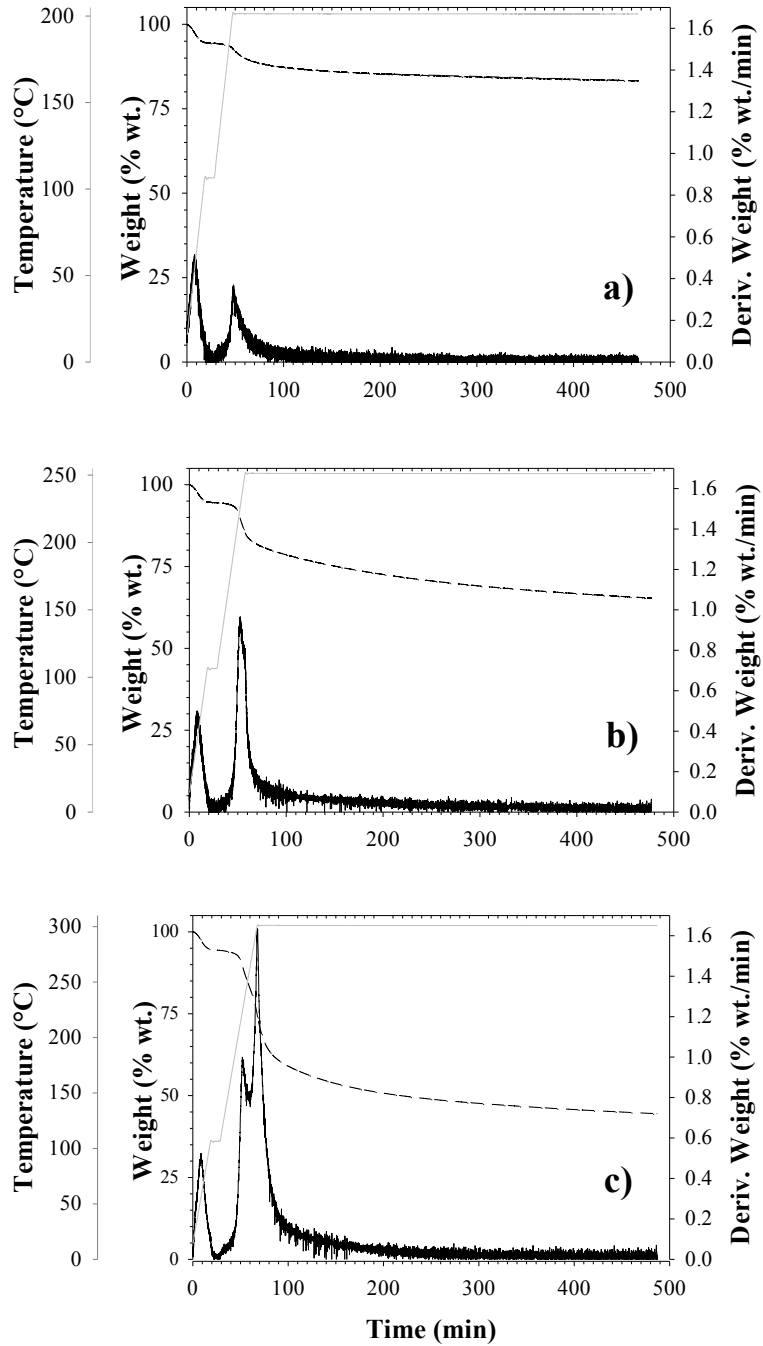
Figure III.6 *TGA (---) and DTG (—) curves of tomato peels recorded under an inert atmosphere, following a quasi-isothermal, preset temperature program (—) up to: a) 200 °C, b) 250 °C and c) 300 °C.*

III.2.2.1 Evolved gas analysis

MS data in the mass to charge ratio (m/z) range 0-200 were scanned during the thermal treatment of air-dried tomato peel samples at three different torrefaction temperatures (i.e., 200, 250 and 300 °C), but many of these only showed noise during the experiments. This is expected to be mainly due to the low release of these volatile compounds and/or condensation in the transfer line. Surely, the tar fraction (compounds having boiling points higher than 200 °C) were lost during measurements. The only MS signals that showed more than just noise are summarized in Table III.3.

Table III.3 *Assignment of Mass Spectrometric signals (Tomato Peels)*

m/z	Assignation	200 °C	250 °C	300 °C
12	C^+, hydrocarbons			
13	CH-	✓	✓	✓
14	CH_2^+, hydrocarbons			
15	CH_3^+, coming from methyl group			
17	OH-	✓	✓	✓
18	H_2O	✓	✓	✓
26	$C_2H_2^+$, hydrocarbons	✓		✓
27	$C_2H_2^+$, hydrocarbons	✓	✓	✓
29	CHO^+, Aldehydes, Hydrocarbons, Formic acid			
31	Methyl alcohols or methoxy (CH_3O-)		✓	✓
42	C_3H_6+, hydrocarbons			
43	Acetic acid (CH_3COOH)			✓
44	Carbon dioxide (CO_2)	✓	✓	✓

For a direct comparison between the gases evolved during the thermal treatment of tomato peels and virgin olive husk all the m/z signals previously listed in Table III.2 are shown in Table III.3, even though not detected during the thermal treatment of TPs. For the assignment of the m/z signals, the same approach described in III.2.1.1 was followed. Data show that the mass spectrum of tomato peel is much simpler than that of the virgin olive husk in Table III.2. Basically, the main gases evolved and their main signals were: i. OH- (m/z = 17) coming from hydroxyl group; ii. water (m/z = 18); iii. several alkyl carbocations (m/z = 13, 26, 27) coming from different hydrocarbons; iv. acetic acid (m/z = 43) and v. carbon dioxide (m/z = 44). Carbon monoxide, which together with the light hydrocarbons is one of the main gas typically evolved during biomass torrefaction, was not monitored in this investigation, due to the interference of the purge gas (i.e., N_2) in its main signal (i.e., m/z = 28). The evolution of gases corresponding to the m/z signals of 27, 31 and 44 from the MS spectra recorded at 300 °C is shown in Figure III.7. The spectra are background corrected. It is worth noting that the MS used is not calibrated for the detected mass to charge ratios, therefore the intensities of two peaks of different m/z ratio cannot be compared. The

zoomed spectra in Figure III.7 show that, unlike the methoxy group coming from methyl alcohols, carbon dioxide exhibits two "well-separated" maxima: the first one corresponding to evolution from hemicellulose decomposition and the second one from cellulose decomposition, as also suggested by the fact that the mass spectrometric intensities belonging to the species plotted in Figure III.7 have a shape and time dependence similar to those of the DTG

c

v
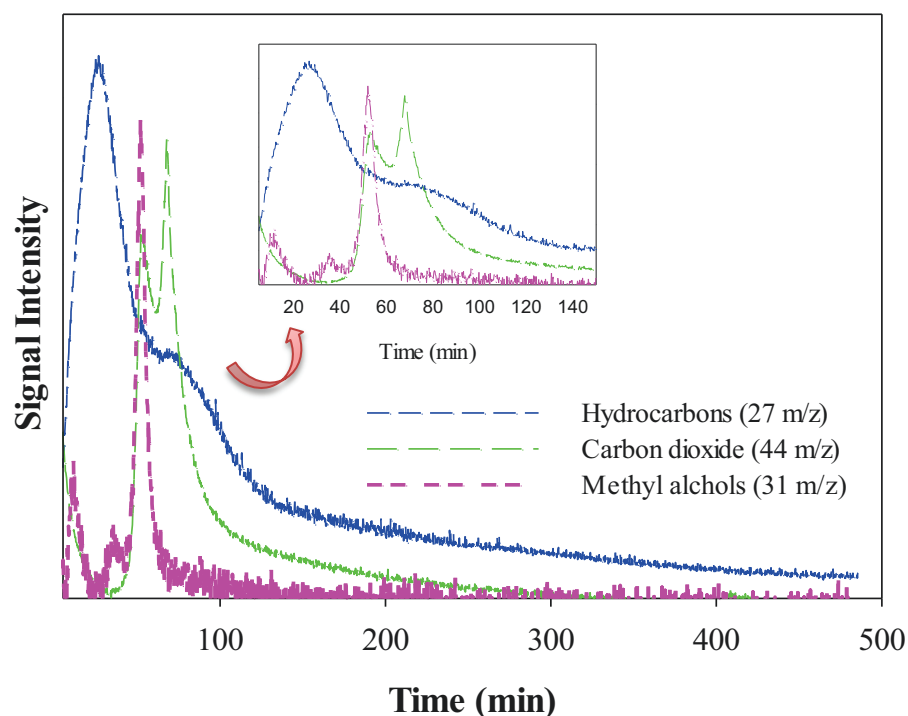
Figure III.7 *MS profiles of the main gases evolved during the isothermal decomposition of tomato peels.*

III.3 Isoconversional decomposition kinetics from non-isothermal

TG/DTG data

In this section, the results from the kinetic analysis of the thermal decomposition of olive husk and tomato peel residues, which are based on the isoconversional methods described in the "*Section II.3*" and non-isothermal thermogravimetric data described in the "*Section III.1*", are presented.

III.3.1 Dependence of activation energy on conversion degree for

the thermal decomposition of virgin olive husk

The OFW plots of $\ln(\beta_i)$ versus $1/T_{\alpha,i}$ for different values of conversion (α) are shown in Figure III.8. For each value of α, the apparent activation energy was calculated from the slope of the plotted regression line. The results obtained and the correlation coefficient (R^2) are listed in Table III.4 together with the values of the apparent activation energy E_α obtained by using the nonlinear Vyazovkin procedure. By comparing the aforesaid values of E_α (Table III.4), it results that the error in the activation energy, as induced by the approximation of the temperature integral used to derive the simplest linear eq. (II.9) on which the OFW method is based, can be considered reasonably small (Brachi et al., 2015a), being lower than the conventionally accepted 10% level of error in the activation energy (Vyazovkin and Wright, 1998). Hence, with regard to virgin olive husk decomposition, this means that the linear procedure may be conveniently used for computation of reliable kinetic parameters. The greatly reduced computational load as compared to the more accurate nonlinear Vyazovkin ation
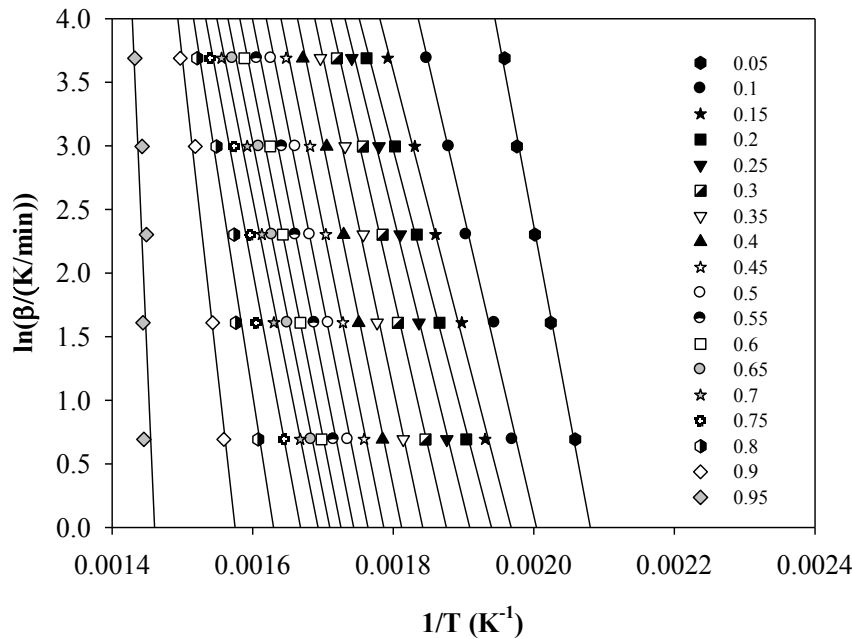
Figure III.8 *Isoconversional Ozawa-Flynn-Wall plot for virgin olive husk decomposition at different values of the conversion degree.*

Figure III.9 shows the dependence of the activation energy on the extent of olive husk conversion, as computed by both linear and nonlinear methods, in a temperature range of interest for a torrefaction process. A small decrease in the E_α appears at low conversion degree ($\alpha \leq 0.15$), followed by an almost constant (no multiple peaks and/or shoulders) value of E_α over the conversion range $0.2 \leq \alpha \leq 0.70$ and by a subsequent rapid rise of E_α for high values of α ranging between 0.75 and 0.95. It is worth noting that such trend reflects, in a way, the three main steps of thermal decomposition of olive husk (Figure III.1b), falling in the range 150-450 °C, where the kinetic evaluation particularly focused on (Brachi et al., 2015a).

Table III.4 *Activation energy for virgin olive husk decomposition by Vyazovkin and Ozawa-Flynn-Wall methods.*

	Vyazovkin method	Ozawa-Flynn-Wall method			
α (-)	E_α KJ·mol^{-1})	E_α KJ·mol^{-1})	Plot equation	R^2 **	Relative error*
0.05	244.76	232.85	$\ln\beta = -29463T^{-1}+61$	1.00	0.05
0.10	189.59	187.78	$\ln\beta = -23760T^{-1}+48$	0.99	0.01
0.15	162.59	169.16	$\ln\beta = -21404T^{-1}+42$	0.99	0.04
0.20	169.68	167.94	$\ln\beta = -21250T^{-1}+41$	1.00	0.01
0.25	196.57	177.87	$\ln\beta = -22506T^{-1}+43$	1.00	0.09
0.30	215.39	192.07	$\ln\beta = -24303T^{-1}+46$	0.99	0.1
0.35	226.59	205.87	$\ln\beta = -26050T^{-1}+48$	0.98	0.09
0.40	227.20	212.32	$\ln\beta = -27005T^{-1}+49$	0.99	0.07
0.45	225.56	216.11	$\ln\beta = -27345T^{-1}+49$	0.99	0.04
0.50	228.35	218.46	$\ln\beta = -27643T^{-1}+49$	0.99	0.04
0.55	227.73	219.27	$\ln\beta = -27745T^{-1}+48$	0.99	0.04
0.60	227.08	219.80	$\ln\beta = -27812T^{-1}+48$	0.99	0.03
0.65	222.22	218.37	$\ln\beta = -27631T^{-1}+47$	0.99	0.02
0.70	228.57	219.40	$\ln\beta = -27762T^{-1}+47$	0.99	0.04
0.75	263.22	219.40	$\ln\beta = -27762T^{-1}+49$	0.97	0.2
0.80	319.52	277.71	$\ln\beta = -35140T^{-1}+57$	0.96	0.1
0.85	407.85	387.98	$\ln\beta = -49093T^{-1}+77$	0.99	0.04
0.90	602.22	521.33	$\ln\beta = -65966T^{-1}+100$	0.92	0.1
0.95	1069.74	994.09	$\ln\beta = -125786T^{-1}+183$	0.44	0.07

* Relative error = $|E_{OFW} - E_{Vyazovkin}|/E_{Vyazovkin}$
**R^2 correspond to the linear fitting in Figure III.8

A comparison of the two trends, based on the values of the conversion degree, reveals that the first trend change observed in Figure III.9 at $\alpha = 0.15$ corresponds roughly to the maximum of the second peak of the DTG curves in the Figure III.1b as well as the second trend change, at $\alpha = 0.7$,

corresponds roughly to the maximum of the third peak of the DTG curves in Figure III.1b. Consistently, the lower the value of activation energy in Figure III.9 and the higher the weight loss rate in Figure III.1b.

Anyway, the apparent activation energy as given by both the linear (i.e., ranging between 167.94 and 994.09 kJ·mol^{-1}) and nonlinear (i.e., ranging between 162.59 and 1069.74 kJ·mol^{-1}) procedures show globally the same increasing dependence upon the conversion degree in the range 0.05-0.95 (Brachi et al., 2015a). This trend can be qualitatively explained by the fact that the residual biomass becomes increasingly more reluctant to further decomposition in a N_2 atmosphere as the conversion progresses. Note, however, that the lower value of the correlation coefficient at α=0.90-0.95 (Table III.4) implies that the corresponding values of E_α might be less reliable. As it is well known, during the torrefaction process, a biomass typically loses 20-35 wt.% of its initial mass, mainly as a consequence of the complete degradation of hemicellulose and of the partial decomposition of c
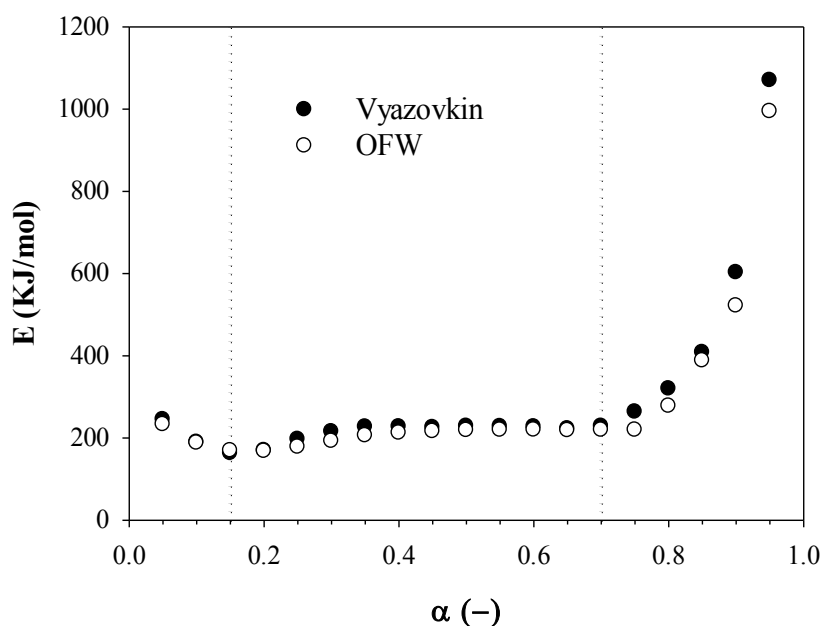
Figure III.9 *Dependence of the activation energy on the conversion degree as determined by the isoconversional Vyazovkin and Ozawa-Flynn-Wall methods.*

Accordingly, this means that over the range of interest for torrefaction (i.e., α ≤ 0.55 based on Eq. (II.14)) in Figure III.9, the apparent activation energy calculated for the thermal decomposing of virgin olive husk may be regarded as roughly constant, amounting to about 200 kJ·mol^{-1} by averaging E_α over α.
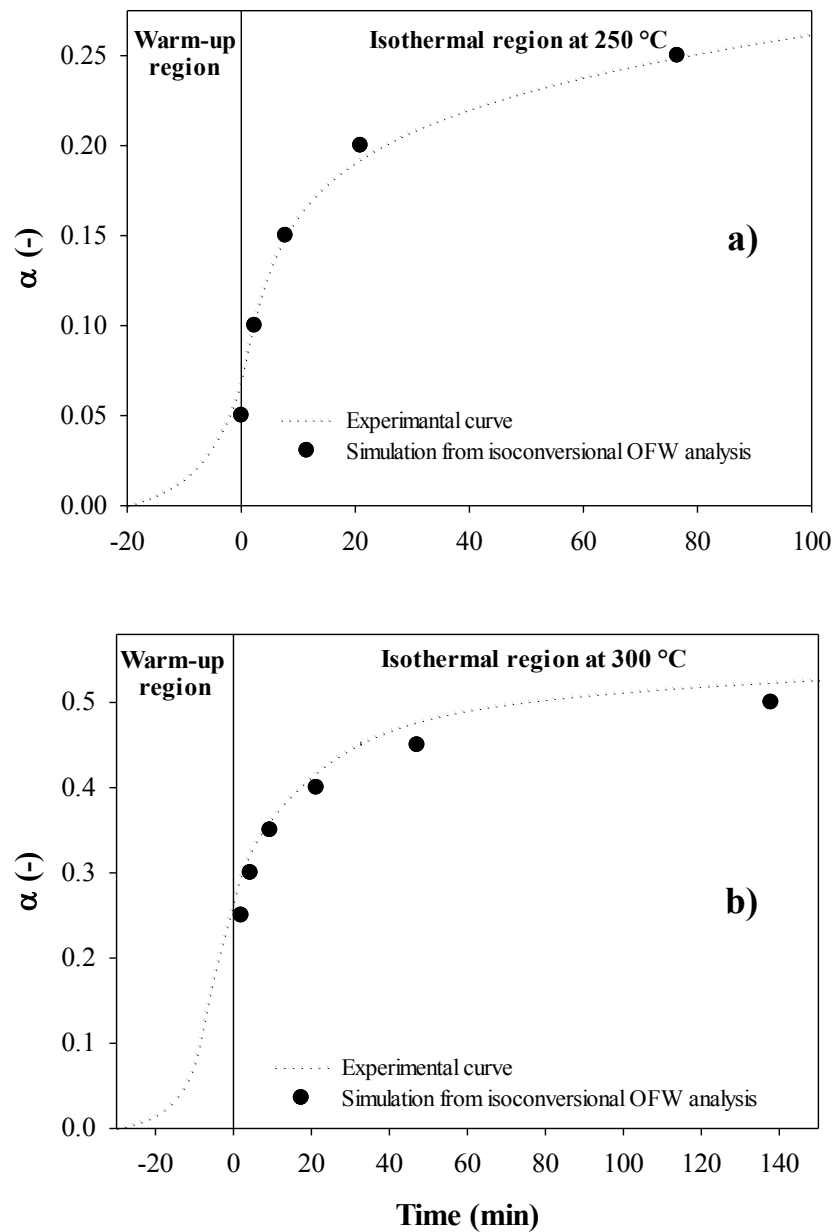
Figure III.10 *Comparison of predicted data and experimental curve for virgin olive husk decomposition at: a) 250 °C and b) 300 °C.*

This finding suggests that the torrefaction of virgin olive husk can be adequately described by a single-step model, which provides an adequate kinetic representation of a multi-step process having a single rate-limiting (Brachi et al., 2015a). Note that the averaging of E_α is a procedure that may

be justified only when a change in E_α as a function of α is just a few percent units of the mean value, but not when such a change is comparable to the mean value (Vyazovkin and Wright, 1998).

III.3.1.1 Validation of kinetic analysis approach

On the basis of the apparent activation energy dependence on the extent of decomposition, as obtained by OFW method, curves representing the conversion profile of virgin olive husk at two different isothermal conditions (i.e., 250 °C and 300 °C) were reproduced by the use of eq. (II.13). To give an indication of the reliability of the kinetic approach employed, the results of the above prediction were then compared with data obtained by isothermal TG analysis (Figure III.4(b)-(c)), not included in the kinetic computations.

It is worth observing that, according to the ICTAC Kinetics Committee (Vyazovkin et al., 2011), the validation of the computed kinetic parameters by demonstrating that they can be used to satisfactorily predict (reproduce) experimental curves non-included in computation rather than experimental curves used to derive the same parameters is a more rigorous approach. As shown in Figure III.10a-b, predictions are in excellent agreement with results from isothermal measurements. It is recalled that the dotted lines in Figure III.10a-b were derived from the isothermal data shown in Figure III.4a-b, respectively, whereas simulation results (i.e., circle symbols) were calculated on the basis of the dynamic TG curves (Figure III.1a), via OFW procedure. Note that, since the above simulations were performed by using eq. (II.13) that allows to compute the time at which a given conversion is reached at an arbitrary temperature under isothermal conditions, the comparison was focused only on the isothermal region of the thermograms at T=250°C (Figure III.4b) and at T=300 °C (Figure III.4c) and, more specifically, limited to the narrow time range (t ≤ 150 min) where the most rapid weight loss occurs.

III.3.2 Dependence of activation energy on conversion degree for

the thermal decomposition of tomato peel residues

The kinetics of the thermal decomposition of tomato peel residues in an inert atmosphere was studied by means of non-isothermal thermogravimetric analysis in the heating rate range 2-60 °C/min. Due to the complexity of the investigated process, which implies simultaneous multi-component degradation reactions, an analytical approach involving the deconvolution of the overlapping degradation steps from the overall differential thermogravimetric curves (DTG curve) and the subsequent application of

Friedman's isoconversional methods (see the "*Section II.3.3*") to the separated peaks was adopted.

III.3.2.1 Deconvoluted DTG curves for the thermal decomposition od

tomato peel residues under non-isothermal conditions

Deconvoluted DTG curves recorded at different heating rates (2, 5, 10, 20, 40 °C/min) are shown in Figure III.11 and the main corresponding separated peak data are listed in Table III.5.
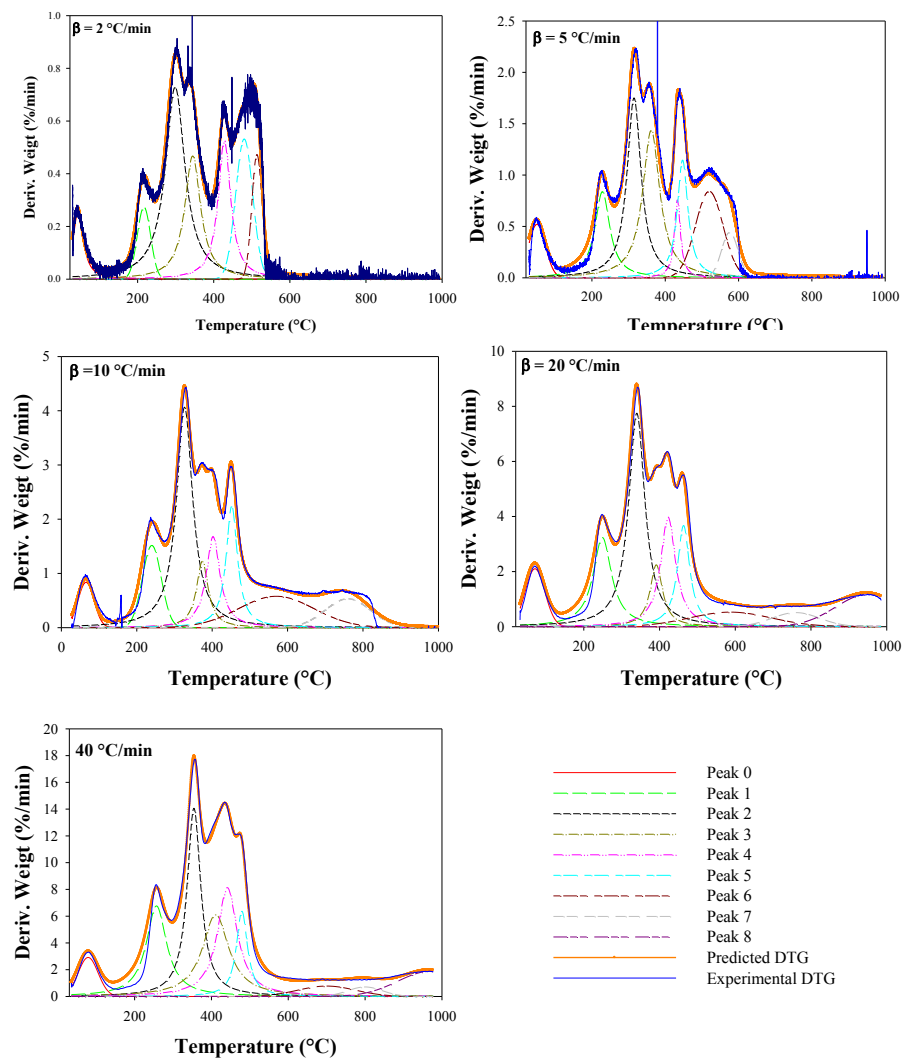
Figure III.11 *Deconvoluted DTG curves recorded at heating rates of 2, 5, 10, 20, 40 °C/min for tomato peel samples.*

Figure III.11 shows that the DTG curves were nicely fitted by Gaussian (eq. II.15) and Lorentzian (eq. II.16) equations. The percentage error of the fitted curves with respect to the experimental ones, as evaluated by the used deconvolution m-functions, was below 5%. The number of deconvoluted peaks was found to depend on the heating rate. Specifically, the deconvolution procedure evidenced seven peaks at the lowest heating rate (i.e., 2 °C/min), eight peaks at medium heating rates (i.e., 5 and 10 °C/min) and nine peaks at higher heating rates (i.e., 20 and 40 °C/min).

III.3.2.2 Activation energies of tomato peels pseudo-components

Based on the above evidence, it was assumed that the pyrolysis of TPs is a multistage process modeled by assuming independent parallel reactions corresponding to the decomposition of seven pseudo-components termed as A, B, C, D, E, F, G, some of which were defined as double or sum peaks, as shown in Table III.6. To obtain the kinetics of each pseudo-component, the corresponding peaks were extracted from the overall differential thermogravimetric curves (DTG curve) recorded at the different heating rates (i.e., 2, 5, 10, 20, 40 °C/min) and were grouped together in Figure III.12. As expected, by increasing the heating rate, the DTG curves of almost all TP pseudo-components are shifted to higher temperatures. The irregular peak shift with increasing heating rates, observed for the pseudo-components F and G, is most likely a result of the observed effects of the heating rate on the TG curve shape, as described in the *"Section III.1.2"*. The activation energies for each pseudo-component were obtained as a function of the conversion degree by using Friedman's isoconversional method, as described in *"Subsection II.3.3.2"*. In order to exclude the errors inherent to the initial and the end periods, only the data in the range of $0.1 \leq \alpha \leq 0.90$ have been considered. The results obtained and the related correlation coefficient, R^2, which reflects the scattering of the experimental data used, are listed in Table III.7. Figure III.13 shows that the activation energies of the separated steps are not all independent on the extent of conversion, which suggests a non-single step mechanism for each separated step, in particular for steps corresponding to pseudo-components B, C and G.

Note also that the lower value of the correlation coefficient observed for pseudo-components F and G (Table III.7) implies that the corresponding value of the activation energy might be less reliable. It is worth noting that the apparent activation energies obtained for pseudo-component B and C are consistent with the values reported in literature for hemicellulose (80-116 kJ/mol) and cellulose (195-286 kJ/mol), respectively (Branca et al., 2005; Gronli et al., 2002). As a consequence, the B and C peak may be associated with the thermal decomposition of hemicellulose and cellulose fractions, respectively (see *"Section III.1.2"*).
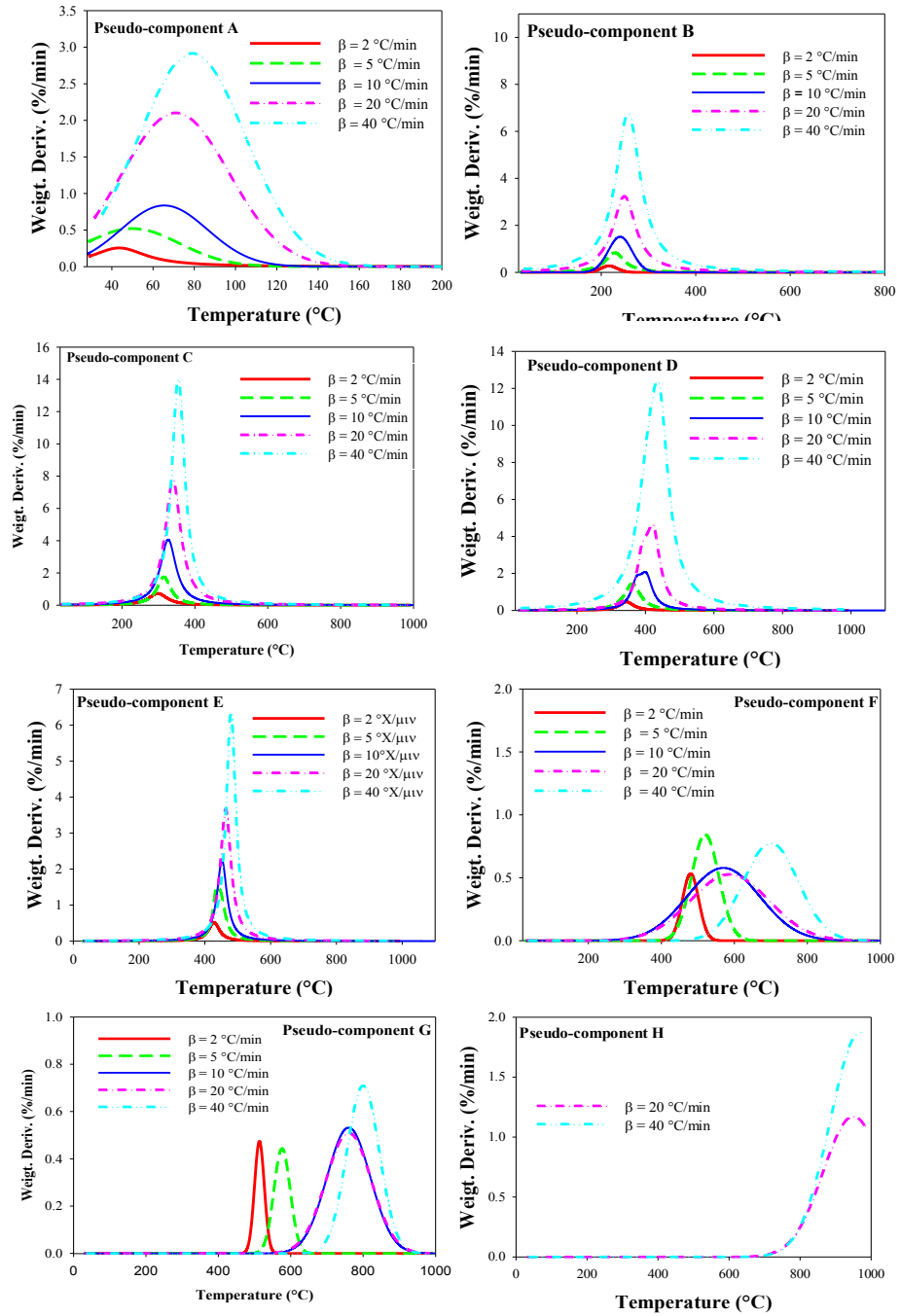
Figure III.12 *DTG of tomato peels pseudo-components obtained by the deconvolution of global DTG curves recorded at different linear heating rates (i.e., 2, 5, 10, 20, 40 °C/min)*

Table III.5 *Characteristics of deconvoluted peaks of TDG curves recorded at different heating rates*

Heating rate (°C/min)	Nr. of peaks	Peak 0		Peak 1		Peak 2		Peak 3		Peak 4		Peak 5		Peak 6		Peak 7		Peak 8	
		x_o	S	x_o	S	x_o	S	x_o	S	x_o	S	x_o	S	x_o	S	x_o	S	x_o	S
2	7	43.57	13	216.5	12	298.5	71	344.5	37	427.7	33	480.0	30	513.5	16	-	-	-	-
5	8	50.22	30	228.5	65	314.8	127	361.8	127	433.0	24	447.3	63	520	79	576.0	25	-	-
10	8	65.4	44	240.0	95	326.8	332	373.9	73	402.3	116	452.0	127	570.0	145	760	80	-	-
20	9	71.0	137	249.0	300	340.0	633	391.5	141	422.5	300	463.5	225	587	142	760	70	950	250
40	9	79.0	190	257	680	354.5	950	411.0	800	441.4	805	479.5	350	700.0	146	799.8	65	970.1	400

x_o, °C
S, %wt./min·°C

Table III.6 *Pseudo-components and deconvoluted peaks association*

Heating rate (°C/min)	A	B	C	D	E	F	G
2	Peak 0	Peak 1	Peak 2	Peak 3	Peak 4	Peak 5	Peak 6
5	Peak 0	Peak 1	Peak 2	Peak 3	Peaks 4+ 5	Peak 6	Peak 7
10	Peak 0	Peak 1	Peak 2	Peaks 3 + 4	Peak 5	Peak 6	Peak 7
20	Peak 0	Peak 1	Peak 2	Peaks 3 + 4	Peak 5	Peak 6	Peak 7
40	Peak 0	Peak 1	Peak 2	Peaks 3 + 4	Peak 5	Peak 6	Peak 7
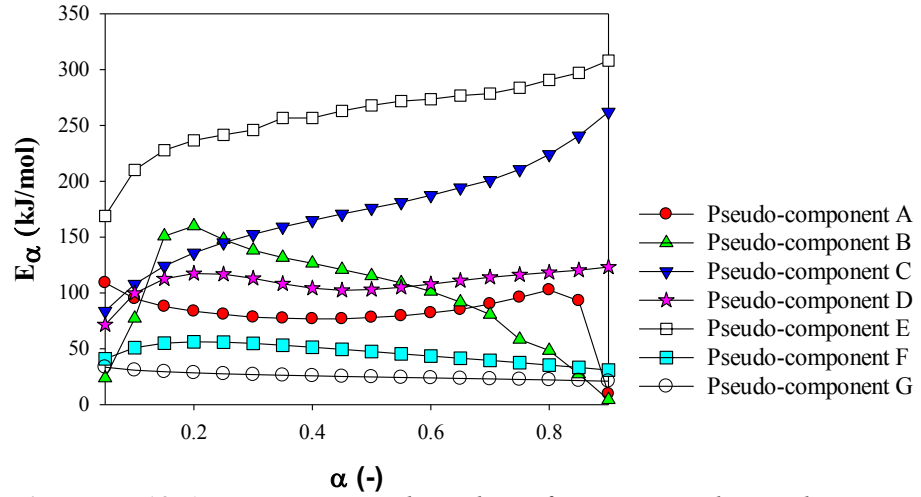
Figure III.13 *Activation energy dependence for tomato peels pseudo-components.*

III.3.2.3 Validation of the kinetic approach

Figure III.14 shows the simulated and the experimental conversion curves of tomato peels under dynamic conditions at the constant heating rate of 60 °C/min. It can be observed that in the range 0.00 to 0.80 of the conversion α, the curve generated by model calculation is a good reproduction of the experimental data (AVP = 2.6 %), though with a slight underestimation.
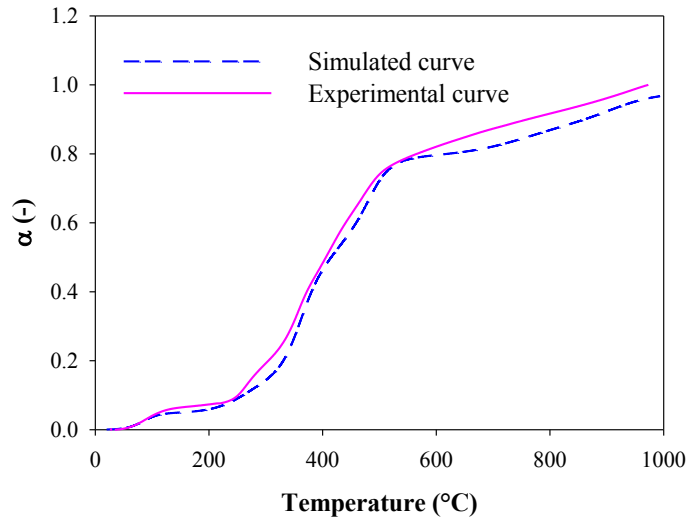
Figure III.14 *Experimental and simulated tomato peel TGA conversion curve under dynamic conditions at a constant heating rate of 60 °C/min.*

Table III.7 *Activation energies of the decomposition of tomato peels pseudo-components by Friedman's isoconversional method. The coefficient R² reflects the scattering of the used experimental data.*

Pseudocomponent	A		B		C		D		E		F		G	
α	E_α	R^2	E_α	R^2	E_α	R^2	E_α	R^2	E_α	R^2	E_α	R^2	E_α	R^2
0.1	94.84	0.90	77.29	0.44	107.88	0.98	99.68	0.88	210.12	0.96	50.99	0.84	30.89	0.47
0.15	87.89	0.93	150.86	0.84	124.14	0.99	112.63	0.96	227.86	0.99	55.06	0.91	29.53	0.46
0.25	80.87	0.96	147.87	0.99	145.06	1.00	116.80	0.99	241.63	0.99	55.95	0.94	27.65	0.43
0.3	78.30	0.97	138.26	0.99	152.54	1.00	113.02	0.99	245.92	0.99	54.83	0.92	26.95	0.42
0.35	77.43	0.98	131.70	0.98	159.15	1.00	108.21	0.99	256.66	0.99	53.24	0.90	26.33	0.41
0.4	76.81	0.98	126.56	0.98	164.97	1.00	104.32	0.99	256.66	1.00	51.45	0.87	25.80	0.41
0.5	78.12	0.98	115.30	0.97	175.96	1.00	103.05	0.99	267.95	1.00	47.52	0.81	24.81	0.39
0.55	79.47	0.97	109.00	0.96	181.09	0.99	105.08	0.99	271.79	1.00	45.54	0.77	24.36	0.39
0.6	82.19	0.96	101.37	0.94	187.40	0.99	107.92	0.99	273.49	1.00	43.53	0.74	23.92	0.38
0.7	90.19	0.91	80.77	0.82	200.85	0.98	114.08	0.99	278.51	0,99	39.61	0.68	23.03	0.37
0.75	96.10	0.84	58.46	0.68	210.70	0.96	116.36	0.98	283.75	0,99	37.57	0.65	22.60	0.36
0.8	102.69	0.71	48.41	0.47	224.10	0.94	118.37	0.97	290.74	0,98	35.45	0.61	22.16	0.36
0.9	9.67	0.01	4.41	0.01	261.98	0.77	123.28	0.91	308.06	0.94	30.93	0.54	21.02	0.34

E_α(MJ/kg) and α(-)

This is probably due to errors introduced, during the deconvolution, by the use of symmetrical functions, such as Lorenzian and Gaussian ones, which are not able to properly fit the asymmetries of the experimental peaks, these latter being due to inhomogeneity in particle size or shape (Perejòn et al., 2011). Again, the greater mismatch (AVP = 4.5%) between simulated and experimental data, above the conversion of 0.8, can be attributed to the lower reliability of values of activation energy related to pseudo-components F and G, which account for the last decomposition steps of tomato peels (i.e., above 600 °C). Anyway, a satisfactory global goodness-of-fit (global AVP = 3.5 %) was achieved. The number of experimental data considered were 1886, 1177 and 708 for conversion α in the range 0.00-1.00, 0.00-0.80 and 0.80-1.00, respectively.

III.4 Fluidization of tomato peels-sand binary mixtures

Figure III.15a-f show the profiles of the measured pressure drop as a function of superficial gas velocity for beds of sand (Fine-SS and Coarse-SS in Figure III.15a) and for the sand/tomato peels binary mixtures (i.e., TP/FSS and TP/CSS consisting of 1-2 mm TP particles mixed with fine and coarse silica sand, respectively) investigated at different mass fractions of TPs in the bed (Figure III.15b-f). Outcomes of cold fluidization tests clearly points out that, for the 1-2 mm TPs particle size, a change of the sand bed size significantly influences the fluidization behavior of the binary mixtures. A larger sand size not only led to a poorer fluidization quality, as confirmed by the more irregular pressure drop patterns observed in the case of the coarser silica sand (CSS) compared to the finer one (FSS) (Figure III.15c-d), but also resulted into a decrease of the maximum allowable biomass batch loading. Specifically, it was found that TP/CSS binary mixtures with a TPs content larger than 3.5 % wt. could not be fluidized since a few minutes after the fluidization medium (i.e. nitrogen) was blown upward and evenly through the bed , it exhibited a cohesive behavior turning into a packed bed, as shown in Figure III.16a-b.; vice versa, the TP/FSS mixtures exhibited a good fluidization behavior up to a TPs mass fraction equal to 9 % wt., as further proved by the data patterns in Figure III.15b-f.

The cohesive behavior of the TP/CSS binary mixtures is likely due to the electrostatic charges generated by sand particle-particle collision and particle-wall contact upon fluidization. Electrostatic charging of sand bed is a very complicate phenomenon, especially when handling of poly-disperse material because of bi-polar charging, with small particles being charged opposite to their larger counterparts (Zhang et al., 2015). In the specific case of sand and tomato peel binary mixture this phenomenon may be further enhanced by the fact that tomato peel particles also proved to be a material prone to charge polarization as shown in Figure III.16c.
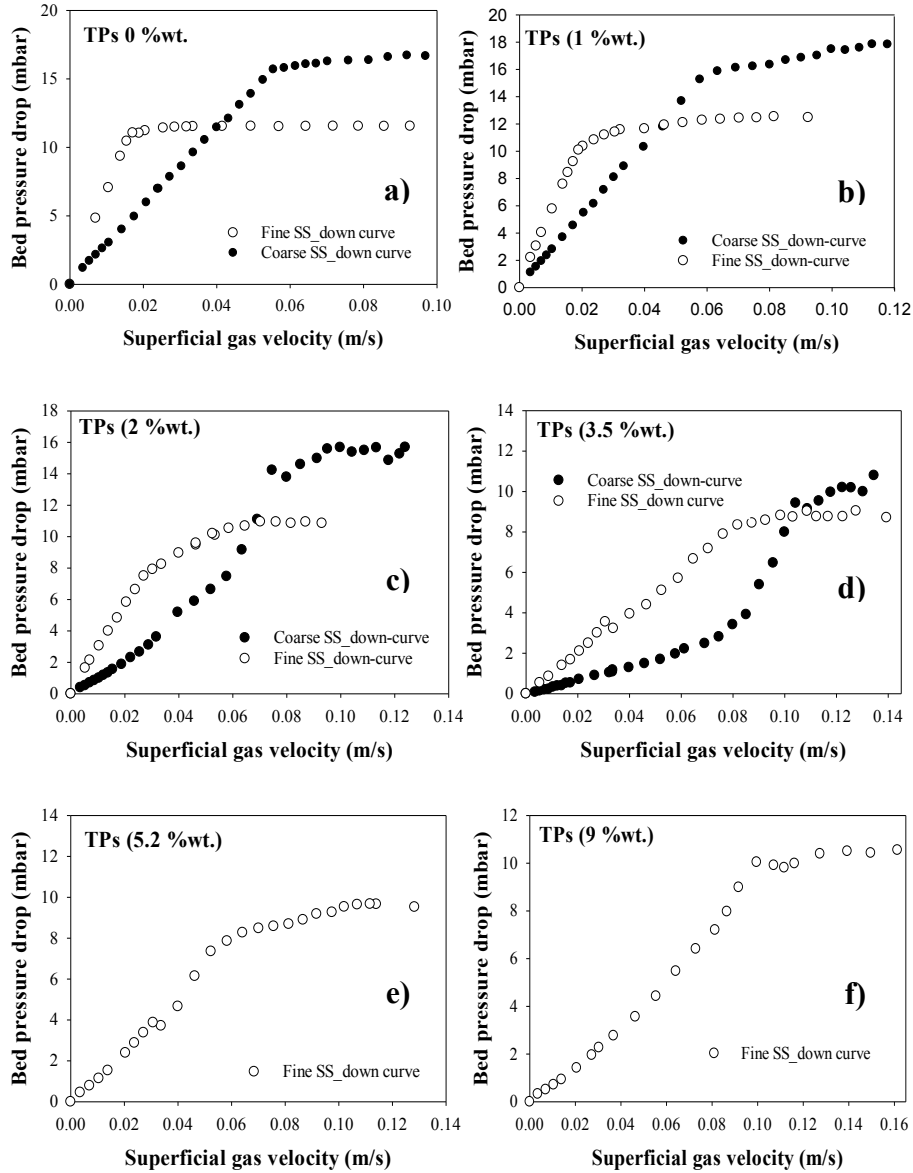
Figure III.15 *Pressure drop as a function of superficial gas velocity at ambient temperature: a) beds of sand (Fine SS or Coarse SS); b) 1 %wt. TP and Fine SS or Coarse SS ; c) 2 %wt. TP and Fine SS or Coarse SS; d) 3.5 % wt. TP and Fine SS or Coarse SS; e) 5.2 %wt. TP and Fine SS; f) 9 %wt. TP and Fine SS.*
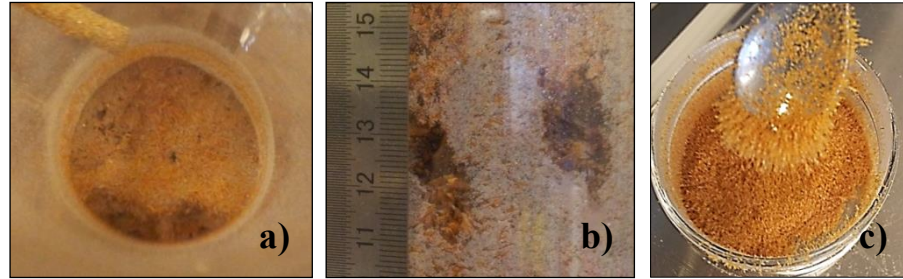
Figure III.16 *Cohesive behavior of a FSS and TPs (5.2 %wt.) binary bed, top view(a) and lateral view (b) and* (c) *tomato peels polarization after sieving (c).*

Table III.8 reports the values of the characteristic velocities (i.e., U_{mf}, U_{cf}, U_{ms}) obtained for the investigated TP/FSS and TP/CSS binary mixtures. It results that all the characteristic velocities increase with increasing the inert bed particle size and the mass fraction of the biomass in the bed. Figure III.17 reports trends of the characteristic velocities at ambient temperature. In more detail, results show that, while U_{mf} and U_{cf} increase quite linearly with the TPs mass fraction in the bed (Figure III.17a-b) for both the binary mixtures investigated, the minimum slugging velocity (U_{ms}) shows a different trend in the two cases (Figure III.17c).

Table III.8 *Characteristic gas superficial velocities as a function of the mass fraction of 1-2 mm tomato peel particles in beds of sand*

TPs (%wt.)	Fine silica sand			Coarse silica sand		
	U_{mf} (m/s)	U_{cf} (m/s)	U_{ms} (m/s)[**]	U_{mf} (m/s)	U_{cf} (m/s)	U_{ms} (m/s)[**]
0	0.017	-	0.093	0.057	-	0.106
1	0.022	0.058	0.092	0.061	0.080	0.113
2	0.040	0.070	0.093	0.083	0.095	0.118
3.5	0.086	0.098	0.122	0.107	0.113	0.122
5	0.082	0.102	0.112	-	-	-
9	0.123	0.127	0.139	-	-	-

[**] U_{ms} was determined by means of bed visual observation

In particular, in the case of TP/FSS mixtures, it remains nearly unchanged from pure sand value up to a biomass mass fraction of 2%, beyond which it also shows a linear growth. Conversely, the minimum slugging velocity of TP/CSS mixtures increases linearly with the biomass mass fraction over the whole investigated range. Since coarse silica sand (CSS) proved to be poorer as fluidizing material compared to the fine silica sand (FSS), this latter was selected to be used as inert bed component in subsequent fluidized bed torrefaction tests. Moreover, data show that, since the minimum slugging velocity of TP/FSS mixtures increases with the biomass mass fraction, but

not as fast as the complete fluidization velocity, when increasing the TPs mass fraction in the bed (Figure III.17d) the regime of good fluidization, whose boundaries are U_{cf} and U_{ms}, narrows.
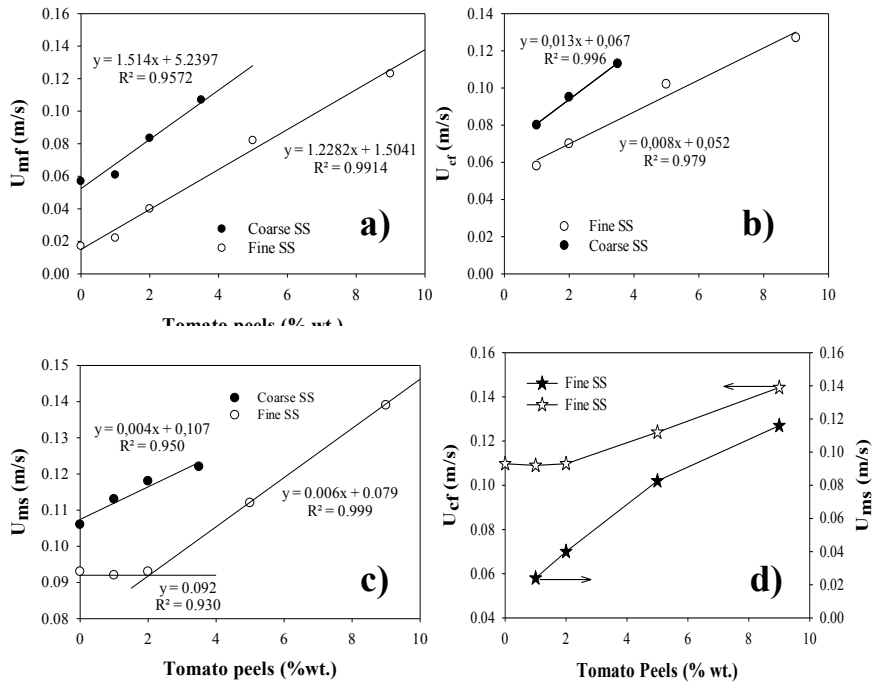
Figure III.17 *Characteristic velocities as a function of the TPs mass fraction in the bed: a. minimum fluidization velocity; b. complete fluidization velocity and c. minimum slugging velocity for both FSS/ TPs and CSS/TPs binary mixtures; d. complete fluidization velocity and minimum slugging velocity for FSS/TPs mixture.*

Therefore, even though it was possible to properly fluidize TP/FSS mixtures up to a biomass weigh fraction of 9 %, as a precaution, a biomass batch loading of 2%wt. (actually corresponding to 20 % by volume) was selected to be use in the subsequent "hot" fluidized bed torrefaction tests. It is worth noting that the present investigation at ambient temperature was not intended to be an exhaustive study of the optimal fluid-dynamics for the operation of the reactor, but rather it is to be considered as a starting point for the operation of the new FB torrefier.

III.5 Torrefaction tests

In this section the results obtained from fluidized bed torrefaction experiments performed on tomato peels are presented and discussed together with those from fixed bed torrefaction tests in order to compare the performance of both torrefaction concepts, mainly in terms of mass and energy yields. The effect of the main process parameters (i.e., temperature and reaction time) on the chemical-physical properties (i.e., elemental composition, calorific value and idrofobicity) of tomato peels are also presented and discussed to understand if such residue could benefit from torrefaction treatment as woody biomass does.

III.5.1 Results from fluidized bed torrefaction experiments

Table III.9 reports in a glance the main results from torrefaction tests performed on tomato peel residues. They are also redrawn in Figure III.18a-d in order to comparatively show the effect of the fluidized torrefaction process variables, i.e., temperature and holding time, on the key performance parameters (i.e., mass yield, M_Y, energy yield, E_Y and energy densification index, I_{ED}) and the main properties of the torrefied tomato peels (i.e., elemental composition, ash content, calorific values). Fluidized bed torrefaction tests were performed in duplicate on all the operating conditions investigated. Errors on mass yield were in the range 1-3 %wt.

As regards tomato peels, it was evident (Figure III.18a) that the dry matter loss was quite limited and lower than 25% wt., on dry-ash free basis (daf), even under the most severe torrefaction conditions (i.e., 285 °C and 30 min). The detected weight losses, however, did not involve a similar loss of energy (Figure III.18b). This suggests that the organic fraction released during the torrefaction treatment was characterized by an energy content lower than that of the residual solid product. An increase in the calorific value of tomato peels by a factor of about 1.2 was, in fact, achieved for the biomass torrefied at 285 °C and 30 min (Figure III.18c), providing a gross calorific value (HHV) on dry basis comparable to that of coal, i.e., ~ 30 MJ/kg (Table III.9). These results are in line with the typical mass and energy yields from woody biomass torrefaction treatment (Chew and Doshi, 2011) and, hence, encourage to consider tomato peels as a good candidate for torrefaction process. As can be seen from Figure III.18a-c, similar trend applies to all of the torrefaction performance parameters when the temperature is raised at constant holding time and, in parallel, when the holding time is increased at constant temperature. The effect of the reaction temperature, however, appears more pronounced than that of the holding time within the tested conditions, in agreement with TGA results (see "*Section III.2.2*"). Commonly, the energy gain versus mass loss of torrefied solids is ascribed to the fact that the latter predominantly arises from the

release of volatiles, which are richer in oxygen and hydrogen than in carbon (Medic et al., 2012). This was confirmed, in the present Ph.D. study, by the TG-MS analysis results (see "*Section III.2.1.1*"), which revealed the presence of water (H_2O), carbon dioxide (CO_2) and hydroxyl group (OH-) in the torgas evolved during the thermal decomposition of tomato peels in the temperature range of interest for torrefaction.
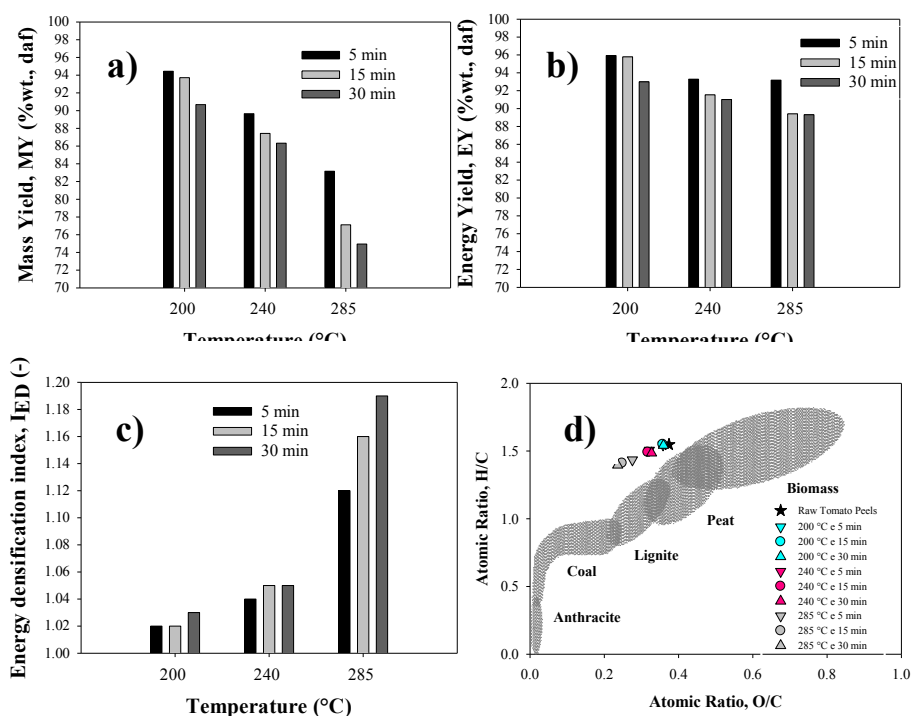
Figure III.18 *Mass yield (a), energy yield (b), energy densification index (c) and Van Krevelen diagram (d) for torrefied tomato peels from fluidized bed torrefaction tests.*

This phenomenon was also responsible for the decrease of the hydrogen-to-carbon (H/C) and oxygen-to-carbon (O/C) elemental ratios in torrefied tomato peels, as clearly emerges from the Van Krevelen diagram in Figure III.18d, where the elemental composition of TPs before (Table II.1) and after (Table III.8) the fluidized bed thermal treatment is reported in terms of O/C and H/C elemental ratios, on dry ash free basis. In more detail, the experimental points placed on this diagram (Figure III.18d) clearly show that the higher the torrefaction temperature, the more the composition of the torrefied tomato peels moves from the characteristic region of biomass to that of low-rank fossil solid fuels such as peat and lignite.

Table III.9 *Results from fluidized bed torrefaction experiments*

Test No	Temperature (°C)	Time (min)	M_Y (%)	E_Y (%)	I_{ED} (-)	HHV (MJ/kg)	LHV (MJ/kg)	Ash (%wt.)	C (%wt.)	H (%wt.)	N (%wt.)	O (%wt.)
1	200	5	94.44	95.93	1.02	25.89	24.23	2.97	58.62	7.61	1.58	29.22
2	200	15	93.72	95.79	1.02	26.07	24.39	2.94	59.29	7.69	1.79	28.29
3	200	30	90.68	92.99	1.03	26.25	24.56	2.57	59.53	7.74	1.82	28.35
4	240	5	89.66	93.29	1.04	26.68	24.98	2.33	61.35	7.76	1.51	27.05
5	240	15	87.43	91.54	1.05	26.75	25.07	2.60	61.88	7.71	1.60	26.22
6	240	30	86.33	91.01	1.05	26.93	25.25	2.58	61.65	7.72	1.52	26.53
7	285	5	83.16	93.18	1.12	28.40	26.71	3.03	64.12	7.72	1.58	23.55
8	285	15	77.12	89.41	1.16	29.21	27.53	3.41	65.36	7.73	1.90	21.60
9	285	30	74.95	89.31	1.19	30.03	28.33	3.29	66.40	7.78	1.66	20.87

Although to a lesser extent, the same occurs when increasing the time that the biomass is exposed to torrefaction. It is worth noting that the decrease of H/C and O/C elemental ratios upon torrefaction makes the biomass feedstock more suitable for fuel application resulting in less smoke and water vapor formation and reduced energy loss during subsequent combustion and gasification processes (Kumar, 2014). Conversely, no significant change in the nitrogen content has been observed from the raw TP (Table II.1) to the torrefied solids (Table III.9).

III.5.2 Equilibrium moisture content of torrefied products

The results from the equilibrium moisture content (EMC) tests performed on raw TPs and selected torrefied samples (i.e., torrefied TPs from fluidized
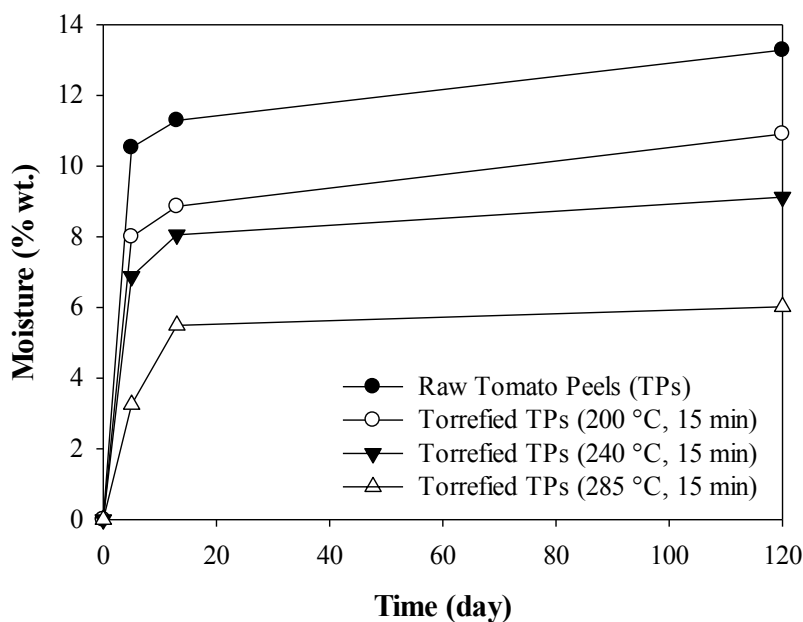
Figure III.19 *Equilibrium moisture content (EMC) of raw and torrefied tomato peel samples after exposure to 80 % relative humidity at ambient temperature.*

It is evident that all the tested samples did not fully reach their equilibrium or saturation levels of moisture content even after a long-term exposure to 80% relative humidity (HR). However, at each time the moisture uptake in torrefied samples was lower compared to that of the raw TPs to an extent that increased with a raising torrefaction temperature. Biomass feedstocks are typically hygroscopic in nature since moisture can be adsorbed into the cell walls and hydrogen-bonded to the hydroxyl groups of

the cell wall components (Chew and Doshi, 2011). Therefore, the loss of the OH⁻ group via dehydration reactions (see "*Section III.2.1.1*"), which tomato peels underwent during torrefaction treatment, can be held responsible for the lower moisture uptake of thermally treated samples compared to raw tomato peels. It is worth noting that the lower EMC associated with torrefied tomato peels can provide three main benefits: 1. reduced moisture level for the energy conversion process; 2. reduced transportation costs and 3. prevention of its decomposition during storage and transportation.

III.5.3 Results from fixed bed torrefaction experiments

Tables III.10 shows the main results obtained from fixed bed torrefaction experiments performed under the same conditions of tests No. 3 and 5 carried out in the fluidized bed reactor. It results that at 200 °C and 30 min the mass and energy yields in the indirect heated fixed bed reactor (i.e., 92.72 % and 94.03 % respectively, daf basis) were higher than that in the directly heated fluidized bed reactor (i.e., 90.68 % and 92.99 % respectively, daf basis). The lower degree of torrefaction (as represented by the weight loss) is further confirmed by the lower carbon and the higher oxygen content of the torrefied TPs from fixed bed test No.3 (Table III.10) compared to those from fluidized bed test (Table III.9), under the same operating conditions.

Table III.10 *Results for fixed bed torrefaction experiments*

	Test No 3	Test No 5
Operating conditions	**200 °C and 30 min**	**240 °C and 15 min**
Process yields (%, daf)		
M_Y	92.72	84.30
E_Y	94.03	91.68
Calorific Value (MJ/kg, db)		
HHV	26.14	27.81
HHL	24.44	26.08
I_{ED} (-)	1.01	1.09
Ash (%wt., db)	2.06	2.53
Ultimate analysis (wt.%, db)		
C	58.72	63.60
H	7.76	7.94
N	1.59	1.68
O (by diff.)	29.87	24.25

The non-uniform temperature distribution throughout the packed bed of TPs, which led to unevenly treated particles, as inferred from the non-uniform color change of torrefied tomato peels (Figure III.20b), might be responsible for the lower conversion degree of the TPs particles in fixed bed reactor compared to that in the fluidized bed reactor under the same operative conditions. In particular, the significant presence of orange-yellow particles (see the middle picture in Figure III.20b), representing almost-unreacted particles, is the primarily responsible for it.
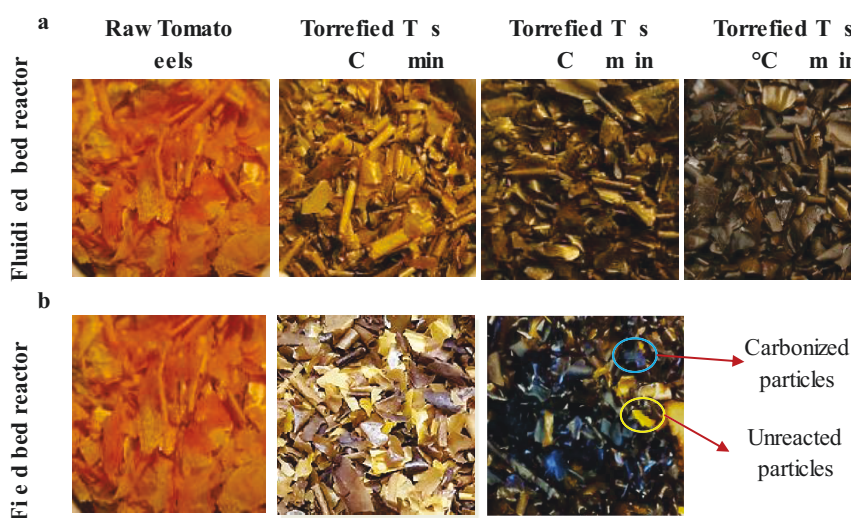
Figure III.20 *Solid product quality from: a). fluidized bed and b) fixed bed torrefaction experiments.*

Instead, the inverted trend in the mass yield which was observed at 240 °C and 15 min (i.e., 84.30 % wt. and 87.43 % wt. for fixed and fluidized bed, respectively) can be attributed to the substantial presence of over-carbonized particles (i.e., dark-black particles as a result of an extensive devolatilization of tomato peel particles), as shown in Figure III.20b (see the picture on the right), most likely arising from the occurrence of overheated zones in the reactor; the latter being, in turn, due to the combined effect of exothermic reactions - that typically appear at high temperature levels (Cavagnol et al., 2015) - and low heat transfer coefficients in packed beds. The higher energy densification (i.e., I_{ED} was equal to 1.09 in fixed bed test and 1.05 in fluidized bed test) arising from the presence of over-reacted particles can justify the fact that comparable values of energy yield were obtained from fixed and fluidized tests No.5, in spite of the lower mass yield from fixed bed test No.5. These results are in agreement with the higher carbon content and the lower oxygen of the torrefied TPs from fixed bed test No.5 (Table III.10)

compared to those from fluidized bed test (Table III.9), under the same operating conditions.

III.5.4 Discussion

Findings from fixed and fluidized bed torrefaction tests suggest that, at the laboratory-scale, where mass and heat transfer limitations are not negligible, the fixed bed torrefaction concept, which is actually the most widely used in torrefaction investigations at a scale larger than TGA, is not suitable to ensure a torrefied product of uniform quality and, consequently, to obtain reliable results on the effect of the main torrefaction parameters on both the solid product properties and the process performance parameters (i.e., M_Y and E_Y). Biomass feedstock has a very low thermal conductivity and heat capacity. These properties coupled with the thermal effect involved in the torrefaction process may create temperature gradients, mostly in torrefaction unit where the heat transfer is low, which may affect the torrefaction performance. The same challenges were, in fact, highlighted by Grigiante and Antolini (2015) who in their paper have recently argued on the significance of the results they obtained from torrefaction tests carried out in a bench-scale fixed bed torrefaction unit (i.e., 200 mm in length and 56 mm in diameter), employing both direct and indirect heat transfer mode. Conversely, sand-assisted fluidized bed technology proved to be particularly suitable for torrefaction applications, thanks to its ability to ensure a uniform temperature profile and consequently an even degree of torrefaction across the whole processed biomass batch, as demonstrated by the uniform change in color that tomato peels particles underwent when subjected to FB treatment within the tested conditions (Figure III.20a).

III.5.5 Mathematical models

By using the experimental data obtained from the fluidized bed torrefaction experiments and by implementing the general model (eq. II.25) in a regression analysis performed by using the SigmaPlot© software, the following multilinear eqs. (III.1)-(III.5) were obtained.

$$C \text{ (\%wt., db)} = 43.7554 + 0.0725 \cdot T(\degree C) + 0.0447 \cdot t(min) \qquad R^2 = 0.97 \quad \text{(III.1)}$$

$$O \text{ (\%wt., db)} = 45.5100 - 0.0783 \cdot T(\degree C) - 0.0506 \cdot t(min) \qquad R^2 = 0.94 \quad \text{(III.2)}$$

$$LHV \text{ (MJ/kg, db)} = 19.9535 + 0.0209 \cdot T(\degree C) + 0.0159 \cdot t(min) \qquad R^2 = 0.96 \quad \text{(III.3)}$$

$$M_Y \text{ (\%, db)} = 130.6892 - 0.1627 \cdot T(\degree C) - 0.2154 \cdot t(min) \qquad R^2 = 0.97 \quad \text{(III.4)}$$

$$E_Y \text{ (\%, db)} = 119.5931 - 0.1057 \cdot T(\degree C) - 0.1664 \cdot t(min) \qquad R^2 = 0.91 \quad \text{(III.5)}$$

Basically, these equations describe the elemental composition of the torrefied tomato peels (i.e., carbon and oxygen content), their calorific value and the mass and energy yields of the fluidized bed torrefaction process as a function of the temperature, T (°C) and holding time, t (min).

Of course, they hold just within the range of values investigated for torrefaction temperature (i.e., 200-285 °C) and holding time (i.e., 5-30 min).

No regression equations were developed for N and H since no significant change in their weight fraction was observed moving from the raw tomato peels to the torrefied ones, regardless of the torrefaction treatment conditions. As a consequence, the measured values N and H were simply averaged over the investigated conditions and turned out to be 1.66 and 7.72 % wt. (on dry basis), respectively.
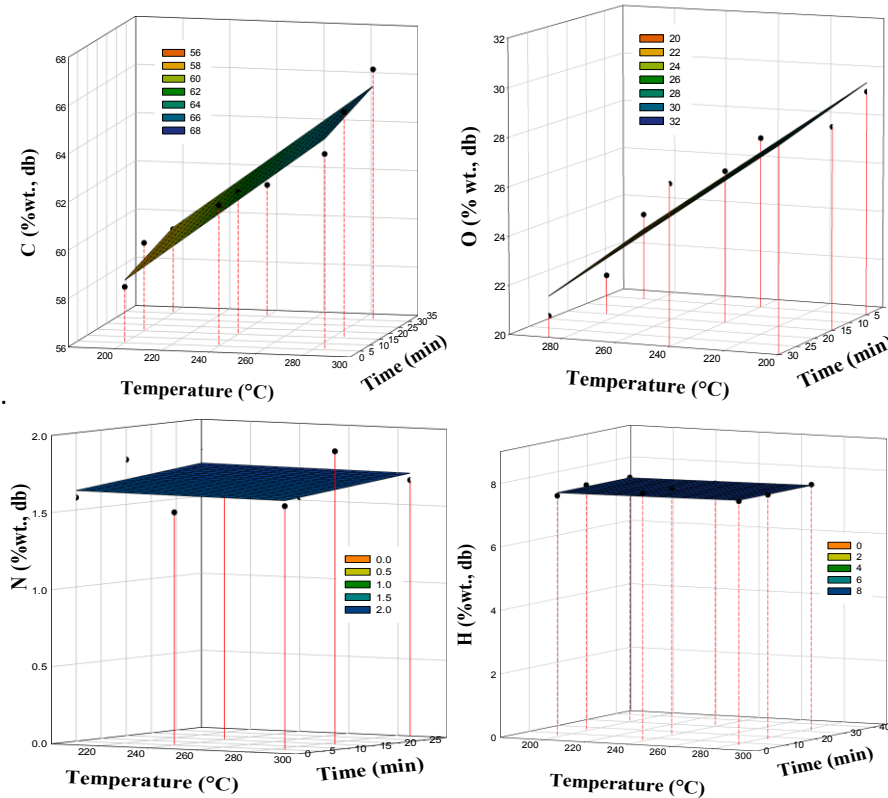
Figure III.21 *3-D plots of elemental composition of torrefied tomato peels with respect to the experimental data points.*

Figure III.21 and III.22 show that the fit between the models (i.e., surface plots) and the experimental data (i.e., points) is reasonably satisfactory. This is also reflected in the values of the correlation coefficient, R^2, which were

0.97, 0.94, 0.96, 0.97 and 0.91 for the carbon content, the oxygen content, the low heating value, the mass yield and energy yield, respectively. This implies that the above regression models can adequately represent the experimental data and can be used to predict the process yields as well as the main solid product properties for tomato peel torrefaction process based on fluidized beds.
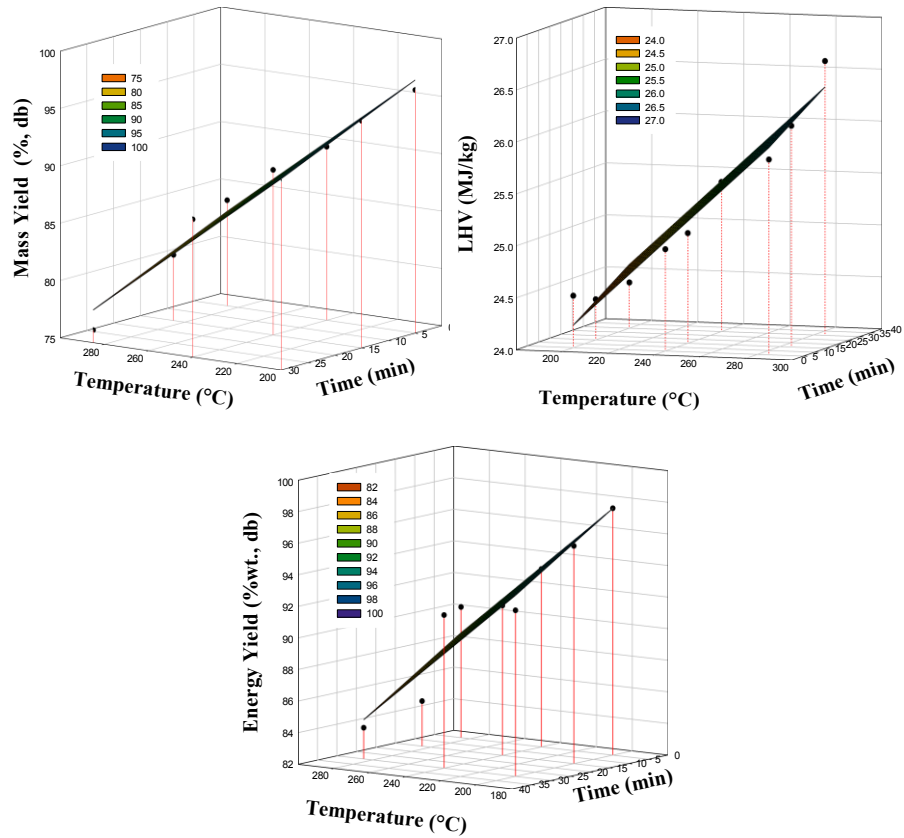
Figure III.22 *3-D plots of the mass yield, the energy yield and the low heating value of torrefied tomato peels with respect to the experimental data points.*

Concluding Remarks
and Future erspect ives

This Ph.D. project successfully explored a new and promising route for the disposal and recovery of low value agro-industrial residues *via* torrefaction treatment. The first phase of the project involved a screening of the agro-industrial residues available in Campania region (Italy) with good potentiality for energy applications. As a result of this analysis, tomato processing residues and olive mill residues, which have stood out as those in need of a more sustainable and environmental friendly disposal solution, were at first selected as biomass feedstocks for this Ph.D. project. However, practical difficulties encountered in the pre-treatment of the virgin olive husk (i.e., specifically in reducing the size of olives stone fragments which compose olive mill residues together with the olive pulp) led afterwards to discard such residue as a potential feedstock for subsequent torrefaction tests.

The potential of the torrefaction treatment for upgrading industrial tomato peels from Campania region (Italy) into high-quality solid energy carriers was investigated in a new lab-scale batch experimental apparatus based on fluidized bed technology, purposely designed and set up for this Ph.D. research work. Firstly, it was investigated the fluidization behavior of tomato peels particles (TPs) also in mixture with inert sands, in order to identify operating conditions (e.g. biomass particle size, mass fraction of biomass in the binary mixture) ensuring a proper fluidization of the bed materials (e.g. preventing channeling and segregation phenomena) during torrefaction experiments. This aspect is essential to achieve a simple and reliable thermal control of the torrefaction process (obtaining isothermal conditions), to avoid hot spots into the reactor, potentially deriving from highly exothermic reaction involved in the torrefaction process, and to obtain a uniform quality of the torrefied product.

Specifically, fluidization tests of air-dried tomato peels showed that the residue could not be fluidized because of its irregular shape (i.e., flat-like particles), pliable nature and large particle size. In addition, air-dried and ground tomato peel particles exhibited the Geldart C cohesive fluidization behavior, with significant channeling, likely as a result of their propensity to electrostatic charging. On the other hand, fluidization studies performed on sand and tomato peels binary mixtures, by varying the biomass weight fraction in the range 2-9 %, showed that the addition of a denser and more regular inert material (i.e. silica sand) to the irregular biomass particles allows to establish proper dynamic fluidization conditions. These findings suggest that the sand-assisted fluidized bed torrefaction concept, not investigated in the pertinent literature so far, could allow to handle a wider spectrum of biomass feedstocks by properly selecting the mixture properties (e.g., biomass particle size, biomass weight fraction, inert bed component size and density). Nevertheless, the separation of the solid inert heat carriers could be a limitation of this technology. Therefore, the possibility to switch the proposed sand-assisted fluidized bed torrefaction process from the batch to a continuous operation mode, the latter conceived to separate the solid product from the inert bed component (e.g., by exploiting mechanisms of density- or size- segregation), should be pursued in the future.

Fluidized bed torrefaction tests were carried out to investigate the effects of the main process variables (i.e. torrefaction temperature and holding time) on the main process performance parameters (i.e., mass and energy yield) as well as the main properties (i.e., elemental composition, calorific value, hydrophobicity) of the solid product . Specifically, experimental runs were performed at 200, 240, and 285 °C and for holding times equal to 5, 15 and 30 min. Results showed that the thermochemical transformations that tomato peels underwent, as a results of the release of volatile matter arising from the thermal decomposition of its organic constituents, led to significant improvements of their chemical and physical properties. In particular, it was observed that higher temperatures and longer holding times (with a more marked effect of the torrefaction temperature) determine an increasing in the calorific value (by a factor of 1.2 for the biomass torrefied at 285 °C and 30 min), a reduction of the O/C (up to approximately 40 % for the biomass torrefied at 285 °C and 30 min) and an improved hydrophobicity of the torrefied biomass with respect to the parent one, while maintaining the mass yield (approximately between 75 and 94 %, daf basis) and energy yield (approximately between 90 and 96 %, daf basis) at acceptable levels. These results are in line with the typical values of mass and energy yields obtained from the more established woody-biomass torrefaction treatment and, hence, encourage to consider tomato peels as a good candidate for the torrefaction process. In this regard, it is worth noting that, under the same torrefaction operating conditions, mass and energy yield and, consequently, the key

properties of the torrefied product can considerably vary for non-woody biomasses (e.g., agro-industrial, herbaceous and crop residues) that are very different in their polymeric composition depending on their origin. In fact, torrefied non-woody biomasses have a wider spread in both mass (typically from 24 to 95% of its original weight) and energy (typically from 29 to 98 %) yields when compared to torrefied woody-biomass.

Outcomes retrieved from this research work also highlighted that sand-assisted fluidized bed reactors are particularly suitable for the torrefaction of agro-industrial residues. In fact, the large thermal inertia and the high heat transfer rate within the dense bed of sand make this technology particularly suited to cope with the exothermicity associated with the thermal degradation of non-woody biomass, which tends to ignite or carbonize easily during torrefaction. This conclusion was also supported, in this Ph.D. Thesis, by a comparison of results obtained from fluidized bed torrefaction tests, employing direct particle-particle heat transfer mode, with those obtained from torrefaction experiments performed in a bench scale fixed bed experimental apparatus, employing indirect wall-particle heat transfer. Outcomes revealed that at the laboratory-scale, where mass and heat transfer limitations are not negligible, the fluidized bed is more suitable to obtain reliable test results, good-quality of the torrefied solids and excellent process performance in terms of mass and energy yields with respect to the fixed bed configuration under identical operating conditions. This is due to the ability of the fluidized bed to ensure a uniform temperature profile and, consequently, an even degree of torrefaction for the whole processed biomass feedstock. However, the comparison with other mixed systems (e.g., rotating tubular reactors), which have already gained some popularity and faced some applications in torrefaction, can be an aspect to be considered for further future investigation developments.

Apart from the reactor technology and the related performances, the viability of the torrefaction process also depends on the heat integration design. Due to its inherent features, it is well suited to be energetically integrated with other processes (e.g., gasification) where available low-value heat can be used for supplying the heat demand of both the drying step, which commands the larger process energy input, and the torrefaction stage. Therefore, an interesting topic for future work may be to investigate different thermal integration scenarios by means of process modeling software, such as ASPEN-Plus®, in order to identify those characterized by the maximum energy and cost efficiency. In this regard, results obtained in this Ph.D. Thesis could be helpful in providing useful tools in the form of: i. simple mathematical models (i.e., multiple regression models) able to predict the changes in the chemical composition and the calorific value of tomato peels over the range of the investigated torrefaction conditions and ii. model-free predictive equations able to predict the characteristic time needed to

achieve a desired conversion degree under typical torrefaction conditions, which were developed through the isoconversional kinetic analysis of thermogravimetric data (TGA).

In this Ph.D. work, the kinetics of the thermal decomposition of both virgin olive husk and tomato peels residues were also investigated by non-isothermal TGA at different heating rates (i.e., 2, 5, 10, 20, 40 °C/min) in order to derive model-free predictive equations, by means of isoconversional methods, for process modeling purposes. Specifically, thermogravimetric measurements performed on tomato peels highlighted that the thermal decomposition of this residue is a rather complex mechanism, which occurs in several simultaneously running stages with overlapping peaks. Therefore, an analytical approach involving the deconvolution of the overlapping degradation steps and the subsequent application of model-free kinetic methods to the separated peaks, was successfully used. In particular, the Friedman's differential isoconversional method allowed to evaluate the dependence of the activation energy on the extent of conversion for individual pseudo-components resulting from the deconvolution procedure. The computed kinetic parameters proved to be suitable for the prediction of the behavior of the sample over the range of the dynamic heating conditions at which the same parameters were determined, i.e., 2-40 °C/min. Specifically, the reliability of the evaluated kinetic parameters was verified by successfully simulating a thermogravimetric profile recorded at the heating rate of 60 °C/min. Theoretical and experimental data showed a good agreement for conversion between 0.2 and 0.8. However, it is believed that better results might be achieved by further refining the deconvolution procedure. In the case of olive husk, a comparison between two different integral isoconversional methods, i.e., the nonlinear Vyazovkin incremental approach, which is more rigorous but time-consuming, and the linear Ozawa-Flynn-Wall (OFW) method, which is computationally simpler but based on mathematical approximations, was carried out. Results showed that the values of the activation energy by OFW method are consistent with those provided by Vyazovkin approach. This implies that the OFW method, more user-friendly compared to the Vyazovkin procedure, is suitable for studying the torrefaction kinetics of residual biomass. The reliability of the evaluated kinetic parameters was checked by simulating two isothermal experimental profiles (i.e., at 250 and 300 °C) that were not used in the kinetic analysis. The theoretical value were in excellent agreement with the experimental data. As a general consideration, the isoconversional methods employed in this Ph.D. work allowed obtaining reliable kinetic parameters that could be used to simulate a steady state model of the torrefaction process involving the investigated agro-industrial residues.

As a general consideration, the results obtained in this Ph.D. project encourage future research efforts in the research field of the torrefaction of agro-industrial residues, as a promising pre-treatment route to upgrade their properties as a fuel and thus to expand their use for fuel and power applications. In particular the composition of the gas evolved during torrefaction deserve further investigation to detect the potential release of alkaline metals and chlorine, typically present in agro-industrial residues, which may affect the integrity (e.g., fouling and corrosion) of the conversion plant devices. This aspect is also important to evaluate the possible valorization routes for the torgas including: i. the production of green chemical from its condensable fraction and ii. the use as a fuel to supply the heat demand of both the drying step, which commands the larger process energy input, and the torrefaction stage.

REFERENCES

Aboyade A.O., Hugo T. J., Carrier M., Meyer E.L., Stahl R., Knoetze J. H., Görgens J. F. (2011) Non-isothermal kinetic analysis of the devolatilization of corn cobs and sugar cane bagasse in an inert atmosphere. *Thermochim. Acta*, 517, 81-89.

Anwar Z., Gulfraz M., Irshad M. (2014) Agro-industrial lignocellulosic biomass a key to unlock the future bio-energy: A brief review. *J. Radiat. Res. Appl. Sci.*, 7, 163-173.

Arena, U. and Mastellone, M.L. (2008) Gassificazione a letto fluido di CDR e imballaggi post-consumo. Available online at: http://docplayer.it/3078663-Gassificazione-a-letto-fluido-di-cdr-e-imballaggi-post-consumo.html.

Arias B., Pevida C., Fermoso J., Plaza M.G., Rubiera F., Pis JJ. (2008) Influence of torrefaction on the grindability and reactivity of woody biomass. *Fuel Process. Technol.*, 89, 169-175.

Assi J.A. and King A.J. (2008) Manganese Amendment and Pleurotus ostreatus Treatment to Convert Tomato Pomace for Inclusion in Poultry Feed. *Poultry Sci.*, 87, 1889-1896.

Atienza-Martìnez M., Fonts I., Abrego J., Ceamanos J., Gea G. (2013) Sewage sludge torrefaction in a fluidized bed reactor. *Chem. Eng. J.,* 222, 534-545.

Balat M., Balat M., Kırtay E., Balat H. (2009) Main routes for the thermo-conversion of biomass into fuels and chemicals. Part 1: Pyrolysis systems, Energy Conversion and Management. *Energ. Convers. Manage.,* 50, 3147–3157.

Bates R.B. (2012) Thesis (S.M.) - Modeling the coupled effects of heat transfer. thermochemistry, and kinetics during biomass torrefaction. Available online at: http://hdl.handle.net/1721.1/70433.

BCHPC (2007) Biomass Combined Heat and Power Catalog of Technologies Published: 2007, U. S. Environmental Protection Agency Combined Heat and Power Partnership. Available online at: http://www.epa.gov/sites/production/files/2015-07/documents/biomass_combined_heat_and_power_catalog_of_technologies_v.1.1.pdf.

Beeckmans J. M., Nilsson J., Large J.F. (1985) Observations on the mechanisms of segregation in flotsam-rich, fully fluidized beds. *Ind. Eng. Chem. Fund.,* 24, 90–95.

Bellur S.R., Coronella C. J., Vàsquez V.R. (2009) Analysis of Biosolids Equilibrium Moisture and Drying. *Environ. Prog. Sustain. Energy*, 28, 291-298.

Berg H.Ø (2013) Comparison of conversion pathways for lignocellulosic biomass to biofuel in Mid-Norway, Master of Energy and Environmental

Engineering. Available online at: http://www.diva-portal.org/smash/get/diva2:649618/FULLTEX$_{T0}$1.pdf.

Bergman, P.C.A., Boersma, A.R., Zwart, R.W.H., Kiel, J.H.A. (2005a) Torrefaction for Biomass Co-firing in Existing Coal-fired Power Stations. ECN Report No.: ECN-C--05-013, Energy Research Centre of the Netherlands. Available online at: https://www.ecn.nl/docs/library/report/2005/c05013.pdf.

Bergman, P.C.A. and Kiel, J.H.A. (2005) Torrefaction for biomass upgrading. ECN Report No.: ECN-RX-05-180, Energy Research Centre of The Netherlands. Available online at: https://www.ecn.nl/docs/library/report/2005/rx05180.pdf.

Bergman, P.C.A., Boersma, A.R., Kiel, J.H.A., Prins, M.J., Ptasinski, K.J., Janssen, F.J.J.G. (2005b). Torrefaction for entrained-flow gasification of biomass. ECN Report No.: ECN-C-05-067, Energy Research Centre of The Netherlands. Available online at: https://www.ecn.nl/docs/library/report/2005/c05067.pdf.

Bettini, O. (2014) Italy's Wine Makers Seal the Bottle on a Very Good Year. GAIN Report Number: IT1406. Available online at: http://files.foodmate.com/2014/files_3893.html.

BISYPLAN (2012) web-based handbook. Available at: http://bisyplan.bioenarea.eu/ash_appendix.html.

Boerrigter, H. and van der Drift, B. (205) "Biosyngas" key-intermediate for production of renewable transportation fuels, chemicals and electricity: optimum scale and economic prospects of Fischer–Tropsch plants. ECN Report No.: ECN-RX--05-181, Energy Research Centre of The Netherlands. Available online at: https://www.ecn.nl/docs/library/report/2005/rx05181.pdf.

Boerrigter, H. and Rauch, R. (2006) Review of applications of gases from biomass gasification. ECN Report No.: ECN-RX--06-066, Energy Research Centre of The Netherlands. Available online at: https://www.ecn.nl/docs/library/report/2006/rx06066.pdf

Bove R. and Lunghi P. (2006) Electric power generation from landfill gas using traditional and innovative technologies. *Energ. Convers. Manage.,* 47, 1391-1401.

Brachi P, Chirone R., Miccio F., Miccio M., Picarelli A., Ruoppolo G. (2014) Fluidized bed co-gasification of biomass and polymeric wastes for a flexible end-use of the syngas: Focus on bio-methanol. *Fuel,* 128, 88-98.

Brachi P., Miccio F., Miccio M., Ruoppolo G. (2015a) Isoconversional kinetic analysis of olive pomace decomposition under torrefaction operating conditions. *Fuel Process. Technol.,* 13, 147-154.

Brachi, P., Miccio, F., Miccio, M., Ruoppolo, G. Fluidized bed torrefaction of industrial tomato peels: set-up of a new batch lab-scale test rig and preliminary experimental results. Proc. of the *22nd International*

121

Conference of Fluidized Bed Conversion, June 14-17, 2015b, Turku (Finland), p. 1-10.

Branca C., Albano A., Di Blasi C. (2005) Critical evaluation of global mechanisms of wood devolatilization. *Termochim. Acta*, 429, 133-141.

Brebu M. and Vasile C. (2010) Thermal degradation of lignin – a review, *Cell. Chem. Technol.*, 44, 353-363.

Bridgeman T.G., Jones J.M., Shiels I., Williams P.T. (2008) Torrefaction of reed canary grass, wheat straw and willow to enhance solid fuel qualities and combustion properties. *Fuel*, 87, 844-856.

Bridgwater A.V. (1995) The technical and economic feasibility of biomass gasification for power generation. *Fuel*, 74, 631-653.

Broadhurst T.E and Becker H.A. (1975) Onset of fluidization and slugging in beds of uniform particles. *AIChE J.*, 21, 238-247.

Canali, S., Stopes, C., Schmid, O., Speiser, B. Current evaluation procedures for fertilizers and coil conditioners used in organic agriculture. Proc. of *a workshop held at Emerson College*, April 29-30, 2014, Great Britain, p. 1-95. Available online at: https://shop.fibl.org/fileadmin/documents/shop/1383-soilconditioners.pdf.

Caputo A.C., Scacchia F., Pelagasse P.M. (2003) Disposal of by-product in olive oil industry: waste to energy solutions, *Appl. Therm. Eng.*, 23,197-214.

Carrasco J.C., Oporto G.S., Zondlo J., Wang J. (2013) Torrefaction kinetics of red oak (querciarubra) in a fluidized bed reactor. *Bioresources*, 8, 5067-5082.

Cavagnol S., Roesler J.F., Sanz E., Nastoll W., Lu P., Perré P. (2015) Exothermicity in Wood Torrefaction and its Impact on Product Mass Yields: From Micro to Pilot Scale. *Can. J. Chem. Eng.*, 9, 331-339.

Cellatoğlu N. and İlkan M. (2015) Torrefaction of Solid Olive Mill Residue. *BioResources,* 10, 5876-5889.

Chen W.H., Peng J., Bi X.T. (2015) A state-of-the-art review of biomass *torrefaction*, densification and applications. *Renew. Sust. Energ. Rev.*, 44, 847-866.

Chew J.J. and Doshi V. (2011) Recent advances in biomass pretreatment - Torrefaction fundamentals and technology. *Renew. Sust. Energ. Rev.*, 15, 4212-4222.

Chiu C.S. and Lu W.C. (2009) Preparation and characterization of solid biomass fuel from rice straw and rice brain. *Fuel Process. Technol.*, 90, 980-987.

Clarke K.L., Pugsley T., Hill G.A. (2005) Fluidization of moist sawdust in binary particle systems in a gas–solid fluidized bed. Chem. Eng. Sci., 60, 6909-6918.

Couhert C., Salvador S., Commandrè J.M. (2009) Impact of torrefaction on syngas production from wood. *Fuel*, 88, 2286-2290.

Cremer, M., Koppejan, J., Middelkamp, J., Witkamp, J., Sokhansanj, S., Melin, S., Madrali, S. (2012) Status overview of torrefaction technologies. IEA Bioenergy Task 32 Report. Available online at: http://www.ieabcc.nl/publications/IEA_Bioenergy_T32_Torrefaction_update_2015b.pdf.

Cui H. and Grace J.R. (2007) Fluidization of biomass particles: a review of experimental multiphase flow aspects. *Chem. Eng. Sci.*, 62, 45-55.

Daleffe R. V., Ferreira M. C., Freire J. T. (2008) Effects of binary particle size distribution on the fluid dynamic behavior of fluidized, vibrated and vibrofluidized beds. *Braz. J. Chem. Eng.*, 25, 83-94.

Davidson, J.F. and Harrison, D. (1963) *Fluidized Particles*. Cambridge University Press, New York (NY), p. 173-196.

DCE (2012) Bioenergy, food and ethics in a globalized world. The Danish Council of Ethics Report. Available on line at: http://www.etiskraad.dk/en/Nyhedsarkiv/2012/maj/~/media/bibliotek/rapporter/2012/Bioenergy-food-and-ethicsin-a-globalized-world-summary.ashx.

de Araújo Sousa B.A. and Correia R.T.P. (2010) Biotechnological Reuse of Fruit Residues as a Rational Strategy for Agro-industrial Resources. *J. Technol. Manag. Innov.*, 5, 104-112.

Demirbas, A. (2009) *Biofuels: Securing the Planet's Future Energy Needs*, Springer, London (UK), p. 43-45.

Deng J., Wang G.J., Kuang J.H., Zhang Y.L., Luo Y.H. (2009) Pretreatment of agricultural residues for co-gasification via torrefaction. J. Anal. Appl. *Pyrol.*, 86, 331-337.

Deutmeyer, M., Bradley, D., Hektor, B., Hess, J. R., Nikolaisen, L., Tumuluru, J., Wild, M. (2012) Possible effect of torrefaction on biomass trade. IEA bioenergy task 40. Available online at: http://www.bioenergytrade.org/downloads/t40-torrefaction-2012.pdf.

Dhungana A., Dutta A., Basu P. (2012a) Torrefaction of Non-Lignocellulose Biomass Waste. *Can. J. Chem. Eng.*, 90, 186-195.

Duhungana, A., Basu, P., Dutta, A. (2012b) Effects of reactor design on the torrefaction of biomass. *J. Energy Resour. Technol.*, 134, 0418011-11.

Di Blasi C., Branca C., Sarnataro F.E., Gallo A. (2014) Thermal runaway in the pyrolysis of some lignocellulosic biomasses. *Energ. Fuel*, 28, 2684-2696.

Duca D., Riva G., Foppa Pedretti E., Toscano G., Mengarelli C., Rossini G. (2014) Solid biofuels production from agricultural residues and processing by-products by means of torrefaction treatment: the case of sunflower chain. *J. Agric. Eng.,* 45, 97-102.

ENAMA (2011) – "Biomasse ed energia. Disponibilità delle biomasse". Available online at: http://www.progettobiomasse.it/it/pdf/studio/p1c2.pdf.

EverGreen Renewable, LLC (2009) Biomass Torrefaction as a Preprocessing Step for Thermal Conversion - Reducing costs in the biomass supply chain. Available online at: http://evergreenrenewable.com/welcome_files/Biomass%20torrefaction.pdf.

Ezejiofor T.I.N., Enebaku U.E., Ogueke C. (2014) Waste to Wealth- Value Recovery from Agrofood Processing Wastes Using Biotechnology: A Review. *Br. Biotechnol. J.*, 4, 418-481.

FAO (2011). FAOSTAT. Food and Agriculture Organization of the United Nations. Available on line at: http://faostat.fao.org/default.aspx.

Fatoni, R., Gajjar, S., Gupta, S., Handa, S., Elkamel, A. Modeling Biomass Gasification in a Fluidized Bed Reactor. Proc. of the *2014 International Conference on Industrial Engineering and Operations Management*, January 7-9, 2014, Bali (Indonesia), p. 1047-1056.

Formisani B. and Girimonte R. (2003) Experimental analysis of the fluidization process of binary mixtures of solids. *KONA Powder Part. J.*, 21, 66-75.

Formisani B., Girimonte R., Longo T. (2008) The fluidization process of binary mixtures of solids: Development of the approach based on the fluidization velocity interval. *Powder Technol.*, 185, 97-108.

Fotovat F., Chaouki J., Bergthorson J. (2014) Distribution of large biomass particles in a sand-biomass fluidized bed: experiments and modeling. *Aiche J.*, 60, 869-880.

Franco C., Pinto F., Gulyurtlu I., Cabrita I. (2003) The study of reactions influencing the biomass steam gasification process. *Fuel*, 82: 835-842.

Fuchs B., Hofbeck K., Faulstich M. (2012) On vacuum-insulated thermal storage. *Energy Procedia*, 30, 255-259.

Gomez A., Zubizarreta J., Rodrgues M., Dopazo C., Fueyo N. (2010) An estimation of the potential of agro-industrial residues in Spain. *Resour. Conserv. Recy.*, 54, 972-984.

Grigiante M. and Antolini D. (2015) Mass yield as guide parameter of the torrefaction process. An experimental study of the solid fuel properties referred to two types of biomass. *Fuel*, 153, 499-509.

Gronli M.G., Varhegyi G., Di Blasi C. (2002) Thermogravimetric analysis and devolatilization kinetics of wood. *Ind. Eng. Chem. Res.*, 41, 4201-4208.

Gupta, C.K. and Sathiyamoorthy, D. (1998) *Fluid Bed Technology in Materials Processing*. CRC Press LLC., Boca Raton (FL), p. 23-33.

Harrison D., Davidson J.F., de Kock J.W. (1961) On the nature of aggregative and particulate fluidization. *Trans. Inst. Chem. Eng.*, 39, 202-211.

Håkansson, K., Nordin, A., Nordwaeger, M., Olofsson, I., Svanberg, M. Process And System Integration Aspects Of Biomass Torrefaction. Proc. of *18th European Biomass Conference and Exhibition*, May 3-7, 2010,

Lyon (France). Available online at: http://www.tfe.umu.se/digitalAssets/61/61395_ob3-4-process-and-system-integration-aspects-of-biomass-torrefaction-submitted.pdf.

Heuzé, V., Tran, G., Hassoun, P., Bastianelli, D., Lebas, F. (2015) Tomato pomace, tomato skins and tomato seeds. Feedipedia, a programme by INRA, CIRAD, AFZ and FAO. Available online at: http://feedipedia.org/node/689.

ISTAT (2006-2013) ISTAT data tables for the reference period 2006-2013. Available on line at: http://agri.istat.it/sag_is_pdwout/jsp/NewDownload.jsp.

Jin, B. and Kelly, J.M. (2009) Wine Industry Residues. In: *Biotechnology for Agro-Industrial Residues Utilisation* (P. Singh nee' Nigam and A. Pandey, Eds), Springer Science + Business Media B.V., Dordrecht, The Netherlands, Chapter 15.

Junsatien W., Soponpongpipat N., Phetsong S. (2013) Torrefaction reactors. *J. Sci. Technol. MSU*, 32, 84-91.

Kaliyan N. and Morey V. (2009) Factors affecting strength and durability of densified biomass product. *Biomass. Bioenerg.*, 33, 337-59.

Kleinschmidt, C.P. Overview of international developments on torrefaction. Proc. of the *Central European Biomass Conference*, January 26-28, 2011, Graz (Austria). Available online at: http://www.ieabcc.nl/workshops/task32_2011_graz_torrefaction/Kleindschmidt_Paper.pdf.

Knoblich M., Anderson B., Latshaw D. (2005) Analyses of tomato peel and seed byproducts and their use and a source of carotenoids. *J. Sci. Food Agric.*, 85, 1166-1177.

Knowlton T. (1977) High-pressure fluidization characteristics of several particulate solids: primarily coal and coal-derived materials. *AIChE Symp. Ser.*, 73, 22-34.

Kongkeaw, N. and Patumsawad, S. Thermal Upgrading of Biomass as a Fuel by Torrefaction. Proc. of *2nd International Conference on Environmental Engineering and Applications (ICEEA 2011)*, August 19-21, 2011, Shanghai (China) p. 38-42.

Koopmans, A., Koppejan, J. Agricultural and forest residues-generation, utilization and availability. Proc. of *Regional Consultation on Modern Applications of Biomass Energy*, January 6-10, Kuala Lumpur (Malaysia) p.1-23. Available online at: http://www.fao.org/docrep/006/AD576E/ad576e00.pdf.

Koppejan, J., Sokhansanj, S., Melin, S., Madrali, S. (2012) Status overview of torrefaction technologies. IEA Bioenergy Task 32 Final Report. Available online at: http://www.ieabcc.nl/publications/IEA_Bioenergy_T32_Torrefaction_review.pdf.

Kumar A., Jones D.D., Hanna M.A. (2009) Thermochemical Biomass Gasification: A Review of the Current Status of the Technology. *Energies*, 2, 556-581.

Kumar, E.Y. (2014) Torrefaction of agricultural residues. *Int. J. Multidiscip. Stud.*, 1, 295-311.

Kunii, D. and Levenspiel, O. (1991) *Fluidization Engineering*, Butterworth-Heinimann, Boston (MA), p. 1-90.

Lam, P.S., Tooyserkani, Z., Naimi, L.J., Sokhansanj, S. (2013) Pretreatment and Pelletization of Woody Biomass. In: *Pretreatment Techniques for Biofuels and Biorefineries* (Z. Fang, Eds), Springer Berlin Heidelberg, New York, Chapter 5.

Lazos E.S. and Kalathenos P. (1988) Technical Note: Composition of tomato processing wastes. *Int. J. Food Sci. Tech*, 23, 649-652.

Leng, Y. (2008) *Materials Characterization: Introduction to Microscopic and Spectroscopic Method*, John Wiley & Sons, Singapore (Asia), p. 319-326.

Li H., Legros R., Bi X.T., Lim C.J., Sokhansanj S. (2012) Torrefaction of sawdust in a fluidized bed reactor. *Bioresour. Technol.*, 103, 453-458.

Lim J.S., Manan Z.A., Wan Alwi S.R., Hashim H. (2012) A review on utilization of biomass from rice industry as a source of renewable energy. *Renew. Sust. Energ. Rev.*,16, 3084-3094.

Lima, F.C.S., Silva, F.L.H., Gomes, J.P., Muniz, M.B., Santiago, A.M. (2014) Evaluation of Cashew apple bagasse for xylitol production. In: *Transport Phenomena and drying of solids and particulate materials - Advanced structured materials* (J.M.P.Q. Delgado and A.G. Barbosa de Lima, Eds), Springer International Publishing (Switzerland), p. 179-204.

Lu J.J. and Chen W.H. (2014) Product Yields and Characteristics of Corncob Waste under Various Torrefaction Atmospheres. *Energies*, 7, 13-27.

Lwin Y. (2000) Chemical equilibrium by Gibbs energy minimization on spreadsheets. *Int. J. Eng. Educ.*, 16, 335-339.

Mafu L.D., Neomagus H.W.J.P., Everson R.C., Carrier M., Strydom C.A., Bunt J.R. (2016) Structural and chemical modifications of typical South African biomasses during torrefaction. *Biores. Technol.*, 202, 192-197.

Manahan, S.E., Enriquez-Poy, M., Molina, L.T, Duran-de-Bazua, C. (2007) Energy and Activated Carbon Production from Crop Biomass Byproducts. In *Towards a Cleaner Planet: Energy for the Future* (J. Klapp, J.L. Cervantes-Cota, J.F. Chavez Alcala, Eds.), Springer-Verlag Berlin Heidenberg, Chapter 23.

Mangut V., Sabio E., Ganan J., Gonzalez J.F., Ramiro A., Gonzalez C.M., Roman S., Al-Kassir A. (2006) Thermogravimetric study of the pyrolysis of biomass residues from tomato processing industry. *Fuel Process. Technol.*, 87, 109-115.

Marzocchella A., Salatino P., Di Pastena V., Lirer L. (2000) Transient fluidization and segregation of binary mixtures of particles. AIChE J., 46, 2175-2182.

Massé D.I., Talbot G., Gilbert Y. (2011) On farm biogas production: A method to reduce GHG emissions and develop more sustainable livestock operations. *Anim. Feed. Sci. Tech.*, 166-167, 436-445.

McKendry P. (2002) Energy production from biomass (part 2): conversion technologies. *Biores. Technol.*, 83, 47-54.

Medic D., Darr M., Shah A., Potter J., Zimmermann J. (2012) Effects of torrefaction process parameters on biomass feedstock upgrading. *Fuel*, 91, 147-154.

Meléndez, J., LeBel, L., Stuart, P.R. (2012) A Literature Review of Biomass Feedstocks for a Biorefinery. In: *Integrated Biorefineries - Design, Analysis, and Optimization* (P. R. Stuart and M.M. El-Halwagi, Eds), CRC Press, Boca Raton, Florida, Chapter 15.

Miranda R., Bustos-Martinez D., Sosa Blanco C., Gutièrrez Villarreal M.H., Rodrigues Cantù M.E. (2009) Pyrolysis of sweet orange (Citrus sinesi) dry peel. *J. Anal. Appl. Pyrol.*, 86, 245-251.

Morillo J.A., Antizar-Ladislao B., Monteoliva-Sánchez M., Ramos-Cormenzana A., Russell N.J. (2009) Bioremediation and biovalorisation of olive-mill wastes. *Appl. Microbiol. Biotechnol.*, 82, 25-39.

Morrin S., Lettieri P., Chapman C., Mazzei L. (2012) Two stage fluid bed-plasma gasification process for solid waste valorisation: Technical review and preliminary thermodynamic modelling of sulphur emissions. *Waste Manag.*, 32, 676-684.

Mussatto S.I. and Teixeira J.A. (2010) Lignocellulose as raw material in fermentation processes. In: *Current Research, Technology and Education Topics in Applied Microbiology and Microbial Biotechnology* (A. Méndez-Vilas, Eds), Formatex Research Center, Badajoz (Spain), pp.897-907.

Nhuchhen D.R., Basu P., Acharya, B. (2014) A Comprehensive Review on Biomass Torrefaction. *Int. J. Renew. Energy. Biofuels*, 2014, 1-56.

Nikolaou, A., Remrova, M., Jeliazkov, I. (2003) Biomass availability in Europe. Lot 5: Bioenergy's role in the EU Energy Market. Available online at: https://np-net.pbworks.com/f/CRES+(2003)+Biomass+availability+in+EU.pdf.

Nordin, A., Pommer, L., Nordwaeger. M., Olofsson, I. (2013) Biomass conversion through torrefaction. In: *Technologies for converting biomass to useful energy: combustion, gasification, pyrolysis, torrefaction and fermentation (*E. Dahlquist, Eds), CRC Press, Boca Raton, Florida, Chapter 7.

Oberberg I. and Thek G. (2004) Physical characterization and chemical composition of densified biomass fuels with regard to their combustion behavior. *Biomass Bioenerg.*, 27, 653-669.

Oka, S.N., (2004) *Fluidized Bed Combustion*, Marcel Dekker, New York (NY), p.73-90.

Orfao J.J.M., Antunes F.J.A., Figueiredo J.L. (1999) Pyrolysis kinetics of lignocellulosic materials-three independent reactions model. *Fuel*, 78, 349-358.

Ozawa T. (1965) A new method of analyzing thermogravimetric data. *Bull. Chem. Soc. Jpn.*, 38, 1881-1886.

Panwar N.L., Kothari R., Tvagi V.V. (2012) Thermochemical conversion of biomass - Eco friendly energy routes. *Renew. Sust. Energ. Rev.*,16, 1801-1816.

Park, J., Meng, J., Lim, K.H., Rojas, O.J., Park, S. (2013) Transformation of lignocellulosic biomass during torrefaction. J. *Anal. Appl. Pyrol.*, 100, 199-206.

Pelizer L. H., Pontieri M. H., Moraes I. O. (2007) Utilização de Resíduos Agro-Industriais em Processos Biotecnológicos como Perspectiva de Redução do Impacto Ambiental. J. *Technol. Manag. Innov.*, 2, 118-127.

Peng J.H., Bi X.T., Sokhansanj S., Lim C.J. (2013) Torrefaction and densification of different species of softwood residues. *Fuel*, 111, 411-421.

Pentananunt R., Mizanur Rahman A.N.M., Bhattacharya S.C. (1990) Upgrading of biomass by means of torrefaction. *Energy*, 15, 1175-1179.

Perejòn A., Sanchez-Jimenèz P.E., Criado J. M., Perez-Maqueda L.A. (2011) Kinetic Analysis of Complex Solid-State Reactions. A New Deconvolution Procedure. *J. Phys. Chem. B*, 115, 1780-1791.

Prins M.J., Ptasinski K.J., Janssen F.J.J.G. (2006) More efficient biomass gasification via torrefaction. *Energy*, 31, 3458-3470.

Prins M.J., Ptasinski K.J., Janssen F.J.J.G. (2006) Torrefaction of wood. Part 2: Analysis of products. *J. Anal. Appl. Pyrol.*, 77, 35-40.

Protásio T.P., Bufalino L., Mendes R.F., Ribeiro M.X., Trugilho P.F., da S. Leite E.R. (2012) Torrefaction and carbonization of briquettes made with residues from coffee grain. *Rev. Bras. Eng. Agríc. Ambient.*, 16, 1415-4366.

Poudel J., Ohm T.I., Oh S.C. (2015) A study on torrefaction of food waste. *Fuel,* 140, 275-281.

Poudel J, Ohm T.I., Lee S.H., Oh S.C. (2015) A study on torrefaction of *sewage* sludge to enhance solid fuel qualities. *Waste Manage.*, 40, 112-118.

Qin W., Egolfopoulos F.N., Tsotsis T.T. (2001) Fundamental and environmental aspects of landfill gas utilization. *Chem. Eng. J.*, 82, 157-172.

Quig, R.H., Granger, T., Ziegler, E.N. (2006) Planning For New Processes: Environmental Aspects. In: *Encyclopedia Of Environmental Science And Engineering* (J.R. Pfafflin and E.N. Ziegler, Eds), CRC Press, Boca Raton (Florida) p. 999.

REACM (2008) Market of Olive Residues for Energy. Available on line at: https://ec.europa.eu/energy/intelligent/projects/sites/iee-projects/files/projects/documents/m.o.r.e._regional_situation_olive_milling_residues_market_en.pdf.

Ren S., Lei H., Wang L., Bu Q., Chen S., Wu J., Julson J., Ruan R. (2013) The effects of torrefaction on compositions of bio-oil and syngas from biomass pyrolysis by microwave heating. *Bioresour. Technol.*, 135, 659-664.

Repellin V., Govin A., Rolland M., Guyonnet R. (2010) Modelling anhydrous weight loss of wood chips during torrefaction in a pilot kiln. *Biomass Bioenerg.*, 34, 602-609.

Rosillo-Calle, F. (2007) *The Biomass Assessment Handbook. Bioenergy for a Sustainable Environment*, Earthscan, London (UK), p. 34-69.

Rossini G., Toscano G., Duca D., Corinaldesi F., Foppa Pedretti E., Riva G. (2013) Analysis of the characteristics of the tomato manufacturing residues finalized to the energy recovery. *Biomass Bioenerg.*, 5, 177-182.

Rossini, G. (2013) Ph.D. Thesis - Valorizzazione energetica mediante tecniche di trattamento fisiche e termochimiche di biomasse residuali da filiere agricole ed agroindustriali. Available online at: http://openarchive.univpm.it/jspui/handle/123456789/86.

Ruiz Celma A., Cuadros F., Lopez-Rodriguez F. (2012) Characterization of pellets from industrial tomato residues. *Food Bioprod. Process.*, 90, 700-706.

Ruoppolo G., Miccio F., Brachi P., Picarelli A., Chirone R. (2013) Fluidized Bed Gasification of Biomass and Biomass/Coal Pellets in Oxygen and Steam Atmosphere. *Chem. Eng. Trans.*,32, 595-600.

Sabio E., Álvarez-Murillo A., Román S., Ledesma B. (2016) Conversion of tomato-peel waste into solid fuel by hydrothermal carbonization: Influence of the processing variables. *Waste Manage.*, 47, 122-132.

Sadaka S. and Negi S. (2009) Improvements of biomass physical and thermochemical characteristics via torrefaction process. *Environ. Progress Sustain. Energy*, 28, 427-434.

Shah A., Darr M.J., Medic D. (2012) Techno-economic analysis of a production-scale torrefaction system for cellulosic upgrading. *Biofuels Bioprod. Biorefin.*, 6, 45-57.

Shang, L., Ahrenfeldt, J., Henriksen, U. B., & Holm, J. K. (2013) Ph.D. Thesis - Upgrading Fuel Properties of Biomass by Torrefaction. Available on line at: http://orbit.dtu.dk/files/56263668/Ph.d.%20thesis%20-%20Lei%20Shang,%20klar%20til%20trykkeri.pdf.

Singh nee' Nigam, P., Gupta N., Anthwal, A. (2009) Pre-treatment of Agro-Industrial Residues. In: *Biotechnology for Agro-Industrial Residues Utilization* (P. Singh nee' Nigam and A. Pandey, Eds), Springer Science + Business Media B.V., Dordrecht, The Netherlands, Chapter 2.

Sogi D.S. and Bawa A.S. (1998) Studies on dehydratation of tomato processing waste. *Indian Food Packer*, 52, 26-29.

Spellman, F. R . (2012) *Forest-Based Biomass Energy Concepts and Applications*, CRC Press, Boca Raton (FL), p. 258-270.

Spinelli R., Kofman P., Magagnotti N. (2007) Il cippato conservato al coperto mantiene più potere calorifico. *L'Informatore Agrario*, 5, 40-45.

Tahmasebpoor, M., de Martin, L., Talebi, M., Mostoufi, N., van Ommen, J.R. Fluidization of Nanoparticles: The Effect of Surface Characteristics. Proc. of the 14th International Conference on Fluidization - From Fundamentals to Products, May 26-31, 2013, The Netherlands, p. 1-9. Avaiilavle online at: http://dc.engconfintl.org/cgi/viewcontent.cgi?article=1094&context=fluid ization_xiv.

Tallaksen, J. (2011) Biomass Gasification: A Comprehensive Demonstration of a Community Scale Biomass Energy System. Final Report to the USDA Rural Development Grant 68-3A75-5-232. Available online at: http://renewables.morris.umn.edu/biomass/documents/USDA_Report/SII _Preprocessing.pdf.

Terrapon-Pfaff J., Fischedick M., Monheim H. (2012) Energy potentials and sustainability-the case of sisal residues in Tanzania. *Energy Sustain. Dev.*, 16, 312-319.

Toscano G., Pizzi A., Foppa Pedretti E., Rossini G., Ciceri G., Martignon G., Duca D. (2015) Torrefaction of tomato industry residues. *Fuel*, 143, 89-97.

Tran K.Q., Trinh T.N., Bach Q.V. (2016) Development of a biomass torrefaction process integrated with oxy-fuel combustion. *Biores. Technol.*, 199, 408-413.

Tumuluru, J.S., Sokhansanj, S., Christopher, O., Wright, T., Boardman, R.D. (2010) Biomass torrefaction process review and moving bed torrefaction system model development. Report INL/EXT-10-19569, U.S. Department of Energy. Available on line at: https://inldigitallibrary.inl.gov/sti/4734111.pdf.

Tumuluru J.S., Sokhansanj S., Hess J.R., Wright C.T., Boardman R. (2011) A review on biomass torrefaction process and product properties for energy applications. *Ind. Biotechnol.*,7, 384-401.

Tumuluru J.S., Boardman R.D., Wright C.T., Hess J.R. (2012) Some Chemical Compositional Changes in Miscanthus and White Oak Sawdust Samples during Torrefaction. *Energies*, 5, 3928-3947.

Uemura Y., Omar W.N., Tsutsui T., Yusup S. Bt. (2011) Torrefaction of oil palm wastes. *Fuel*, 908, 2585-2591.

UNFCCC (2005) Clarification of definition of biomass and consideration of changes in carbon pools due to a CDM project activity. EB-20 Report, Annex 8, p.1. Available online at: https://cdm.unfccc.int/EB/020/eb20repan08.pdf.

Uslu A., Faaij A.P.C., Bergman P.C.A. (2008) Pretreatment technologies and their effect on international bioenergy supply chain logistics: Techno-economic evaluation of torrefaction, fast pyrolysis, and pelletization. *Energy*, 33, 1206-1223.

Van der Stelt M.J.C., Gerhauser H., Kiel J.H.A., Ptasinski K.J. (2011) Biomass upgrading by torrefaction for the production of biofuel: A review. *Biomass Bioenerg.*, 35, 3748-3762.

Vasile C., Popescu C.M, Popescu M.C., Brebu M., Willfor S. (2011) Thermal behaviour/treatments of some vegetable residues. IV. Thermal decomposition of eucalyptus wood. *Cellulose Chem. Technol.*,45, 29-42.

Varhegyi G., Jakab E., Till F., Szekely T. (1989) Thermogravimetric-mass spectrometric characterization of the thermal decomposition of sunflower stem. *Energ. Fuel.*, 3, 755-760.

Vasquez V.R., Coronella C.J. (2009) A simple model for vapor-moisture equilibrium in biomass substrates. *AIChE J.*, 55, 1595-1603.

Vyazovkin S. (1996) A unified approach to kinetic processing of nonisothermal data. *Int. J. Chem. Kinet.*, 28, 95-101.

Vyazovkin S. (1997) Evaluation of activation energy of thermally stimulated solid-state reactions under arbitrary variation of temperature. *J. Comput. Chem.*, 18, 393-402.

Vyazovkin S. (2000) Modification of the integral isoconversional method to account for variation in the activation energy. *J. Comput. Chem.*, 22, 178-183.

Vyazovkin S. and Dollimore D. (2006) Linear and nonlinear procedures in isoconversional computations of the activation energy of nonisothermal reaction in solids. *J.Chem. Inf. Sci.*, 36,42-45.

Vyazovkin S. and Sbirrazzuoli N. (2006) Isoconversional kinetic analysis of thermally stimulated process in polymers. *Macromol. Rapid. Commun.*, 27, 1515-1532.

Vyazovkin S. and Wight C.A. (1998) Isothermal and non-isothermal kinetics of thermally stimulated reactions of solids. *Inter. Rev. Phys. Chem.*, 17, 407-433.

Vyazovkin S., Burnham A.K., Criado J.M., Pérez-Maqueda L.A., Popescu C., Sbirrazzuoli N. (2011) ICTAC Kinetics Committee recommendations for performing kinetic computations on thermal analysis data. *Thermochim. Acta*, 520, 1-19.

Wang M.J., Huan Y.F., Chiueh P.T., Kuan W.H., Lo S.L. (2012) Microwave-induced torrefaction of rice husk and sugarcane residues. *Energy*, 37, 177-184.

Wender I. (1996) Reactions of synthesis gas. *Fuel Process. Technol.*, 48, 189-297.

Williams, R.B., Jenkins, B.M., Nguyen, D. (2003) Solid waste conversion: a review and database of current and emerging technologies. Final Report. CIWMB Interagency Agreement IWM-C0172. Available on line at:

http://energy.ucdavis.edu/files/05-06-2013-2003-solid-waste-conversion-review-and-assessment.pdf.

Winston P.W. and Bates D.H. (1960) Saturated Solutions For the Control of Humidity in Biological Research. *Ecology*, 41, 232-237.

Wu K.T., Tsai C.J., Chen C.S., Chen H.W. (2012) The characteristics of torrefied microalgae. *Appl. Energy*, 100, 52-57.

Yang, W.C. (2003) Bubbling Fluidized Beds. In: *Handbook of fluidization and fluid-particle systems* (W.C. Yang, Eds), Marcel Dekker, New York, Chapter 3.

Yang H., Yan R., Chen H., Lee D.H., Zheng C. (2007) Characteristic of hemicellulose, cellulose and lignin pyrolysis. *Fuel*, 86,1781-1788.

Yuan H., Wang Y., Kobayashi N., Zhao D., Xing S. (2015) Study of Fuel Properties of Torrefied Municipal Solid Waste. *Energ. Fuel.*, 29, 4976-4980.

Zhang Y., Jin B., Zhong W. (2008) Fluidization, mixing and segregation of a biomass-sand mixture in a fluidized bed, *Int. J. Chem. React. Eng.*, 6, 1-29.

Zhang Y., Jin B., Zhong W. (2009a) Experimental investigation on mixing and segregation behavior of biomass particle in fluidized bed. *Chem. Eng. Process.*, 48, 745-754.

Zhang, Y., Jin, B., Zhong, W., Ren, B., Xiao, R. (2009b) Characterization of fluidization and segregation of biomass particles by combining image processing and pressure fluctuations analysis. *Int. J. Chem. React. Eng.,* 7, 1-19.

Zhang L., Xu C.C., Champagne P. (2010) Overview of recent advances in thermo-chemical conversion of biomass. Energ. Convers. Manage., 51, 969-982.

Zhang L., Bi X., Grace J.R. (2015) Measurements of electrostatic charging of powder mixtures in a free-fall test device. *Procedia Eng.*,102, 295-304.

Zheng A., Zhao Z., Chang S., Huang Z., He F., Li H. (2012) Effect of Torrefaction Temperature on Product Distribution from Two-Staged Pyrolysis of Biomass. *Energ. Fuel.*, 26, 2968-2974.

Zuorro A., Lavecchia R., Medici F., Piga L. (2014) Use of cell wall degrading enzymes for the production of high-quality functional products from tomato processing waste. *Chem. Eng. Trans.*, 38, 355-360.

LIST OF SYMBOLS

a	Regression coefficient [%wt.·°C^{-1}] in eqs.III.1-III.2
	[MJ·kg^{-1}·°C^{-1}] in eqIII.3
	[%·°C^{-1}] in eqs.III.4-III-5
A	Pre-exponential factor [min^{-1}]
A$_\alpha$	Pre-exponential factor value at a fixed conversion degree [min^{-1}]
A$_j$	Pre-exponential factor of the jth biomass pseudo-component [min^{-1}]
b	Regression coefficient [%wt.·min^{-1}] in eqs.III.1-III.2
	[MJ·kg^{-1}·min^{-1}] in eqIII.3
	[%·min^{-1}] in eqs.III.4-III-5
E	Apparent activation energy [J·mol^{-1}]
E$_\alpha$	Apparent activation energy value at a fixed conversion degree [J·mol^{-1}]
E$_j$	Apparent activation energy of the jth biomass pseudo-component [J·mol^{-1}]
E$_{\alpha j}$	Apparent activation energy of the jth biomass pseudo-component at a fixed conversion degree [J · mol^{-1}]
E$_Y$	Energy yield [%]
f(α)	Reaction model [-]
f(T, t)	Dependent variable of the regression equation [%wt.] in eqs. III.1-III.2 [MJ·kg^{-1}] in eq. III.3 [%wt.] in eqs. III.4-III.5

133

$g(\alpha)$	Integral form of the reaction model [-]
i	Integer number representing dynamic thermogravimetric experiments performed at the different heating rate [-]
$I(E,T)$	Temperature integral in eq. II.8 [°C]
$I(E_\alpha, T_\alpha)$	Temperature integral in eq. II.10 [°C]
$I^*(E_\alpha, T_\alpha)$	Temperature integral in eq. II.12 [°C]
I_{ED}	Energy densification index [-, daf]
k	Integer number representing the experimental points employed to evaluate the quality of fit between simulated and experimental conversion curves [-]
M_Y	Mass yield [%, daf]
R	Gas constant [J K^{-1} mol^{-1}]
S	Total area under the curve from the baseline for Gaussian and Lorentzian peak-shape functions [%wt. min^{-1} °C^{-1}]
S_{ji}	Total area under the jth deconvoluted peak from the DTG curve recorded at the ith heating rate β_i [%wt. min^{-1} °C]
t	Time [min]
t_α^*	Time at which the conversion degree α is experimentally achieved at an arbitrary temperature T_o under isothermal conditions [min]
T	Temperature [°C]
T_o	Temperature [°C]
$T_{\alpha,i}$	Temperature at which the conversion degree α is experimentally achieved at the ith heating rate βi [K].

$T_{\alpha j,i}$ Temperature at which the conversion degree α of the jth pseudo-component is reached under the ith heating rate β_i [°C].

T_{α}^{*} Temperature at which the conversion degree α is experimentally achieved at the heating rate $\beta*$ [°C].

T_i Onset temperature for DTG peaks [°C].

T_f End temperature for DTG peaks [°C].

T_{max} Temperature at which maximum weight loss occur during a TGA tests [°C].

w   Weight at half height of the deconvoluted DTG peaks [°C].

W_f Normalized mass value at the end of the weight loss event of interest in a TGA [-]

W_t Normalized mass value at a generic time t [-]

W_o Normalized mass value at the beginning of the weight loss event of interest in a TGA [-]

W_{jf} Normalized mass value of the jth pseudo-component at the end of the weight loss event of interest in a TGA [-]

W_{jt} Normalized mass value of the jth pseudo-component at a generic time t [-]

W_{j0} Normalized mass value of the jth pseudo-component at the beginning of the weight loss event of interest in a TGA [-]

W_{max} Maximum weight loss rate corresponding to DTG peak maxima[%wt. min^{-1}]

x   Independent variable of Gaussian and Lorentzian peak-shape functions [°C]

x_o	Center of Gaussian and Lorentzian peak-shape functions [°C]
y	Dependent variable of Gaussian and Lorentzian symmetric peak-shape functions [%wt. min^{-1}]
y_O	Baseline offset of Gaussian and Lorentzian peak-shape functions [%wt. min^{-1}]
z_O	Regression coefficient [%wt.] in eqs. III.1-III.2 [MJ·kg^{-1}] in eq. III.3 [%wt.] in eqs. III.4-III.5

GREEK SYMBOLS

α	Conversion degree [-]
α^*	Experimental value of the degree of conversion [-]
$\alpha_{(k,exp)}$	Conversion degree from the experimental TG curve recorded at 60 °C/min [-]
$\alpha_{(k,calc)}$	Conversion degree from the simulated dynamic TG curve at 60 °C/min[-]
β	Linear heating rate [°C min^{-1}]
β_i	ith linear heating rate [°C min^{-1}]
β_h	hth linear heating rate [°C min^{-1}]
γ_j	Contribution of jth pseudo-component to the total mass loss during a TGA test run [-]
$\Phi(E_\alpha)$	Objective function f to be minimized according to the non-linear Vyazovkin isoconversional method [-]

ABBREVIATIONS

CSS	Coarse Silica Sand
FSS	Fine Silica Sand
GRD	Generalized Reduced Gradient
OH	Virgin Olive Husk
TPs	Tomato Peels
TP/CSS	Coarse sand and tomato peels binary mixture
TP/FSS	Fine sand and tomato peels binary mixture